WID

Water Injectivity Decline Simulator

Technical Documentation

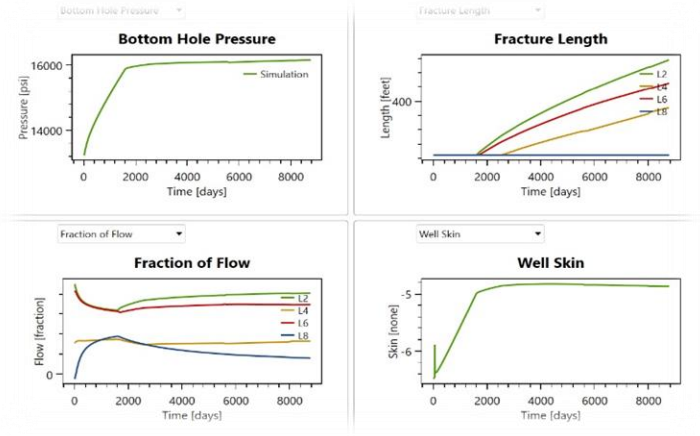

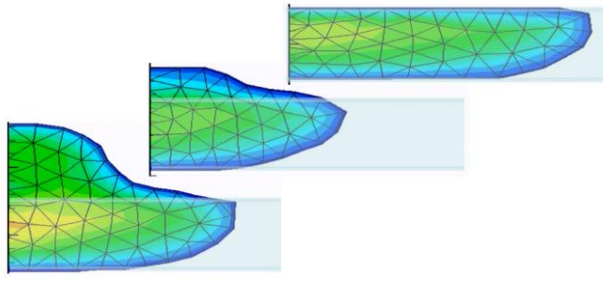

- ✓ 2-D and 3-D Induced Fracture Propagation Simulation
- ✓ Injectivity, Fraction of Flow in Vertical & Horizontal Injectors
- ✓ Comprehensive Filtration Physics for Injection Wells
- ✓ History Match Injection Well Performance

Last updated on February 14, 2018 for WID3D 18.01

License Information

This software documentation is provided for internal use only by companies have a license agreement to use this software. The license is non-exclusive, non-sub licensable, non-transferable and non-assignable.

Table of Contents

Table of Contents 3
Chapter 1: Introduction 7
1.1 Background 7
1.2 WID Simulator 7
Chapter 2: Injectivity Decline 9
2.1 Introduction 9
2.2 Particle Retention 9
2.3 Flow of Particle Suspensions in Porous Media 9
2.4 Filtration Coefficient 11
2.7.1 Filtration Coefficient Modified at High Darcy Velocities 13
2.5 Permeability Reduction Model 14
2.6 Transition Time 15
2.7 Flow Resistance 16
2.7.1 Flow Resistances for Linear Geometry 17
2.7.2 Flow Resistances for Radial Geometry 18
Chapter 3: Two Dimensional Fracture Model 25
3.1 Introduction 25
3.2 Modeling Fracture Growth in Injection Wells 25
3.3 In-Situ Stresses 26
3.4 Effect of Thermoelastic Stresses 27
3.5 Determination of Temperature and Saturation Profiles 28
3.6 Effect of Pore Pressure 30
3.7 Fracture Propagation 31
Chapter 4: Development of 2-D Fracture Simulator 37
4.1 Introduction 37
4.2 Model Features 37
4.3 Method of Solution for Fracture Growth Model 38
4.4 Fluid Flow Equations 39
4.5 Permeability Decline for a Fracture of Fixed Length 40
4.6 Permeability Reduction for a Growing Fracture 42
4.7 Fracture Plugging Model 43
4.8 Pressure Drop Along the Fracture 44
4.9 Method of Solution for Determining Fracture Length 45
4.10 Examples and Discussion 46
4.10.1 Injection below the Fracture Pressure 46
4.10.2 Effect of Particle Concentration 46
4.10.3 Effect of Injection Rate 47
4.10.4 Effect of Formation Permeability 47
4.10.5 Effect of Thermal Stresses 48
Chapter 5: Injection in Multi-layered Reservoir 60
5.1 Introduction 60
5.2 Flow Distribution into Multiple Layers 60
5.2.1 Flow into an Unperforated Layer from an Adjacent Perforated Layer 61
5.2.2 Flow into an Unperforated Layer from Multiple Perforated Layer 62
5.2.3 Flow into Multiple Unperforated Layers from Multiple Perforated Layers 63

5.2.4 Flow into Layered Reservoir with Shale Barriers 66
Chapter 6: Injectivity Decline in Horizontal Wells 69
6.1 Introduction 69
6.2 Background: Injectivity of Horizontal Wells 69
6.3 Model Development 70
6.3.1 Flow Resistance for Flow into the Reservoir from a Horizontal Well with a Longitudinal Fracture 71
6.3.2 Flow Resistance for Flow into the Reservoir from a Horizontal Well with a Transverse Fracture 72
6.3.3 Flow Resistance for Flow into the Reservoir from the Horizontal Well up to the Drainage Boundary 73
6.3.4 Flow Resistance for Flow into the Reservoir from the Transverse Fracture up to the Drainage Boundary 74
6.4 Model Implementation 74
6.5 Results and Discussion 75
6.5.1 Effect of Horizontal Well Length 76
6.5.2 Effect of Water Quality 76
6.5.3 Effect of Reservoir Thickness 76
6.5.4 Other Factors Affecting Injector Performance and Fracture Growth 77
6.6 Conclusions 78
6.6 Nomenclature (All variables are in SI units) 79
6.6.1 Greek symbols 81
6.7 References 82
6.8 Appendix 83
Chapter 7: Injection into Frac-Packed Wells 95
7.1 Introduction 95
7.2 Model Formulation 96
7.2.1 Pressure Profile and Flow Distribution around a Frac-Packed Well 97
7.2.1.1 Comparison of Bilinear Model with Prats Solutions 97
7.2.2 Filtration and Permeability Decline Model 97
7.2.2.1 Permeability Reduction Model 99
7.2.3 Flow Resistance Model for Bilinear Flow 100
7.2.3.1 Flow Resistance along the Frac-pack 100
7.2.3.2 Flow Resistance Perpendicular to the Frac-pack 101
7.2.3.3 Flow Resistance between the Wellbore and the Equi- pressure Ellipse 103
7.2.3.4 Total Flow Resistance up to the Equi-pressure Ellipse 104
7.2.3.5 Flow Distribution around the Wellbore and the Frac- pack 104
7.2.4. Pressure Distribution in the Reservoir and the Frac-pack 105
7.2.5. Frac-Pack Widening and Channeling 107
7.2.6. Frac-Pack Lengthening 109
7.3 Model Implementation and Results 109
7.4 Conclusions 111
7.5 Nomenclature (All variables are in SI units) 113
7.6 References 115
7.7 Appendix 116
Chapter 8: Pressure Transient Model in WID 127
8.1 A Simple Model for Estimating Pressure in an Injection Well with 2-phase Flow. 127
8.2 Comparison of Analytical Model Results with CMG 127

8.3 Comparison of WID Early Pressure Model with CMG 130
8.4 A Simple Model for Estimating BHP for a Fractured Injector 131
8.5 Superposition for Variable Injection Rates 132
Chapter 9: Injection Modeling with Fracture Closure 134
9.1 Injection Well Modeling with Fracture Closure 134
9.2 Algorithm for Injection Well Modeling with Fracture Closure 134
9.3 An Example of Injection Well Modeling with Fracture Closure 135
9.4 Equivalent Frac Pack Porosity as it Extends or Closes 136
Chapter 10: Skin Distribution and Cross-Flow in Vertical Well Layers 140
10.1 Skin Distribution between Layers with Initial Well Skin 140
10.2 Skin Evolution with Injection 144
10.3 Flow Distribution when Layers are not in Hydrostatic Equilibrium 145
Chapter 11: 3-Dimensional Fracture Propagation Model 148
11.1 Introduction 148
11.2 Model Formulation 150
11.3 Model Algorithm 154
11.4 Discussion 155
11.5 Conclusion 158
11.7 Nomenclature 158
11.7 References 159
11.8 Figures 161

Chapter 1: Introduction

1.1 Background

Injection of fluids into the subsurface is of great importance in various aspects of the petroleum industry. Waterflooding is the most widely used improved oil recovery process. Injection of sea and surface water is increasing in mature fields. Water injection is also used for pressure maintenance. As oil fields mature, the volumes of produced water requiring disposal increase significantly. The increasing ratio of produced water to oil calls for handling and disposal of large amounts of produced water. With strict offshore quality requirements, subsurface injection is becoming more favorable. Large sums of money are being spent on subsurface injection.

Injection wells are susceptible to formation damage. Injectivity decline could occur due to plugging of the near wellbore region by suspended particles in the injected water, precipitation due to incompatibility of injected and formation water, fines migration, swelling of clay minerals, or by the growth of bacteria. A decline in injectivity can have a large impact on the economic feasibility of water injection operations. It is therefore important to develop reliable models to predict the injectivity decline of water injection wells.

Injectivity decline can potentially lead to fracture initiation. In order to maintain a constant flow rate, the bottomhole pressure is increased. In field operations, injection may continue at a bottomhole pressure that is high enough to initiate and propagate hydraulic fractures. These fractures can have a significant impact on reservoir performance. Unlimited fracture growth can have a number of undesirable consequences.

1.2 WID Simulator

The software tool has been developed at University of Texas at Austin to simulate well injectivity decline and fracture propagation during waterflooding and subsurface produced water disposal. The software is aimed at providing a better understanding and an engineering basis for modeling the fracture propagation in injection wells and the impact of fracturing on waterflood performance. The program is a PC based, user-friendly program that can predict the injectivity and growth of injection well fractures due to the combined influence of changes in pore pressure, thermal stresses and formation damage due to particle plugging.

The results from the simulations can help the oil company engineer answer important questions such as

- How clean is clean? What filtration specifications should I use?
- Can I inject raw seawater?
- How much oil in water can my injection well tolerate?
- How fast is the fracture growing?
- How often will the injection well require a remedial treatment to regain injectivity?
- What rates can I inject at without extending a fracture too far into the reservoir?
- How can the drilling program be adjusted to account for fracture growth in injectors?

- How will the reservoir simulation results be impacted by the dynamic growth of injection well fractures?
- What is the optimal strategy for injecting water at the lowest cost of facilities while achieving good reservoir sweep?
- How the flow is distributed between layers in a multilayered injection scenario?
- Will there be height growth of induced fractures into the bounding layer?

Chapter 2: Injectivity Decline

Water is injected into subsurface formations for waterflooding applications, pressure maintenance and produced fluids management. In mature fields, a substantial amount of oil recovery is achieved through waterflooding. In offshore operations, the injection of produced water for waterflooding and pressure maintenance is increasing. The water has suspended solids and oil droplets, which cause the injectivity to decline. A decline in injectivity can have a large impact on the economic feasibility of water injection operations. Filtration can usually reduce the concentration of suspended solids, but at a substantial cost. For these reasons, it is important to have reliable models to predict the injectivity of water injection wells.

2.1 Introduction

The prediction of injectivity decline provides an important tool to specify water quality requirements and to estimate the extent of impairment. To predict injectivity decline due to particle plugging, the nature of the impairment and its impact on well injectivity needs to be known. Past studies have shown that permeability decline due to internal filtration and the formation of an external filter cake are the primary reasons for injectivity decline (Fig. 2.1). This section discusses particle retention in porous media and details a model to predict injectivity decline due to particle plugging.

2.2 Particle Retention

Based on experimental observations, it has been proposed (Pang[1]) that particle retention occurs mainly by four mechanisms: size exclusion, surface deposition, bridging and log-jam (Fig. 2.2). Size exclusion occurs when the particle size is larger than the size of the pore throat and the particles are retained by straining. A second mechanism for particle trapping is surface deposition. Here particles are retained due to attractive surface forces acting on particles that are transported to the vicinity of the grains. The third mechanism, bridging, refers to the dynamic process where particles are retained by previously retained particles, and form bridges. Log-jam or multi particle hydrodynamic retention (MPHR occurs at high concentrations, when more than one particle tries to flow through the pore throat simultaneously and a log-jam similar to a traffic jam is formed. This mechanism is not of significant importance in injection wells since the concentration of injected particles is low and is usually below the critical concentration required for forming log-jams. It may be a significant mechanism in waste disposal wells such as those used for drill cuttings injection where the solids content is very high.

The retention mechanism and the extent of solids retained depend on various factors such as: (I) Size distribution, concentration, shape and surface properties of the injected particles. (II) Grain or pore size distribution, shape, structure and surface properties of the formation (III) Fluid properties – interstitial velocity, physico-chemical properties.

2.3 Flow of Particle Suspensions in Porous Media

Consider the flow of a dilute suspension containing particles through a porous medium. A general mass conservation equation for the flowing particles can be written as

$$\nabla.(uc - D\nabla c) + \frac{\partial}{\partial t}(\phi c + \sigma) = 0 \qquad (2.1)$$

where u is the Darcy velocity, c is the concentration of suspended particles (volume of particles per unit fluid volume), D is the dispersion coefficient, ϕ is the porosity and σ is the specific deposit (volume of deposited particles per unit bulk volume).

To simplify the equation, certain approximations are introduced. First, the flow is assumed to be incompressible which renders $\nabla u = 0$. Next, dispersion is neglected, as diffusion is negligible for particles larger than 1μm (Herzig et al.[2]). Incorporating these approximations, Eq. (2.1) becomes

$$u.\nabla c + \frac{\partial}{\partial t}(\phi c + \sigma) = 0 \qquad (2.2)$$

Considering particle plugging to be the only mechanism changing the porosity, we have

$$\frac{\partial}{\partial t}\phi = -\frac{\partial \sigma}{\partial t} \qquad (2.3)$$

The rate of deposition is assumed to be proportional to the particle concentration and the Darcy velocity, as proposed by Iwasaki [5].

$$\frac{\partial \sigma}{\partial t} = \lambda u c \qquad (2.4)$$

where the constant of proportionality λ, is called the filtration coefficient. With all the above assumptions, Eq. (2.2) in one dimension simplifies to

$$u.\frac{\partial c}{\partial x} + \phi \frac{\partial}{\partial t} c + \lambda u c = 0 \qquad (2.5)$$

We assume that λ is a constant equal to λ_o. Further, the injection velocity u and the porosity are assumed to be independent of time. Eq (2.5) is solved analytically for the one-dimensional case. The initial and boundary conditions are $c(x,0) = 0$ (2.6)

$$c(0,t) = c_{in} \qquad (2.7)$$

where c_{in} is the concentration of particles at the inlet and is equal to the injected particle concentration.

Solving Eq. (2.5) with the above initial and boundary conditions for one dimension yields

$$c(x,t) = 0, \qquad t < \frac{\phi x}{u} \qquad (2.8)$$

$$c(x,t) = c_{in} \exp(-\lambda_o x), \qquad t > \frac{\phi x}{u} \qquad (2.9)$$

Eq. (2.8) and Eq. (2.9) describe the concentration profile of the suspended particles at any instant.

Introducing these into Eq. (2.4) and solving the differential equation

$$\sigma(x,\theta) = \lambda_0 u \theta c_{in} \exp(-\lambda_o x), \quad \theta > 0 \tag{2.10}$$

$$\sigma(x,\theta) = 0, \quad \theta \le 0 \tag{2.11}$$

where θ is the corrected time measured from the time the suspension reaches a location *x*.

$$\theta(x) = t - \int_0^x \frac{dx'}{u(x')/\phi(x')} \tag{2.12}$$

The difference between *t* and θ is important for the first few pore volumes (PV) only. In water injection, thousands of pore volumes flow through the near wellbore region where most of the deposition takes place. Hence, θ can be replaced by *t* for all practical purposes. Hence

$$\sigma(x,\theta) = \lambda_0 u t c_{in} \exp(-\lambda_o x), \ t >> 1\,\text{PV} \tag{2.13}$$

The corresponding decrease in porosity is expressed as

$$\phi(x,t) = \phi_0 - \sigma(x,t) \tag{2.14}$$

Fig. (2.3) shows the effect of filtration coefficient on the concentration profile. Fig. (2.4) shows the evolution of specific deposit with time, for λ=0.1, *u*=0.1cm/s, ϕ=0.2, and c_{in}=10 ppm. Fig. (2.5) shows the corresponding decrease in porosity with time.

2.4 Filtration Coefficient

The filtration coefficient determines the rate of particle entrapment and is, therefore, of great importance. For dilute suspensions, the filtration coefficient is assumed to be independent of *c*, resulting in a first order rate dependence of the particle trapping on the suspended particle concentration. Most hazardous wastes and produced waters contain low to moderate concentrations of total suspended solids (TSS). For the applications under consideration, it is reasonable to assume that the filtration coefficient is independent of *c*.

The filtration coefficient can change as particle deposition proceeds. This can be written in general as,

$$\lambda = \lambda_0 f(\sigma) \tag{2.15}$$

where λ_o is the initial filtration coefficient.

The variation of λ with time is represented as

$$\lambda = \lambda_0 (1 + b\sigma) \tag{2.16}$$

where *b* is a constant which can either be positive or negative. Values for *b* are hard to obtain theoretically and can be deduced from experiments. Our default value for *b* is zero.

The initial filtration coefficient λ_o can be found experimentally. If a suspension is injected into a core of length *L* and the inlet and effluent concentrations, c_{in} and c_{eff} are measured, Eq. (2.8) yields

$$\lambda = \frac{1}{L} \ln(\frac{c_{in}}{c_{eff}}) \tag{2.17}$$

Experiments have been done to study the effect of various parameters on λ. Results often show a power-law dependence.

$$\lambda \propto u^{-\gamma_u}, d_p{}^{\gamma_p}, d_g{}^{\gamma_g} \tag{2.18}$$

where γ_u, γ_p and γ_g are constants and d_p and d_g are the particle and grain diameters.

Several authors have developed methods to calculate o based on computer simulations. A semi-empirical expression based on Happel's model, developed by Rajgopan and Tien3 has been used to calculate the filtration coefficient. Based on extensive computer simulations, they have expressed the initial collector efficiency as,

$$\eta = (1-\phi)^{2/3} A_s N_{Lo}{}^{1/8} N_R{}^{15/8} + 3.375\times10^{-3}(1-\phi)^{2/3} A_s N_G{}^{1.2} N_R{}^{-0.4} + 4A_s{}^{1/3} N_{Pe}{}^{-2/3}$$

Rajagopalan assumed f ~ 0.39 for filter beds and simplified the above equation to the following:

$$\eta = 0.72 A_s N_{Lo}{}^{1/8} N_R{}^{15/8} + 2.4\times10^{-3} A_s N_G{}^{1.2} N_R{}^{-0.4} + 4A_s{}^{1/3} N_{Pe}{}^{-2/3} \tag{2.19}$$

where A_s is Happel's geometric factor, N_{Lo} (London group parameter), N_G (gravity number) and N_{Pe} (Peclet number) are dimensionless parameters. η is the collection efficiency, which is the ratio of trapped concentration to initial concentration.

$$\eta = \frac{(c_{i-1} - c_i)}{c_{i-1}} \tag{2.20}$$

For Happel's cell, the relation between λ and η can be represented as

$$\lambda = \frac{3(1-\phi)}{2d_g} \eta \tag{2.21}$$

Figure 2.8 shows a comparison of model filtration coefficient values with experimental values as a function of superficial velocity. The filtration coefficient decreases with increasing fluid velocity. Figure 2.9 shows a comparison of model filtration coefficient values with a set of 105 experiments conducted by 13 different researchers.

2.7.1 Filtration Coefficient Modified at High Darcy Velocities

The filtration coefficient reduces with increasing velocities. In general the trend is that λ is proportional to u^{-a} where "a" is usually between 0.5 and 1 for u (Darcy velocity) less than 1 cm/s. Most filtration experiments that were used to fit Tien and Rajagopalan's model were done at flow velocities (Darcy velocities) less than 1 cm/s and gave reasonable model results. However at flow velocities the model starts to give higher filtration coefficient values than found experimentally. Maroudas, A. et al. 1965 have presented experimental data for filtration coefficients at high Darcy velocities (> 1 cm/s) (*Clarification of suspensions: a study of particle deposition in granular media Part II - A Theory of Clarification*). Based on their experiments, an empirical equation is developed and implemented into WID 7.2.

Modified Filtration Coefficient Model: The experiments by Maroudas et al. 1965 showed that above a critical velocity there is no particle trapping of the injected particles in the media, i.e. the filtration coefficient is zero (though the model predicts a finite filtration coefficient). Therefore, equations for critical interstitial velocities (Vc) were developed for any given size of injected particles into any given size of media grains. These equations were best fit to the experimental data presented by Maroudas et al. 1976 as shown below.

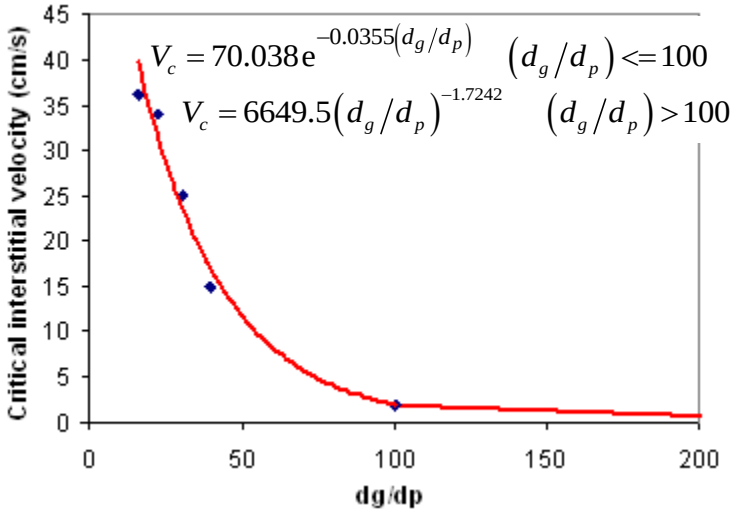

$$V_c = 70.038e^{-0.0355 d_g/d_p} \qquad (d_g/d_p) \le 100$$

$$V_c = 6649.5(d_g/d_p)^{-1.7242} \qquad (d_g/d_p) > 100$$

Above a critical interstitial velocity the filtration coefficient is zero. Even at velocities smaller than critical velocities, the filtration coefficient calculated by Rajagopalan and Tien's model is higher than measured by Maroudas et al. and other researchers. Therefore a velocity

correction factor (VCF) is introduced to lower the filtration coefficient at high interstitial velocities (lower than the critical velocity) and is given as followed:

$$VCF = (V_c - u/\phi)/V_c \qquad u/\phi \le V_c$$
$$VCF = 0 \qquad u/\phi > V_c$$

$$\lambda_{om} = VCF\,\lambda_o$$

Where λ_o is the initial filtration coefficient calculated from Rajagopalan and Tien's model and λ_{om} is the modified/corrected filtration coefficient. Vc is the critical interstitial velocity beyond which there is no particle trapping and u is the Darcy velocity.

2.5 Permeability Reduction Model

As particles are trapped in the pore throats and reduce the porosity, the permeability too declines which in turn leads to a decline in injectivity. There are several relationships available in the literature, which relate the decline in permeability to the concentration of deposited particles. We use the permeability reduction model proposed by Pang[1]. Starting from the Kozeny-Carman equation

$$k = \frac{\phi^3}{K_K(1-\phi)^2 S^2 \tau} \qquad (2.22)$$

where *k* is the permeability, *S* is the specific surface area (per unit grain volume), K_K is the Kozeny constant and τ is the tortuosity. The best-fit value for factor $k' = K_K\tau$ has been found by Carman to be 5. The ratio of permeability at any instant to the initial permeability is

$$\frac{k}{k_o} = \frac{\phi^3(1-\phi_0)^2 S_o{}^2 k_o'}{\phi_0{}^3(1-\phi)^2 S^2 k'} \qquad (2.23)$$

Pang proposed that the reduction in permeability could be broken down into permeability reduction due to three factors namely reduced porosity (k_{dp}), increased surface area (k_{ds}) and increased tortuosity (k_{dt}).

$$k/k_o = k_{dp}k_{ds}k_{dt} \qquad (2.24)$$

where

$$k_{dp} = \frac{\phi^3(1-\phi_0)^2}{\phi_0{}^3(1-\phi)^2} \qquad (2.25)$$

In calculating the reduction in permeability due to increased surface area (k_{ds}), the particles and grains are viewed as spheres with their entire surface exposed to flow.

$$k_{ds} = \left(\frac{1+\sigma/(1-\phi_0)}{1+(d_g/d_p)\sigma/(1-\phi_0)} \right)^2 \qquad (2.26)$$

The reduction in permeability due to increased tortuosity is difficult to predict. This has been accounted for by the introduction of an empirical parameter β, which is dependent on the pore structure and is called the damage factor. Normally $\beta \geq 0$.

$$k_{dt} = \frac{1}{1+\beta\sigma} \qquad (2.27)$$

In our simulations, the default value for β is 0.

2.6 Transition Time

When a fluid containing suspended particles is injected into a porous medium, the particles invade the formation and form an internal filter cake in the porous medium. As the injection continues and more particles are trapped, a point is reached where very few particles can invade the formation and an external cake (filter cake on the formation face) starts to form. The time when the transition from internal cake build up to external cake build up occurs is called the transition time (t^*). The transition time is assumed to occur when the porosity at the formation face reaches a critical porosity ϕ^*.

From Eq. (2.4) and Eq. (2.16),

$$\frac{\partial\sigma}{\partial t} = \lambda_0(1+b\sigma)uc \qquad (2.28)$$

The solution for constant flow rate is,

$$\sigma = \frac{1}{b}\left(e^{\lambda_0 buct} - 1\right), \qquad b \neq 0 \qquad (2.29)$$

$$\sigma = \lambda_0 uct\,, \; b = 0 \qquad (2.30)$$

At transition time (t^*), the critical porosity (ϕ^*) is reached. The specific deposit is equal to the difference between the initial porosity and the critical porosity.

$$\sigma = \phi_0 - \phi^* \qquad (2.31)$$

Inserting Eq. (2.31) into Eq. (2.29) and Eq. (2.30)

$$t^* = \frac{1}{buc\lambda_0}\ln\left[b(\phi_0 - \phi^*)\right], \qquad b \neq 0 \qquad (2.32)$$

$$t^* = \frac{\phi_0 - \phi^*}{uc\lambda_0}, \ b = 0 \qquad (2.33)$$

If the filtration coefficient λ is constant or increases with σ (i.e. $b \geq 0$), the pores at the inlet will be filled with captured particles and an external cake will start to form. However if the filtration coefficient λ decreases with σ (i.e. $b<0$), it could reach 0 before the critical porosity is reached, thus allowing the particles to penetrate deeper into the formation before being deposited. Under these circumstances, the transition to an external cake does not occur ($t^* \to \infty$).

Experimental data on the transition time and specific deposit is unavailable. Hence the critical porosity (ϕ^*) needs to be estimated theoretically. Assuming that the entire initial pore space is filled by particles, the resulting porosity would be a product of the initial porosity of the formation and the porosity of the internal filter cake. Hence a reasonable estimate of the critical porosity is

$$\phi^* = \phi_{formation} \times \phi_{cake} \qquad (2.34)$$

When an external filter cake forms, its properties (cake porosity and permeability) greatly influence the injectivity decline. These properties can be measured in the laboratory using core flood experiments. In the absence of core flood data, theoretical correlations such as the Blake-Cozeny equation can be used to estimate the porosity from the permeability data.

2.7 Flow Resistance

It is often convenient to represent the injectivity of a well in terms of flow resistance from the wellbore to the external drainage boundary. The flow resistance is defined as

$$R = \frac{P_{wf} - P_R}{q} \qquad (2.35)$$

where P_{wf} is the bottomhole injection pressure, P_R is the pressure at the external drainage radius and q is the flow rate.

The flow resistance is the inverse of the injectivity index, I,

$$I = \frac{q}{P_{wf} - P_R} \qquad (2.36)$$

$$R = \frac{1}{I} \qquad (2.37)$$

The total flow resistance can also be expressed as the sum of flow resistances between various regions. For a constant rate injection, R is calculated as shown below:

$$R = \frac{1}{q}\int_{P_R}^{P_{wf}} dP \tag{2.38}$$

This approach also makes it convenient to add the near wellbore damage for various completion geometries. The flow resistance in the near wellbore region is broadly broken up into three parts – resistance due to the formation unaffected by particle plugging (no damage), resistance due to the formation that is invaded by particles (internal filter cake) and the resistance due to external filter cake (Fig. 2.6 and Fig. 2.7). The flow resistance due to the formation unaffected by the particles would remain constant with time if there are no mobility effects (single-phase flow). The resistance due to the formation invaded by particles increases with time until the transition time is reached. After the transition time, internal filtration stops and an external cake start to form. From then on, the resistance due to the external cake comes into play and increases with increasing cake thickness.

2.7.1 Flow Resistances for Linear Geometry

The flow equation for linear geometry is

$$q(x) = \frac{Ak(x)}{\mu}\frac{dP}{dx} \tag{2.39}$$

where *A* is the cross sectional area, *k* the permeability and μ is the viscosity.

- **Undamaged Region**

From Eq. (2.38) and (2.39) the flow resistance is given by

$$R_U = \frac{\mu L}{Ak} \tag{2.40}$$

where *L* is the length of the undamaged formation.

- **Invaded Region**

The invaded region is modeled as N linear cores of length Δx connected in series with constant damaged permeability.

$$R_I = \frac{\mu}{A}\int_{x_i}^{x_o}\frac{dx}{k(x)} = \frac{\mu}{A}\sum_{i=1}^{N}\frac{\Delta x}{k(x_i)} \tag{2.41}$$

k(x) is determined using Eq. (2.24).

- **External Filter Cake**

The flow resistance imposed by external filter cake with cake thickness equal to h_c and cake permeability equal to k_c is given by:

$$R_C = \frac{\mu h_c}{A k_c} \tag{2.42}$$

2.7.2 Flow Resistances for Radial Geometry

The flow equation for radial geometry is

$$q(r) = A(r)\frac{k(r)}{\mu}\frac{dP}{dr} \tag{2.43}$$

where *A* is the cross sectional area, *k* the permeability and μ is the viscosity.

- **Undamaged Region**

From Eq. (2.38) and (2.43) the flow resistance is given by

$$R_U = \frac{\mu \ln(r_e / r_o)}{2\pi k h} \tag{2.44}$$

where r_e is the external drainage radius, r_o is the outer radius of the region invaded by particles.

- **Invaded Region**

The invaded region is modeled as a number of radial regions of radii r_i connected in series. From Eq. (2.31) and (2.32)

$$R_I = \frac{\mu}{A}\int_{r_w}^{r_o}\frac{dr}{k(r)} = \frac{\mu}{2\pi h}\sum_{i=1}^{N-1}\frac{\ln(r_{i+1}/r_i)}{k(r_i)} \tag{2.45}$$

$k(r)$ can be determined by solving the filtration equations for specific deposit $\sigma(r,t)$ and then calculating the corresponding permeability with the permeability model.

- **External Filter Cake**

The flow resistance imposed by external filter cake in a radial geometry with cake permeability, k_c is given by:

$$R_C = \frac{\mu \ln(r_w / r_c)}{2\pi k_c h} \tag{2.46}$$

where r_w is the original radius of the well and r_c is the radius of the well with the external cake.

A cased and perforated well is treated as a special case of radial geometry. The particle plugging is treated as though the flow was occurring through a well of circular cross section having the same area of flow as the perforated case. The radius of the wellbore r_w in Eq. (2.45) and Eq. (2.46) can be replaced by an equivalent radius r_{eq}, which is shown as below:

$$r_{eq} = nr_p l_p \tag{2.47}$$

where n is the number of perforations per unit well length, r_p is the radius of perforations and l_p is the length of perforations.

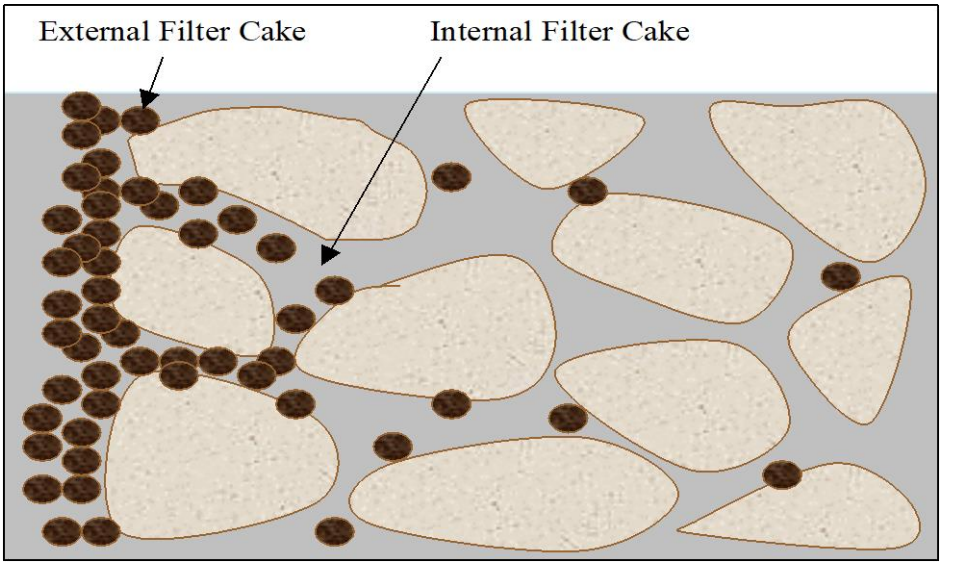

Figure 2.1: Permeability decline due to internal and external filter cakes

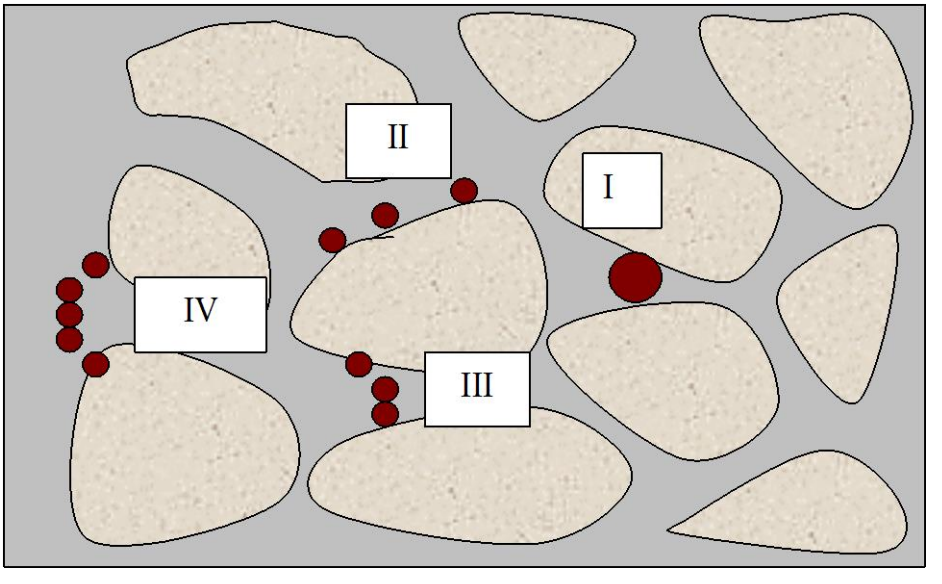

Figure 2.2: Mechanisms of particle retention

I. Size exclusion **II**. Surface deposition **III**. Bridging **IV**. MPHR

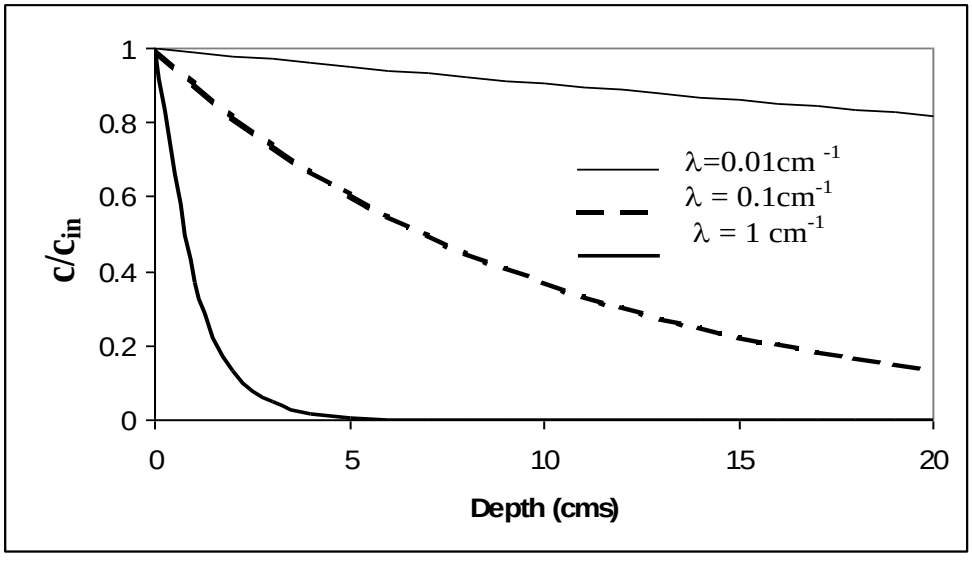

Figure 2.3 Effect of filtration coefficient on concentration profile

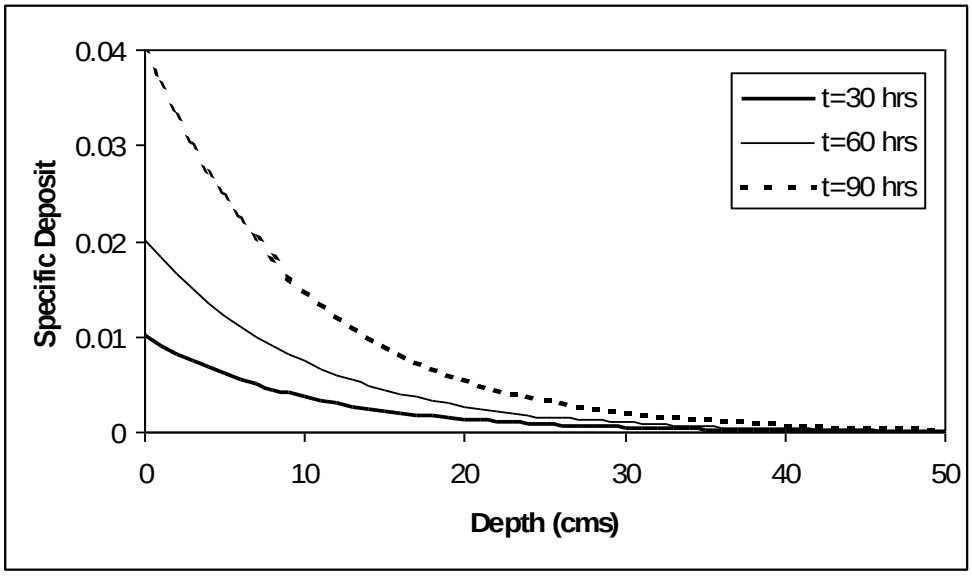

Figure 2.4: Evolution of specific deposit with time

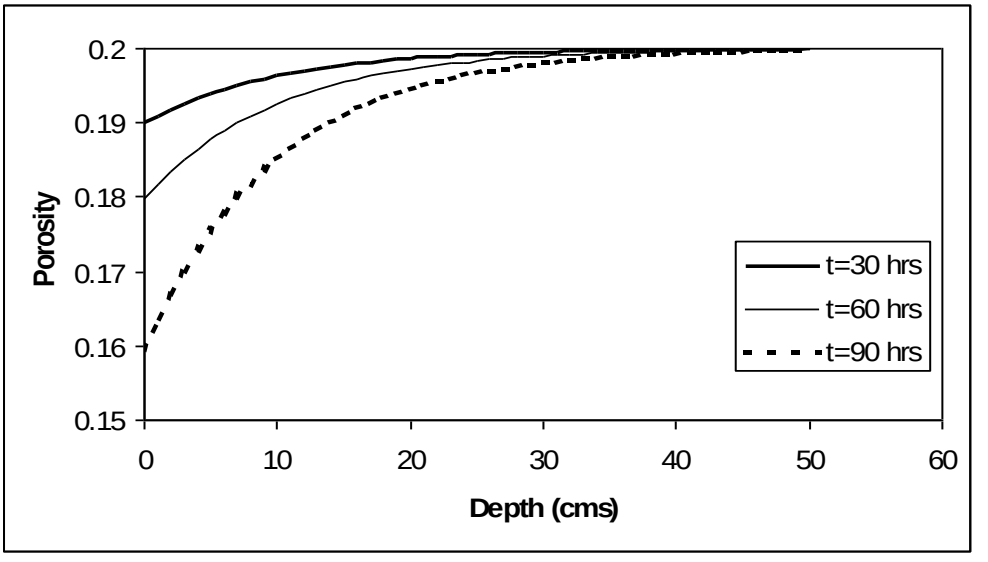

Figure 2.5: Decrease of porosity with time

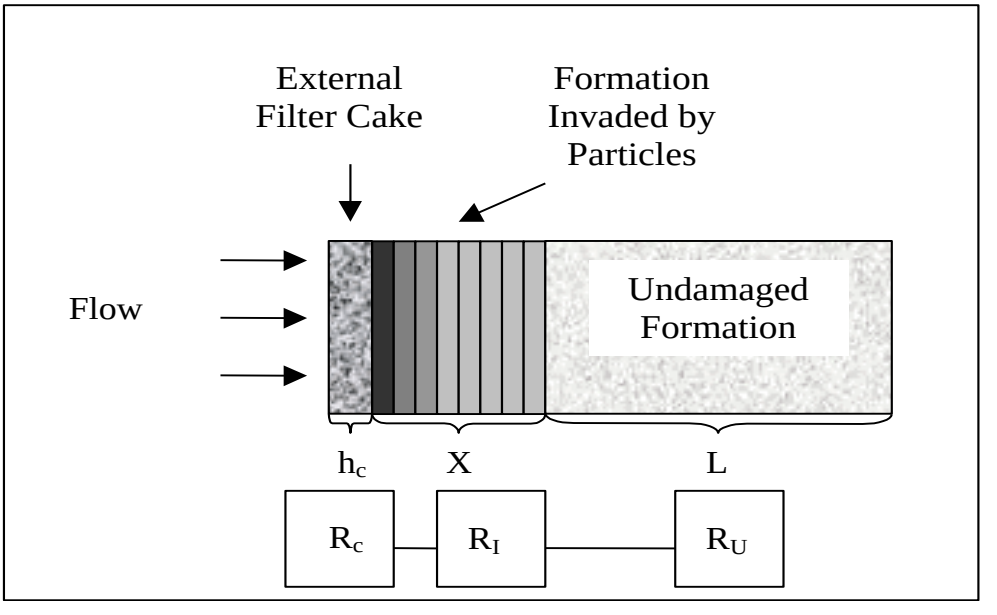

Figure 2.6: Flow resistance for linear geometry

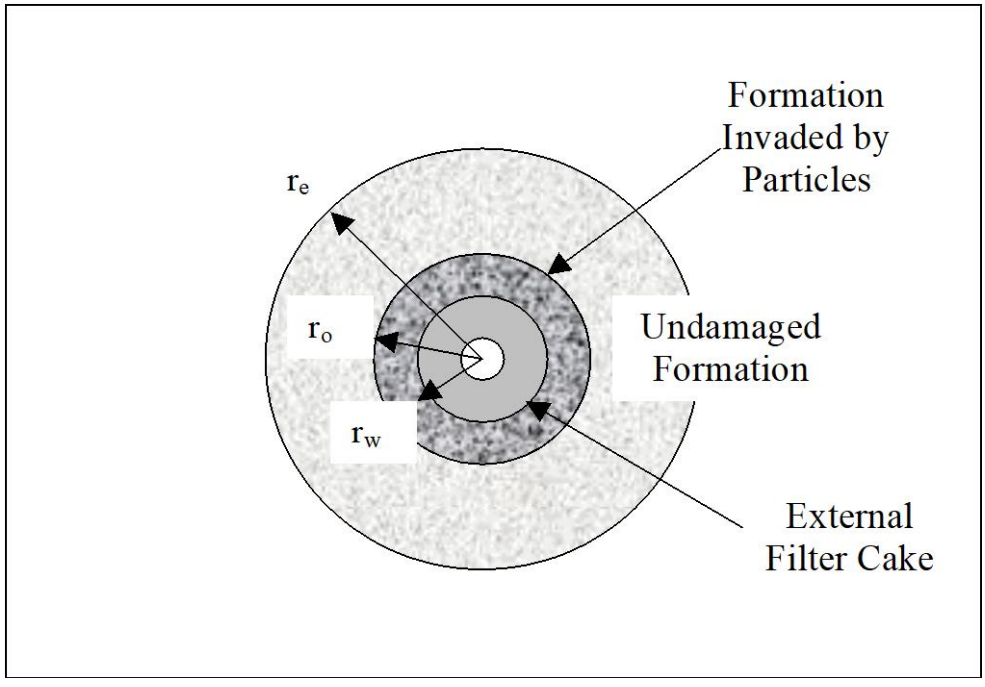

Figure 2.7: Flow resistance for radial geometry

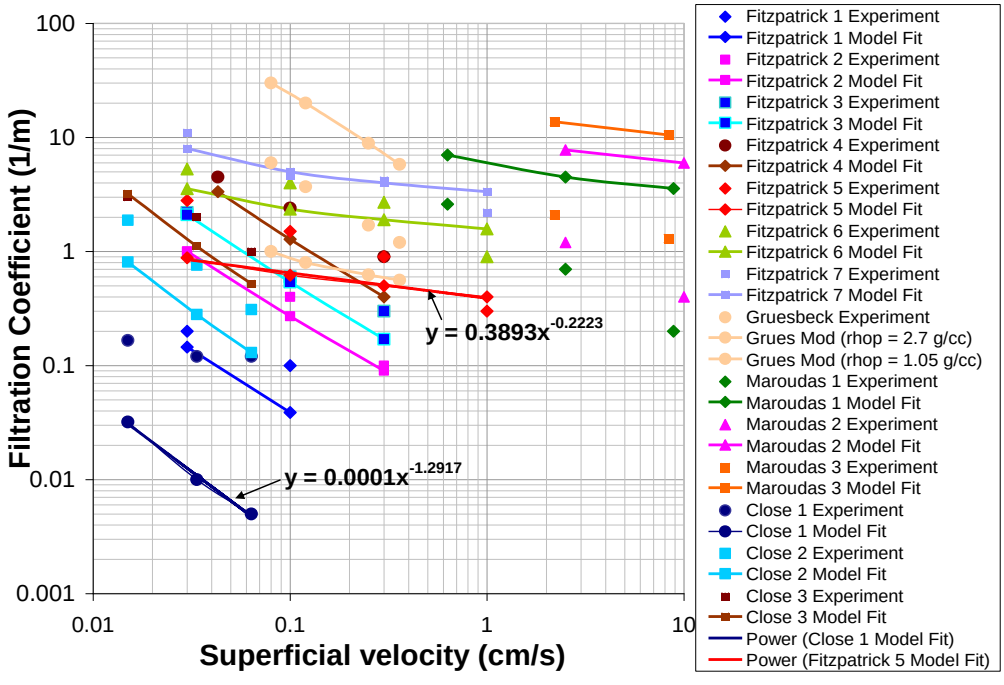

Figure 2.8: Comparison of filtration coefficient values as a function of Darcy velocity.

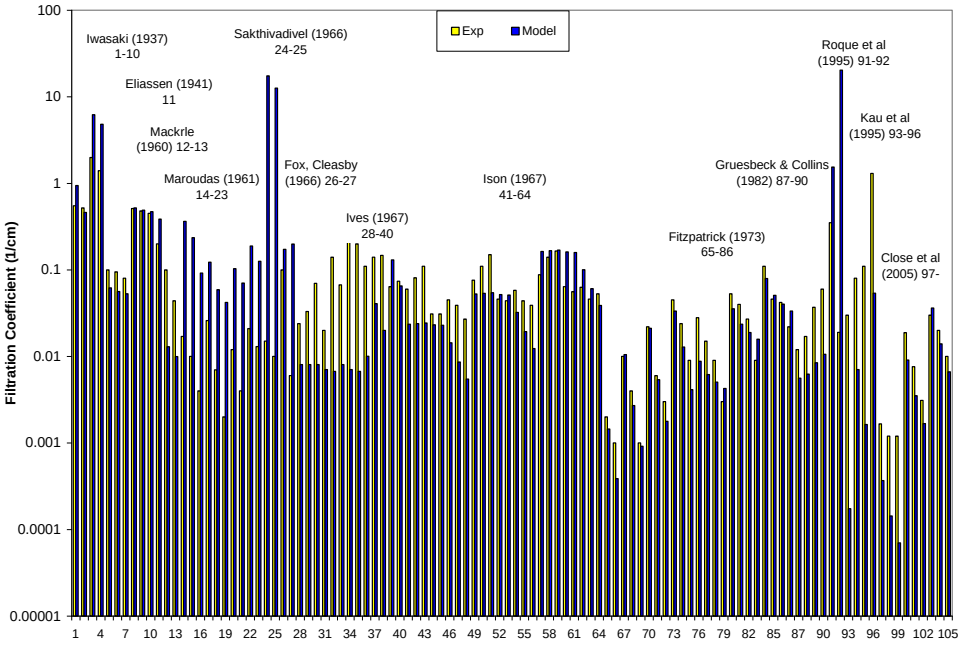

Figure 2.9: Comparison of filtration coefficient values (Experiments vs. Model).

Chapter 3: Two Dimensional Fracture Model

3.1 Introduction

Water injected into injection wells contains suspended particles, which plug the formation. This reduces the permeability in the near wellbore region and causes a decline in the injectivity. In order to maintain a constant flow rate the bottomhole pressure is increased. In field operations, injection may continue at a bottomhole pressure that is high enough to initiate and propagate hydraulic fractures. When the fracture pressure is exceeded fractures are initiated. Further, when the fracture face gets plugged during the course of injection, and the pressure exceeds the fracture propagation criteria, fractures are propagated.

The fluids injected into the formation are typically cooler than the formation. This causes a region of cooled rock to develop around injection wells. Formation rock in the cooled region contracts and this leads to a decrease in the horizontal earth stresses around the injection well. The reduction in horizontal stresses cause hydraulic fractures to be induced at pressures lower than the original fracturing pressures for the rock. This is termed 'thermally induced fracturing'. The increase in bottomhole pressure due to particle plugging and the reduction in fracture pressure from cold fluid injection lead to the initiation and propagation of hydraulic fractures in injection wells.

For unfractured injection wells, Sharma et al.[4] have shown that the injectivity depends strongly on water quality. In a case study for the offshore Gulf of Mexico water injection wells, data presented for five wells showed a rapid decline in injectivity. Such declines may be expected even for relatively clean waters for unfractured wells.

A model to predict the initiation and propagation of fractures in injection wells was proposed by Perkins and Gonzalez[5]. They recognized the importance of thermal stresses and particle plugging on fracture growth. They proposed estimating the skin resistance using an empirical model based on laboratory core flood experiments. Several other authors too highlight the importance of particle plugging on fracture initiation and propagation (Dikken and Niko[6], Detienne et. al.[7]). A model, which combines our current understanding of particle deposition and injection well fracturing to quantify the effect of these competing phenomena on injectivity, is developed in section 4.

3.2 Modeling Fracture Growth in Injection Wells

Formation injectivity decline may potentially lead to fracture initiation and growth if the injection rates are to be maintained. Fracture propagation can also be caused by temperature difference between the injected water and the reservoir. The fracture geometry and propagation rates depend on the formation properties, injection rate, water quality and the temperature difference.

The reservoir rock is in a state of stress, which results from the weight of the overburden and tectonic movements of the earth. To inject a fluid into the formation, a bottomhole pressure determined by the reservoir pressure, the injectivity and the flow rate is applied.

This fluid pressure exerts a radial force on the surrounding reservoir rock thereby deforming the rock. The radial expansion of the wellbore results in a tangential stress. If the fluid pressure is high enough, the tangential stress, which was previously compressive due to the overburden and earth movements, turns into a tensile stress. When this tensile stress exceeds the tensile strength of the rock, a fracture is initiated. In developing a model for fracture propagation in injection wells, it is assumed that the stress-strain relationship is linear. Because of this assumption of linear elasticity, this work applies only to consolidated rocks.

Injection well fracturing is affected by two factors – thermal and pore pressure effects. The state of stress of the rock is affected by changes in the temperature of the rock. Injecting cool fluids cools the formation rock and causes the matrix to contract, thereby reducing the compressive tangential stress. This will facilitate fracturing.

Pore fluids in the reservoir support a portion of the total applied stress. Due to the high wellbore pressures associated with injection, the pore pressure in the surrounding formation increases. Since the weight of the overburden is carried both by the grains and the fluid within the pores, an increased pore pressure reduces the effective stress on the rock matrix thereby inducing the rock matrix to expand. Since there is little room for expansion, internal compressive stresses are developed in the rock. This increased compressive stress tends to oppose the tensile tangential stress caused due to the increase in wellbore pressure. An increase in pore pressure therefore suppresses fracture propagation.

3.3 In-Situ Stresses

The state of stress in the sub-surface is a complex function of the depth and the regional tectonic activity. The vertical stress corresponds to the weight of the overburden. For a formation of depth *H*, the vertical stress σ_v is

$$\sigma_v = g\int_0^H \rho_o dH \tag{3.1}$$

where ρ_0 is the density of the overburden.

This can be calculated by integrating the density log. This weight is supported both by the rock matrix and the fluid in the pores. The effective stress (σ_v') on the rock matrix is given as

$$\sigma_v' = \sigma_v - \alpha_B p \tag{3.2}$$

where p is the pore pressure and α_B is Biot's poroelastic constant. This is approximately equal to 0.7-1 for most hydrocarbon reservoirs.

During diagenetic processes, the earth's movement in the horizontal direction is limited and hence stresses are assumed to be accommodated by strains only in the vertical direction. Treating the rock as an isotropic elastic body, the effective horizontal stress σ_H', can be obtained using Poisson's relationship (by equating the horizontal strains to zero)

$$\sigma_H' = \frac{\nu}{1-\nu}\sigma_v' \tag{3.3}$$

where ν is the Poisson's ratio. The total horizontal stress is obtained by adding the pore pressure to the effective horizontal stress.

$$\sigma_H = \frac{\nu}{1-\nu}(\sigma_v - p) + p \tag{3.4}$$

Because of tectonic activity, the stresses in the horizontal direction are usually unequal. The stress given by Eq. (3.4) is the minimum horizontal stress. The maximum horizontal stress is given by

$$\sigma_{H,\max} = \sigma_{H,\min} + \sigma_{tect} \tag{3.5}$$

where σ_{tect} is the tectonic stress.

The direction of fracture propagation is normal to the direction of the minimum stress. In our fracturing model, it is assumed that the minimum horizontal stress is smaller than the vertical stress and hence the fracture created is vertical and propagates in a direction normal to the minimum horizontal stress.

3.4 Effect of Thermoelastic Stresses

If the temperature of the injected fluid is different from the formation, a thermal front with a temperature different from the original rock temperature propagates from the injection well. In the presence of a two-winged vertical fracture during injection, the flow geometry would be elliptical. If a fluid of constant viscosity is injected, the outer boundary of the flood front at any time will approximately be an ellipse that is confocal with the fracture (Fig. 3.1). The outer boundary of the region of changed temperature is also elliptical and confocal with the fracture. This change in temperature causes the rock to contract or expand, thereby altering the stresses both in the region of changed temperature and in the surrounding rock, which is at the initial temperature.

The thermoelastic stresses in an infinitely tall cylinder of elliptical cross section are available from the literature. The thermoelastic stresses $\Delta\sigma_{1T,}$ perpendicular to the major axis of the ellipse are shown by Mindlin and Cooper[8] to be

$$\frac{(1-\nu)}{E\alpha\Delta T}\Delta\sigma_{1T} = \frac{(b_0/a_0)}{1+b_0/a_0} \tag{3.6}$$

where a_0 and b_0 are the major and minor axes of the thermal front ellipse and α is the linear coefficient of thermal expansion. The thermal stresses $\Delta\sigma_{2T,}$ parallel to the major axis of the ellipse are given as

$$\frac{(1-\nu)}{E\alpha\Delta T}\Delta\sigma_{2T} = \frac{1}{1+b_0/a_0} \tag{3.7}$$

Perkins and Gonzalez[5] have determined the thermoelastic stresses for a region of elliptical cross section and finite thickness by a numerical procedure. Empirical equations were then developed to give an explicit method to estimate the average stresses in an elliptically cooled region of any height.

The thermoelastic stresses $\Delta\sigma_{1T,}$ perpendicular to the major axis of the ellipse are expressed as

$$\frac{(1-\nu)}{E\alpha\Delta T}\Delta\sigma_{1T} = \frac{(b_0/a_0)}{1+b_0/a_0} +$$

$$\left(\frac{1}{1+b_0/a_0}\right)\left[1+0.5\left\{1.45\left(\frac{h}{2b_0}\right)^{0.9}+0.35\left(\frac{h}{2b_0}\right)^{2}\right\}\left\{1+\left(\frac{b_0}{a_0}\right)^{0.774}\right\}\right]^{-1} \tag{3.8}$$

where h is the thickness of the formation.

The thermoelastic stresses $\Delta\sigma_{2T,}$ parallel to the major axis of the ellipse are expressed as

$$\frac{(1-\nu)}{E\alpha\Delta T}\Delta\sigma_{2T} = \frac{1}{1+b_0/a_0} +$$

$$\left(\frac{b_0/a_0}{1+b_0/a_0}\right)\left[1+0.5\left\{1.45\left(\frac{h}{2b_0}\right)^{0.9}+0.35\left(\frac{h}{2b_0}\right)^{2}\right\}\left\{1+\left(\frac{b_0}{a_0}\right)^{0.774}\right\}\right]^{-1} \tag{3.9}$$

3.5 Determination of Temperature and Saturation Profiles

When a cooler fluid is injected into a formation, the fluid cools the formation surrounding the injection well. The dimensions of this cooled region depend on the thermal properties of the injected fluids, the reservoir fluids and the mineral grains of the reservoir rock. The temperature distribution can be calculated using simple energy balance equations.

In the presence of a fracture, the outer boundary of the region of changed temperature is elliptical and confocal with the fracture. The true temperature profile can be obtained using numerical methods. In this work, the temperature profile is approximated as a step profile (Fig 3.2). The waterflood displacement is assumed to be piston like. This leads to a step

profile for the water saturation, where oil is at the residual oil saturation behind the flood front and water is at the initial water saturation ahead of the flood (Fig. 3.3). The heat conduction to the overlying and the underlying formations is neglected.

For the system under consideration, Marx and Langenheim[9] (1959) have shown that the volume of the cooled region V_c, can be determined by an energy balance.

$$V_c = \frac{\rho_w C_w W_i}{\rho_{gr} C_{gr}(1-\phi) + \rho_w C_w \phi(1-S_{or}) + \rho_o C_o \phi S_{or}} \tag{3.10}$$

where V_c is the volume of the cooled zone, ρ_w, ρ_o and ρ_{gr} are the densities of water, oil and mineral grains, C_w, C_o and C_{gr} are the specific heats of the water, oil and mineral grains, ϕ is the porosity and S_{or} is the residual oil saturation.

The dimensions of the waterflood ellipse can be obtained by solving the equations for elliptical geometry. Let L_f be the half-length of the fracture. The major and minor axes of the thermal front ellipse a_0 and b_0 (Fig. 3.1) can be expressed in cylindrical coordinates as

$$a_0 = L_f \cosh\xi_0 \tag{3.11}$$

$$b_0 = L_f \sinh\xi_0 \tag{3.12}$$

The volume of the cooled zone can be expressed as

$$V_c = \pi {L_f}^2 h \sinh\xi_0 \cosh\xi_0 = \frac{\pi {L_f}^2 h}{4}\left\{\exp(2\xi_0) - \exp(2\xi_0)^{-1}\right\} \tag{3.13}$$

Let $X_0 = exp\,(2\xi_0)$ (3.14)

Then Eq. (3.13) can be expressed as, $${X_0}^2 - \frac{4V_c}{\pi {L_f}^2 h} X_0 - 1 = 0 \tag{3.15}$$

Solving for X_0 $$X_0 = \frac{2V_c}{\pi {L_f}^2 h} + \frac{1}{2}\sqrt{\left(\frac{4V_c}{\pi {L_f}^2 h}\right)^2 + 4} \tag{3.16}$$

From Eq. (3.11) and Eq. (3.14), the major axis of the thermal front ellipse can be expressed as

$$a_0 = \frac{L_f}{2}\left(\sqrt{X_0} + \frac{1}{\sqrt{X_0}}\right) \tag{3.17}$$

From Eq. (3.12) and Eq. (3.14), the minor axis of the thermal front ellipse can be expressed as

$$b_0 = \frac{L_f}{2}\left(\sqrt{X_0} - \frac{1}{\sqrt{X_0}}\right) \tag{3.18}$$

If a fluid of constant viscosity is injected, the outer boundary of the flood front at any time would approximately be an ellipse that is confocal with the fracture. The volume of the waterflooded region V_{wf}, is given by

$$V_{wf} = \frac{W_i}{\phi(1 - S_{or} - S_{wi})} \tag{3.19}$$

where S_{wi} is the initial water saturation.

Let L_f be the half-length of the fracture. The major and minor axes of the thermal front ellipse a_1 and b_1 (Fig. 1) can be written as

$$a_1 = L_f \cosh\xi_1 \tag{3.20}$$

$$b_1 = L_f \sinh\xi_1 \tag{3.21}$$

As discussed above, the major and minor axes can be solved for and be expressed as,

$$a_1 = \frac{L_f}{2}\left(\sqrt{X_1} + \frac{1}{\sqrt{X_1}}\right) \tag{3.22}$$

$$b_1 = \frac{L_f}{2}\left(\sqrt{X_1} - \frac{1}{\sqrt{X_1}}\right) \tag{3.23}$$

where

$$X_1 = \frac{2V_{wf}}{\pi L_f{}^2 h} + \frac{1}{2}\sqrt{\left(\frac{4V_{wf}}{\pi L_f{}^2 h}\right)^2 + 4} \tag{3.24}$$

3.6 Effect of Pore Pressure

The weight of the overburden is carried both by the grains and the fluid within the pores. A change in pore pressure would induce a change in the state of stress of the rock. Lubinski[10] has shown that for a non-deformable pore structure, i.e. assuming the porosity and permeability of the rock to be independent of the pressure, the change in stresses due to thermal phenomena are analogous to those due to pore pressure effects. The linear

coefficient of pore pressure expansion β_p, is analogous to the linear coefficient of thermal expansion, α.

$$\beta_p = \frac{1-2\nu}{E} - \frac{c_{gr}}{3} \qquad (3.25)$$

The stresses induced by a pore pressure change Δp, can be computed in a manner similar to the computation of stresses induced due to a change in temperature ΔT, with β_p replacing α and ΔP replacing ΔT.

Hence from Eq. (3.8), the poroelastic stresses $\Delta\sigma_{1p,}$ perpendicular to the major axes of the ellipse are expressed as

$$\frac{(1-\nu)}{E\beta_p \Delta p}\Delta\sigma_{1p} = \frac{(b_0/a_0)}{1+b_0/a_0} +$$

$$\left(\frac{1}{1+b_0/a_0}\right)\left[1+0.5\left\{1.45\left(\frac{h}{2b_0}\right)^{0.9}+0.35\left(\frac{h}{2b_0}\right)^{2}\right\}\left\{1+\left(\frac{b_0}{a_0}\right)^{0.774}\right\}\right]^{-1} \qquad (3.26)$$

Similarly, the poroelastic stresses $\Delta\sigma_{2p,}$ parallel to the major axes of the ellipse are expressed as

$$\frac{(1-\nu)}{E\beta_p \Delta p}\Delta\sigma_{2p} = \frac{1}{1+b_0/a_0} +$$

$$\left(\frac{b_0/a_0}{1+b_0/a_0}\right)\left[1+0.5\left\{1.45\left(\frac{h}{2b_0}\right)^{0.9}+0.35\left(\frac{h}{2b_0}\right)^{2}\right\}\left\{1+\left(\frac{b_0}{a_0}\right)^{0.774}\right\}\right]^{-1} \qquad (3.27)$$

3.7 Fracture Propagation

Fracture propagation is of immense importance for injection wells. Fracture propagation provides the potential for higher injection rates and relaxed water quality specifications. However, uncontrolled fracture propagation may also induce problems, such as poor vertical sweep due to fracturing through barriers, and early water breakthrough. The successful application of tertiary oil recovery processes may also be adversely affected by the presence of these fractures.

In this work, the fracture is assumed to be confined between the overlying and underlying formations. The fracture is initially assumed to grow as an enlarging penny shaped crack (Fig. 3.5) until it is confined above and below. After the confinement, it starts extending laterally (Fig 3.6). The leading edge of the fracture is assumed to be circular.

The strains associated with a hydraulic fracture are relatively small and hence the formation can be assumed to be deformed in a linearly elastic manner. However, for a

sharp edged crack, the linear theory predicts infinitely large values of stresses and strains at the fracture tip. Such stresses cannot be sustained in a real material. To work around this, it has been proposed that an inelastic region exists near the fracture tip. The inelastic behavior would relieve the large induced stresses and would result in absorption of substantial surface energy upon extension of fractures.

The energy balance approach for fracture propagation is used in this work. In this approach, the fracture extension pressure is the pressure that will make the work done during the fracture extension equal to the total energy accounted for in the fracture system. Perkins and Krech[11] proposed an approximate energy balance equation including the inelastic tip behavior. They have shown that when the earth stresses are large compared to the rock tensile strength, the energy balance reduces to

$$p = s + \sqrt{\frac{\pi UE}{2(1-\nu^2)r_f}} \tag{3.28}$$

where p is the average pressure in the circular area near the extending ends of the fracture, s is the earth stress perpendicular to the fracture plane, U is the specific surface energy and r_f is the radius of the extending end of the fracture. The direction of fracture propagation would be normal to the direction of the minimum stress. Hence s equals $\sigma_{H,min}$ and the fracture propagation pressure is given by,

$$p = \sigma_{H,\min} + \sqrt{\frac{\pi UE}{2(1-\nu^2)r_f}} \tag{3.29}$$

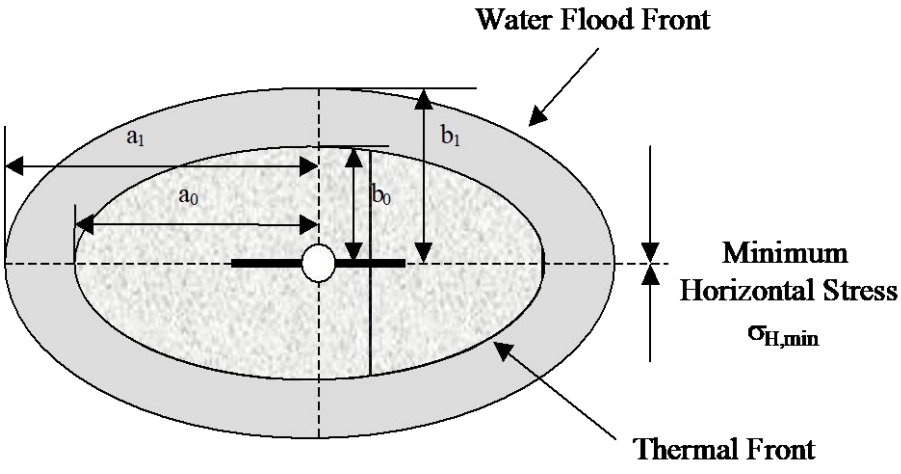

Figure 3.1: Elliptical flow geometry in the existence of a fracture perpendicular to the direction of minimum horizontal stress

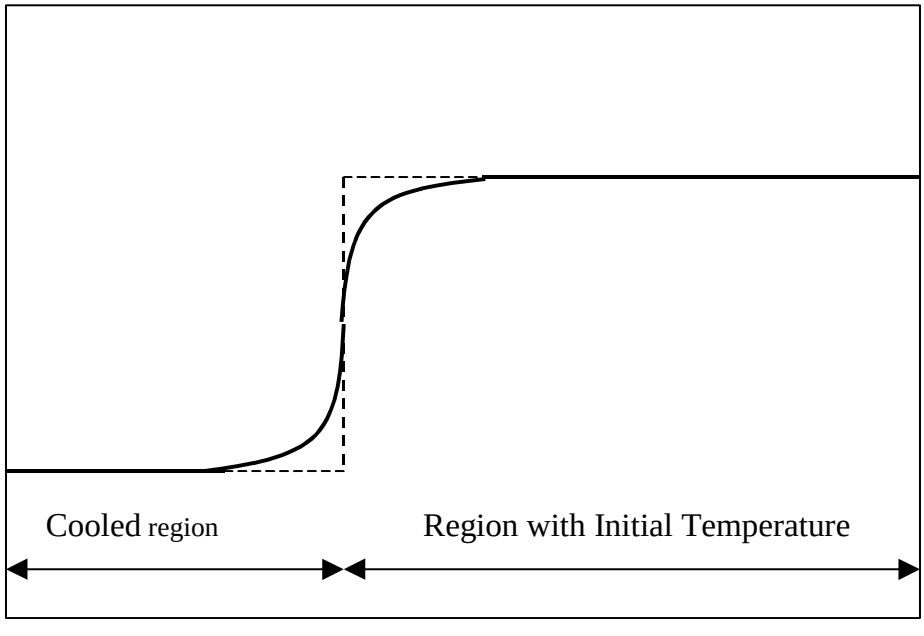

Figure 3.2: Approximation of the temperature profile by a step profile

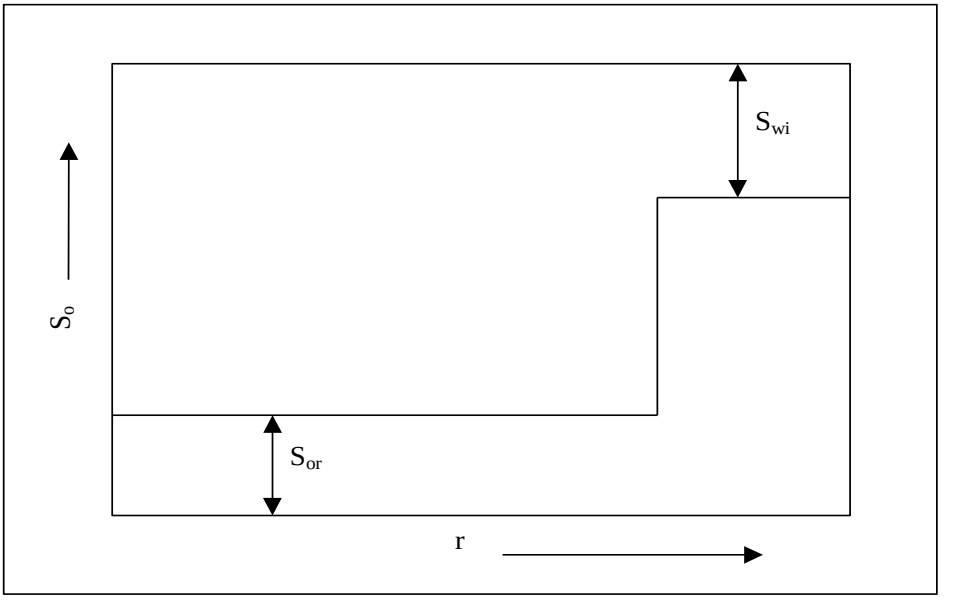

Figure 3.3: Approximation of the saturation profile by a step profile

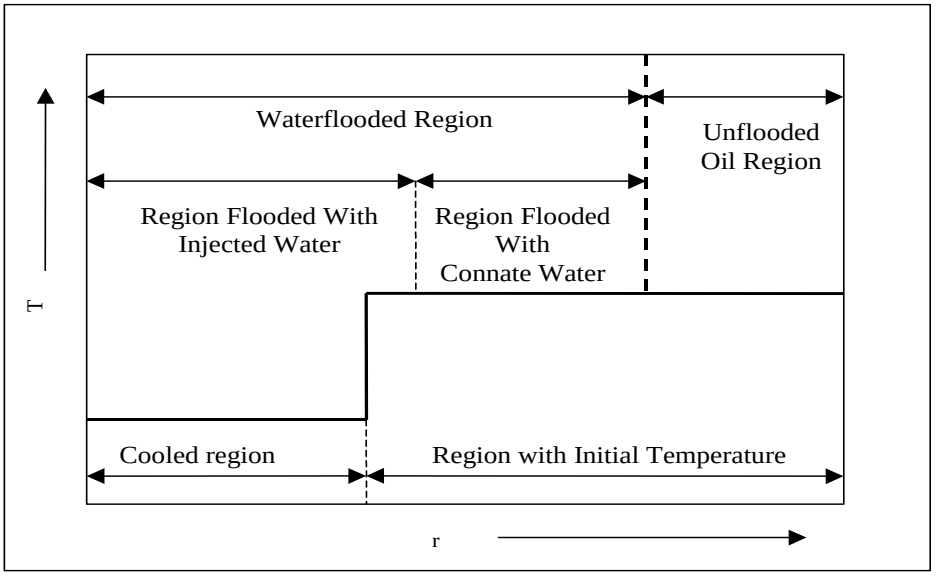

Figure 3.4: Simplified view of saturation and temperature distributions

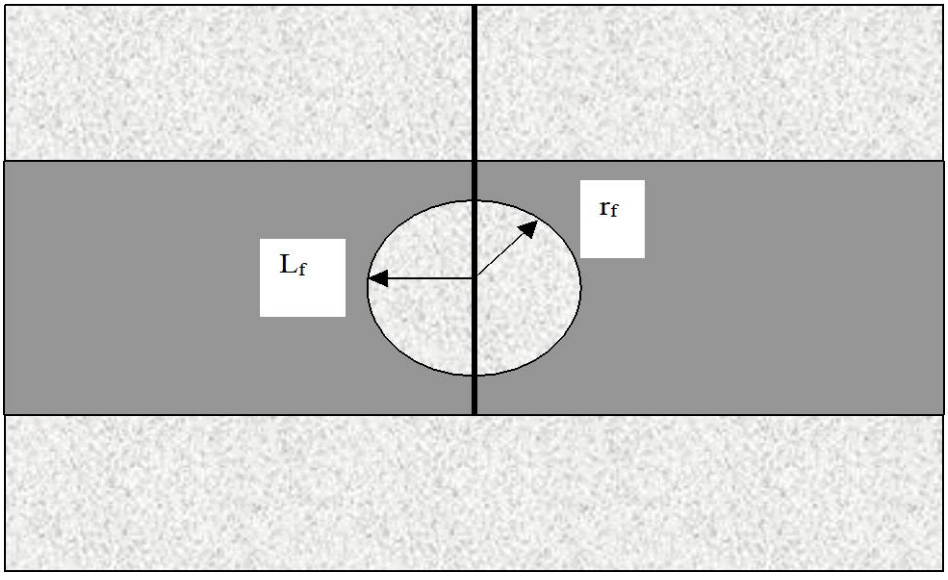

Figure 3.5: View of the fracture shortly after initiation

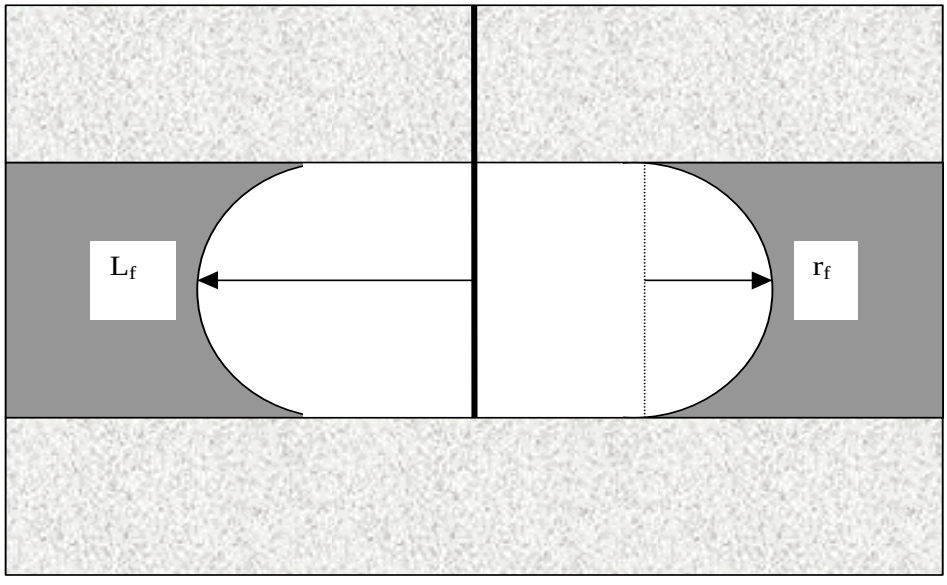

Figure 3.6: View of the fracture after confinement

Chapter 4: Development of 2-D Fracture Simulator

4.1 Introduction

A model to predict the growth of injection well fractures due to the combined influence of injection pressure, changes in pore pressure, thermal stresses and formation damage due to particle plugging is presented. Fracture growth and fracture face plugging are treated as dynamically coupled phenomena. The models and equations outlined in sections 3 and 4 have been implemented in a user-friendly simulator, WID 7.2. This extends the previous work by Wennberg (UT WID 3.1), which dealt with predicting the injectivity decline due to particle plugging for unfractured wells. The current version can predict the growth of injection well fractures as well. This section provides an overview of the development of the simulator.

Deposition of particles in the near wellbore region has an important influence on fracturing of water injection wells. It is well established that maintaining injectivity requires minimizing formation damage in the near wellbore region. Deposition of injected solids and oil droplets lead to a decline in well injectivity. One important outcome is an increased bottomhole injection pressure required to maintain a given injection rate. In field operations, injection may continue at a bottomhole pressure that is high enough to initiate and propagate hydraulic fractures. When the fracture pressure is exceeded fractures are initiated. Further, injection of water colder than the reservoir temperature induces thermal stresses which facilitate fracture growth by reducing fracturing pressure. As the injection continues, the face of the fracture could get plugged by the suspended particles, thus impairing the flow. This results in an increase in the pressure in the fracture, which causes the fracture to grow further. Thus particle plugging and fracture growth are two mutually sustaining processes, which together dictate the pressure behavior and injectivity of water injection wells.

4.2 Model Features

The object of the model is to predict the injectivity decline and growth of injection well fractures due to particle plugging, thermal and pore pressure effects. The following assumptions are made in developing UT WID model.

1. The reservoir is homogeneous and isotropic.
2. The vertical stress exceeds the horizontal stresses and therefore the fractures created are vertical.
3. There is a large difference between the minimum and maximum horizontal stresses which lead to fracture propagation as a single two-winged fracture (Figure 3.6).
4. The fracture is contained and extends vertically through the entire thickness of the reservoir.
5. Formation damage due to particle plugging is uniform over the entire fracture face.

6. The leak-off is uniform over the entire fracture face.
7. The leak-off is one dimensional and perpendicular to the fracture face.
8. The filtration coefficient is constant and can be obtained either from core flow experiments or from the empirical relations built into the model.
9. The temperature front is approximated as a step profile and heat conduction to overlying and underlying formations is neglected.
10. The injection rate is constant.
11. The reservoir fluid displacement is piston like, with step profiles having residual reservoir fluid (usually oil) saturation behind the water flood front and initial water saturation ahead of the water flood front.

4.3 Method of Solution for Fracture Growth Model

The wellbore bottomhole injection pressure with an injection induced fracture is calculated using the following equation.

$$P_i = P_r + \Delta P_1 + \Delta P_2 + \Delta P_3 + \Delta P_4 + \Delta P_s + \Delta P_f + \Delta P_p$$

where Pr is the pressure at the far-field drainage boundary, ΔP1, ΔP2, ΔP3 and ΔP4 are the pressure drops across regions discussed in the next section, ΔPs is the additional pressure drop due to particle plugging and cake build up, ΔPf is the pressure drop along the fracture from the wellbore to the tip of the fracture, and ΔPp is the pressure drop across the perforations..

The pressure at the fracture tip, Ptip is calculated as followed:

$$P_{tip} = P_i - \Delta P_f - \Delta P_p$$

Therefore, $P_{tip} = P_r + \Delta P_1 + \Delta P_2 + \Delta P_3 + \Delta P_4 + \Delta P_s$

Note: The model presented above is an improvement over the Perkins and Gonzalez model which uses the average pressure in the fracture. Their equation was as followed:

$$P_{tip} = P_r + \Delta P_1 + \Delta P_2 + \Delta P_3 + \Delta P_s - (2/3)\Delta P_f \qquad *$$

Note in Perkins and Gonzalez SPE paper the equation is presented in a different form than *; and accounts only for water injection (not polymer injection, which resulted in only three regions with ΔP1, ΔP2, and ΔP3). The Perkins and Gonzalez model is a good approximation for fractures with high conductivity, i.e. for small ΔPf . However, if ΔPf becomes large relative to the other pressure drop terms, Ptip may become smaller than Pr (drainage boundary pressure). The pressure at the fracture tip should clearly be more than the drainage boundary pressure. This discrepancy in the Perkins and Gonzalez model arises because the fracture is represented as an ellipse with a pressure equal to the average pressure in the fracture. This is a good approximation if the pressure drop along the fracture is small. Therefore, to avoid such cases, equation * was modified to equation (3.11). For most cases a large ΔPf is calculated as the fracture is plugged by solids.

4.4 Fluid Flow Equations

In the presence of a two-winged vertical fracture or a cased-hole frac pack during injection, the flow geometry is elliptical. If a fluid of constant viscosity is injected, the outer boundary of the flood front at any time will approximately be an ellipse that is confocal with the fracture (Fig. 4.1).

At any given time there are four distinct regions - the region ahead of the flood front where oil is the mobile phase, the region behind the flood front where the formation may have the connate water displaced from the region behind and is at its original temperature, the region behind the connate water front with injected fluid front at reservoir temperature and the region with the injected fluid at injected fluid temperature. Each of these regions is elliptical and confocal with the fracture and has relevant relative permeabilities and viscosities. The pressure drops across each of these regions can be obtained using equations for flow between confocal elliptical regions.

The pressure drop between the far-field drainage boundary and the waterflood front is given as

$$\Delta P_1 = \frac{q\mu_o}{2\pi k k_{ro} h} \ln\left(\frac{2r_e}{a_2 + b_2}\right) \tag{4.1}$$

Where, a_2 and b_2 are the major and minor axes of the connate water flood front, μo is the viscosity of oil and k_{ro} is the end-point relative permeability to oil and r_e is the far-field drainage radius. The pressure drop between the connate water front and the injected fluid front is given by

$$\Delta P_2 = \frac{q\mu_{wr}}{2\pi k k_{rw} h} \ln\left(\frac{a_2 + b_2}{a_1 + b_1}\right) \tag{4.2}$$

Where k_{rw} is the end-point relative permeability to water and μ_{wr} is the viscosity of water at the initial reservoir temperature, a_1 and b_1 are the major and minor axes of the injected fluid front. The pressure drop between the injected fluid front and the thermal front is given as

$$\Delta P_3 = \frac{q\mu_{wi}}{2\pi k k_{rw} h} \ln\left(\frac{a_1 + b_1}{a_0 + b_0}\right)$$

Where k_{rw} is the end-point relative permeability to water and μ_{wi} is the viscosity of water at the injected water temperature, a_0 and b_0 are the major and minor axes of the thermal front. Note, it is assumed that the injected fluid is water, in case of injected fluid being a polymer solution, ΔP_3 and ΔP_4 will be different from what is presented. If you need those equations please contact us. The pressure drop between the thermal front and the fracture assuming water being the injected fluid is given as

$$\Delta P_4 = \frac{q\mu_{wi}}{2\pi k k_{rw} h} \ln\left(\frac{a_o + b_o}{L_{fp}}\right) \quad (4.3)$$

Where k_{rw} is again the end-point relative permeability to water, μ_{wi} is the viscosity of water at the injection water temperature and L_{fp} is the cased-hole frac pack half-length or the fracture length.

The pressure drop due to solids in the injected fluid is calculated as followed:

$$\Delta P_s = qR_s \quad (4.4)$$

Where R_s is the flow resistance due to solids (both internal and external). The pressure drop due to the perforations is calculated as followed (Perkins and Gonzalez, 1985):

$$\Delta P_p = 0.8338\rho v_p^{\ 2} \quad (4.5)$$

Where ρ is the injected fluid density and v_p is the velocity of the injected fluid through the perforations.

4.5 Permeability Decline for a Fracture of Fixed Length

When fluids containing suspended particles are injected into a fracture, the particles first invade the formation adjacent to the fracture faces and reduce the permeability. When the transition time is reached, an external cake starts to form on the fracture face. A model to predict permeability decline for various geometries has been presented in Section 2. This model is applied to predict the permeability decline due to fracture face plugging.

For filtration purposes, we treat the flow from the fracture as linear. This is because most of the damage occurs in a narrow region close to the fracture face (Fig. 4.2). In this region, the flow can be safely assumed to be one dimensional, perpendicular to the fracture face. Because of this linear flow assumption, the filtration equations for linear geometry determine the permeability decline. Plugging on each face of the fracture is modeled as the plugging of a corresponding series of linear cores whose inlet is perpendicular to the fracture face (Fig. 4.3).

Let c_0 be the concentration of suspended particles in the injection water. Let the fracture half-length be L_f. The filtration coefficient (λ) is assumed to be constant. The length of the damaged zone (L_D) or the distance from the fracture face which has experienced a change in permeability due to particle plugging is set equal to 10 to 20 times $1/\lambda$. Beyond this distance, the effects of particle plugging are minimal. This damaged zone is broken up into a series of N linear cores of length Δx connected in series.

After injection for time t, the concentration of deposited particles, σ at a distance x from the fracture face is given by Eq. (2.13) as:

$$\sigma(x,t) = \lambda u c_0 t \exp\{-\lambda x) \quad (4.7)$$

where u is the average velocity. Assuming that the specific deposit remains constant over the length Δx of each core, the specific deposit for the ith core can be written as:

$$\sigma(i,t) = \lambda u c_0 t \exp\{-\lambda(i-1)\Delta x) \tag{4.8}$$

The corresponding reduction in porosity for each core can be written as:

$$\phi(i,t) = \phi_0 - \sigma(i,t) \tag{4.9}$$

where ϕ_0 is the initial porosity of the undamaged formation.

The corresponding reduction in permeability can be written as:

$$k(i,t)/k_0 = k_{dp} k_{ds} k_{dt} \tag{4.10}$$

where k_0 is the initial permeability of the formation,

$$k_{dp} = \frac{\phi(i,t)^3 (1-\phi_0)^2}{\phi_0{}^3 (1-\phi(i,t))^2} \tag{4.11}$$

$$k_{ds} = \left(\frac{1+\sigma(i,t)/(1-\phi_0)}{1+(d_g/d_p)\sigma(i,t)/(1-\phi_0)} \right)^2 \tag{4.12}$$

where d_p is the diameter of injected particles and d_g is the diameter of the formation grains and

$$k_{dt} = \frac{1}{1+\beta} \tag{4.13}$$

where β is the damage factor whose default value is 0.

The flow resistance due to the damage (permeability reduction of the reservoir near the f racture faces) at any time is calculated by:

$$R_I(t) = \frac{\mu_{wi}}{A_f} \sum_{i=1}^{N} \frac{\Delta x}{k(i,t)} \tag{4.14}$$

where A_f is the area of the fracture faces. The fracture has four faces. Therefore, the total area of the fracture faces is calculated by:

$$A_f = 4 L_f h_f \tag{4.15}$$

where h_f is the height of the fracture and L_f is the half length of the fracture. The initial total flow resistance of the reservoir up to the damage zone is given by the following equation

$$R_I(0) = \frac{\mu_{wi} L_d}{A_f k} \tag{4.16}$$

After the transition time *t**, an external filter cake starts to form. The following two scenarios are possible:

- One possibility is that due to high fluid shear forces, all the injected particles are transported to the fracture and the tip starts to fill up, i.e. the external filter cake is formed at the tip and is non-uniform across the fracture face.

- The other possibility is that fluid shear stresses have little influence on the external filter cake build up and particles deposit uniformly along the length of the fracture. After the fracture is almost filled up, there could be worm-holing within the fracture.

We consider the second possibility assuming a uniform deposition of particles over the fracture face for calculating the flow resistance due to external filter cake. This is an approximation of the more realistic phenomenon, which is most likely to yield a non-uniform distribution of filter cake along the fracture face. This simplification also allows us to preserve the assumption of a uniform line source in an elliptical flow domain, considered in UT WID where the flow equations are solved for elliptic geometry, treating each of the ellipses as constant pressure surfaces. This assumption is only valid if both the external filter cake is uniform and the internal damage is uniform across the fracture face. The flow resistance due to the external cake is calculated as:

$$R_c(t) = \frac{\mu_{wi} h_c(t)}{A_f k_c} \tag{4.17}$$

where k_c is the external filter cake permeability and $h_c(t)$ is the thickness of the external filter cake at time *t* which is uniform over the entire fracture face.

The total flow resistance at any given instant would be the sum of flow resistances due to internal and external filter cakes and is given as:

$$R_{tot}(t) = R_I(t) - R_I(0) + R_c(t) \tag{4.18}$$

The pressure drop because of formation damage ΔP_s caused by particle plugging in the formation and any cake build up in the fracture is given as followed:

$$\Delta P_s = q \mu_{wi} R_{tot}(t) \tag{4.19}$$

where q is the injection rate and μ_{wi} is the viscosity of the injected water.

4.6 Permeability Reduction for a Growing Fracture

Deposition of particles in the near wellbore region has an important influence on fracturing of water injection wells. Deposition of injected solids and oil droplets lead to a decline in well injectivity. Hence an increased bottomhole injection pressure is required to maintain a given injection rate. In field operations, injection may continue at a bottomhole pressure that is high enough to initiate and propagate hydraulic fractures. When the fractures propagate, the fracture length is changing with time. Hence the equations developed in the previous sections need to be modified to account for the growing fractures.

When water is injected through a fracture, the water leaks off from the fracture faces. The suspended particles plug the formation adjacent to the fracture face and reduce the permeability. When the pressure exceeds the propagation pressure, the fracture propagates. Injection well fractures grow very slowly. The rate of fracture growth could vary from a few inches per day to a few feet per day. The newly exposed fracture at the tip has a higher permeability than the rest of the fracture face because it has not been invaded by the particles (Fig. 4.4). So a large proportion of the fluid leaks off from the newly exposed fracture face. The higher fluid leak off at the tip would mean a higher rate of deposition of particles and a higher rate of permeability decline. Hence, very quickly the permeability at the fracture tip would approach the permeability over the rest of the fracture face and the permeability over the entire fracture face becomes uniform. This phenomenon could be represented in a different way. It is similar to what would be observed had all the injection occurred through the fracture at its current half-length.

We model the dynamic process of fracture growth and filtration as a pseudo-static process. At any given instance, the fracture has a half-length determined by the fracture mechanics. At this half-length, we compute the particle plugging and permeability decline assuming that the fracture has been fixed at that given half-length since the instant of initiation of injection. Thus, it is assumed that all flow from the time of initiation to the present has entered the fracture at its current geometry. In modeling the filtration as a pseudo-static process, it is important to maintain the mass balance on particles.

4.7 Fracture Plugging Model

It has been discussed in the earlier sections that when fluids containing suspended solids are injected into a formation, the particles first enter the formation and form an internal filter cake. When a critical porosity is reached and no more particles can enter the formation, an external filter cake begins to form. Based on the filtration model, the length of the fracture can be modeled as consisted of four different regions (Fig 4.5). Region 1 is the portion of the formation ahead of the fracture tip. This region has not been contacted by the fracture and therefore it has not been invaded by the particles. Region 2 is the region immediately behind the fracture tip. This region has just been contacted by the fracture and is relatively less damaged. Particles are still invading the formation and forming an internal filter cake. Region 3 is the region behind the fracture tip where the internal filtration has stopped and an external cake is still forming. Region 4 is the region where an equilibrium cake thickness has been reached.

In an injection well fracture, particle deposition and fracture propagation (exposing of undamaged formation) are two mutually dependent processes. The suspended solids in the injected fluid are constantly plugging the formation and thus impairing leak-off through the fracture faces. The damage results in increased pressure at the fracture face to sustain

injection rates. When the pressure at the tip exceeds the propagation pressure, the fracture propagates exposing undamaged formation. This increases the area available for leak-off. Moreover, the newly exposed formation is undamaged initially and thereby allows better fluid leakoff. This increased leakoff causes the pressure at the tip to fall below the fracture propagation pressure. The fracture stops propagating till the newly exposed region is plugged by the particles and the pressure at the tip again exceeds the fracturing pressure. There exists a delicate balance between fracture propagation and fracture tip plugging.

It has been observed in the large block injectivity tests[1] that in a propagating fracture, most of the leak off occurs at the fracture tip and injected particles are transported and deposited at the tip. The higher fluid leak off at the tip would mean a higher rate of deposition of particles and a higher rate of permeability decline. Sometimes the internal filter cake is not effective at controlling leakoff. In such cases, once the internal filtration is complete, an external filter cake begins to form. If the external cake too is not impermeable enough to effectively control leakoff, the growing external filter cake slowly fills the fracture as the injection continues. Based on these observations, the fracture-plugging model presented above can be simplified. Since the formation gets damaged very rapidly at the tip, the permeability at the fracture tip would approach the permeability over the rest of the fracture face rapidly and the permeability over the entire fracture face becomes uniform. Also since most of the leak off occurs near the fracture tip, the external filter cake growth too is most pronounced at the tip. The growing external filter cake can fill the narrow tip. Hence the fracture-plugging model simplifies to a two zone model (figure 4.6). Zone 2 is the region behind the tip, which is filled with external filter cake. Figure 4.7a shows Zone 2 where relatively larger portions of the fracture are filled by external cake and a few flow channels exist. Figure 4.7b shows Zone 1 where the filter cake thickness is small and the fracture is open to flow (unfilled by external cake).

4.8 Pressure Drop Along the Fracture

Using the PKN model the average width of a fracture can be expressed as

$$\overline{W}(y,t) = 1/h \int_{-h/2}^{h/2} \frac{1-\nu}{G} \sqrt{h^2 - 4z^2}.\Delta P(y,t) \qquad (4.20)$$

where h is the height of the fracture and ΔP is the excess pressure.

The width of the fracture open to flow, W_o is given by

$$W_o = \overline{W}(y,t) - 2h_c \qquad (4.21)$$

where h_c is the thickness of the external filter cake.

The flow resistance and corresponding pressure drop along the length of the fracture is given in the table below:

Table 1: Flow resistance for flow in the fracture.

When no filter cake along the face of the fracture, i.e. $h_c = 0$:

$$R_{fi} = \left[\frac{16}{3\pi} \frac{(2n_p+1)^{n_p} k_p L_f E^{2n_p+1}}{{n_p}^{n_p} 2^{2n_p-1} (1-\nu^2)^{2n_p+1} {h_f}^{3n_p+1}} \right]^{\frac{1}{2n_p+2}} q^{-\left[\frac{n_p+2}{2n_p+2}\right]};$$

$$w_{fi} = \frac{2(1-\upsilon^2)h_f}{E} q * R_{fi}$$

$$\Delta P_f = \frac{w_{fi} E}{2(1-\upsilon^2)h_f}$$

For $h_c > 0$: $w_f = w_{fi} + 2h_c$; $\Delta P_f = \frac{w_f E}{2(1-\upsilon^2)h_f}$

4.9 Method of Solution for Determining Fracture Length

The model predicts the injectivity and fracture growth by integrating a fracture propagation model with a particle plugging model coupled together. The following sections provide a detailed description of the method of solution.

i. A fracture length is assumed.

ii. The dimensions of the thermal and water flood ellipses are calculated from the cumulative water volume injected.

iii. The change in minimum horizontal stress because of thermal and pore pressure effects is calculated.

$$\sigma'_{H\min} = \sigma_{H\min} + \Delta\sigma_{1T} + \Delta\sigma_{1P} \tag{4.26}$$

iv. The fluid flow equations are solved and the pressure at the outer boundary of the damage zone is given by

$$P_D = P_r + \Delta P_1 + \Delta P_2 + \Delta P + \Delta P_4 \tag{4.27}$$

where P_r is the pressure at the far-field drainage boundary, ΔP_1, ΔP_2, ΔP_3 and ΔP_4 are the pressure drops across the four regions shown in figure 4.1 and discussed in the previous section.

v. The Ptip is calculated by the fracture propagation equation and the reservoir flow equations. The fracture length is changed until Ptip is found equal in both the systems.

The model equations outlined have been implemented in WID (Well Injectivity Decline Simulator) as a user-friendly simulator running on a Windows-based operating system. The injectivity and fracture lengths are calculated in WID using a user-specified initial time step and repeating the algorithm until the maximum time of injection is reached.

4.10 Examples and Discussion

WID simulations were conducted using a perforated injection well injecting water into a 25m thick sandstone formation bounded by impermeable layers at the top and bottom. The injection and formation parameters are chosen to represent a typical water injection operation. Injected water quality (as represented by the particle size and concentration), reservoir permeability and injection rate have a strong influence on the particle plugging and hence on fracture initiation, propagation and injectivity behavior of the formation.

4.10.1 Injection below the Fracture Pressure

To demonstrate the effect of fracturing coupled with filtration on injectivity behavior of a water injection well, it is illustrative to consider first a case where the injection pressures and skin resistance together are not sufficient to cause fracturing. Results shown in Fig. 4.8 depict the injectivity and skin histories for the case when no fracture is initiated. Increasing the injected particle concentration leads to a faster rate of plugging and hence a faster rate of injectivity decline. The injectivity histories for these runs (Fig. 4.8a) indicate that, in the absence of fracturing, injectivity decline is both rapid and severe at larger injected particle concentrations. The effect of formation damage due to internal and external filtration can be seen from the skin history (Fig. 4.8b). This shows that the injectivity of unfractured wells is strongly dependent on injection water quality.

4.10.2 Effect of Particle Concentration

To understand the role of particle plugging on injection well fracturing and injectivity decline, we consider a case in which the thermal stresses are negligible. Also, to avoid any injectivity changes due to difference in fluid mobilities, the water is injected into an aquifer. Fig. 4.9 show simulations for injectors in which fractures are induced by an increase in bottomhole pressure due to particle plugging. The wells are initially unfractured. As the injection proceeds, the suspended particles plug the formation and reduce the permeability. As the bottomhole pressure increases and reaches the fracturing pressure, a fracture is initiated. Note that the rate of fracture growth is faster in the beginning. This is because the fracture is initially assumed to grow as an enlarging penny shaped crack (Fig. 3.5) until it is confined above and below. After the confinement, it starts extending laterally (Fig 3.6). Hence in the early time, at small fracture lengths, a small increase in fracture length would only expose only a small surface area. The smaller surface area available for particle retention leads to a faster rate of permeability reduction and hence a faster rate of fracture growth.

It is interesting to note that once the fracture is initiated, the injectivity almost becomes constant. This is because once the fracture is initiated, the pressure at the fracture tip equals the fracture propagation pressure. The pressure at the tip plus the pressure drop along the fracture gives the pressure at the wellbore. In the absence of thermal effects, the minimum horizontal stress remains almost constant. This means that the pressure at the fracture tip remains constant. The pressure drop along the fracture is small because the fracture has a high permeability. The increase in pressure drop along the fracture due to increasing fracture length is negligible. Hence, the pressure

at the wellbore, which is the sum of fracture propagation pressure and the pressure drop along the fracture, remains almost a constant.

Increasing the particle concentration increases the rate of permeability decline and to maintain a constant flow rate, the bottomhole pressure needs to be increased at a faster rate. Hence, for the higher particle concentration, the fracture is initiated earlier. Also, once the fracture is initiated, the fracture face gets plugged faster for a higher particle concentration and so the fracture propagates faster. One important thing to note is that, once the fracture is initiated the injectivity of the well is almost independent of water quality. This is because the bottomhole pressure stays close to the fracture propagation pressure. The injection water quality determines the rate of permeability decline and hence determines when the fracture is initiated and how fast the fracture grows to accommodate the particle plugging. This is evident from Fig. 4.9. The injection water quality only determines the time of initiation of the fracture and the rate of fracture growth and not the injectivity.

4.10.3 Effect of Injection Rate

To understand the role of injection rate on injection well fracturing and injectivity decline, we consider injection into an aquifer and without thermal stresses. Fig. 4.10 shows the effect of flow rate on fracturing of injectors due to particle plugging.

When the formation permeability and the reservoir pressure are held constant, a higher injection rate would mean a higher bottomhole pressure. Also, a higher injection rate at the same particle concentration would mean a faster rate of permeability decline. So, for a higher injection rate, not only does the bottomhole pressure start off higher, but it also grows faster. Hence the fracture criterion is met earlier and a fracture is initiated earlier. Also, the fracture grows faster because of the faster rate of plugging of the fracture face. This is evident from Fig. 4.9b.

Note that for this case as well, once the fracture is initiated, the injectivity remains almost constant. Unlike the previous case, the injectivity ratios for the different flow rates do not fall upon each other after the fracture initiation. This is because each of these wells started with a different bottomhole pressure depending on the flow rate and once the fracture is initiated, they end up with the same bottomhole pressure, which is close to the fracture propagation pressure.

4.10.4 Effect of Formation Permeability

Fig. 4.11 shows the effect of initial formation permeability on the injectivity and fracturing of injectors. When the flow rate and the reservoir pressure are held constant, a lower formation permeability would mean a higher bottomhole pressure. Also, a lower permeability would mean a better particle trapping efficiency. Hence at the same particle concentration, a lower initial formation permeability would cause a faster rate of permeability decline. So for a lower permeability, not only does the bottomhole pressure start off higher, but it also grows faster. Hence the fracture criterion is met earlier and a fracture is initiated earlier. Also, the fracture increases faster because of the faster rate of plugging of the fracture face. This is evident from Fig. 4.11b.

4.10.5 Effect of Thermal Stresses

When the injected fluid is substantially cooler than the formation, it will not heat up to the formation temperature as it travels from the surface to the bottom of the well. The cooler fluid induces thermal stresses. These thermal stresses reduce the minimum horizontal stress and hence the fracture propagation pressure. Fig. 4.12 shows the effect of thermal stresses. The minimum horizontal stress is decreasing because of thermal stresses. The bottomhole pressure is increasing because of particle plugging. A fracture is initiated when the pressure at the fracture tip exceeds the modified minimum horizontal stress. This clearly occurs sooner when the thermal stresses are large and reduce the minimum horizontal stress by a large amount. Hence a combination of particle plugging and thermal stresses controls fracturing. If the difference in temperature between the injected fluid and the formation is large, the thermal stresses can dominate the fracturing process.

Fig. 4.13 shows the effect of thermal stresses on the injectivity and fracturing of injectors when a fluid cooler than the formation is injected into the formation. As the difference in temperature increases, the fractures grow longer because of a larger reduction in the minimum horizontal stress. One important thing to note is that, unlike the previous cases where the injectivity became constant once the fracture is induced, the injectivity increases after fracture is initiated and can even become higher than the initial injectivity. This is because the minimum horizontal stress was constant in the previous cases when there were no thermal effects. The bottomhole pressure, which was close to the minimum horizontal stress, also remained constant. However, when thermal stresses are induced, the minimum horizontal stress decreases with time as the injection proceeds. Hence once the fracture is initiated and the bottomhole pressure has started to follow the minimum horizontal stress, the reduction in minimum horizontal stress causes a reduction in bottomhole pressure as well (Fig. 4.12). This reduction of bottomhole pressure at the same injection rate causes an increase in injectivity. If the thermal stresses are high and the minimum horizontal stresses reduce by a large amount, the injectivity of the well could increase beyond the initial injectivity.

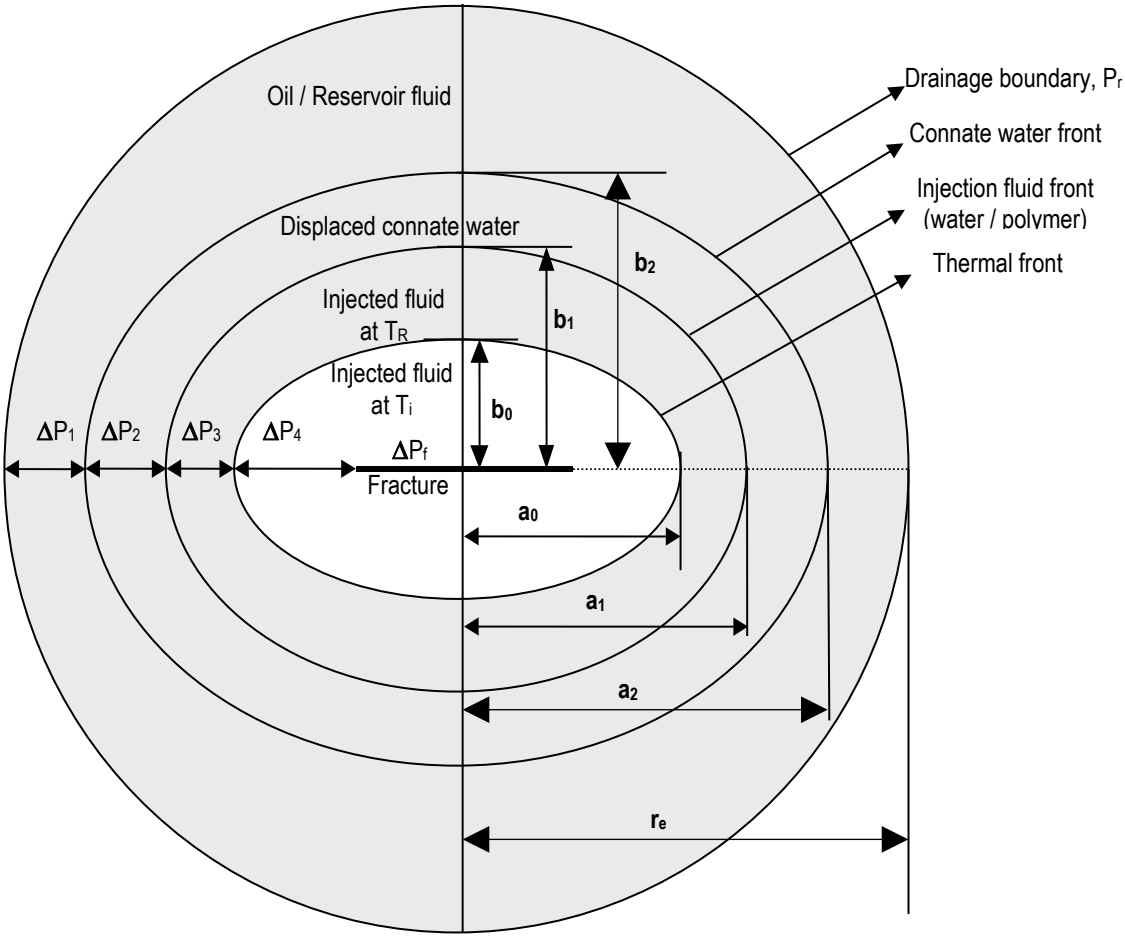

Figure 4.1: Plan view of a growing two-winged fracture

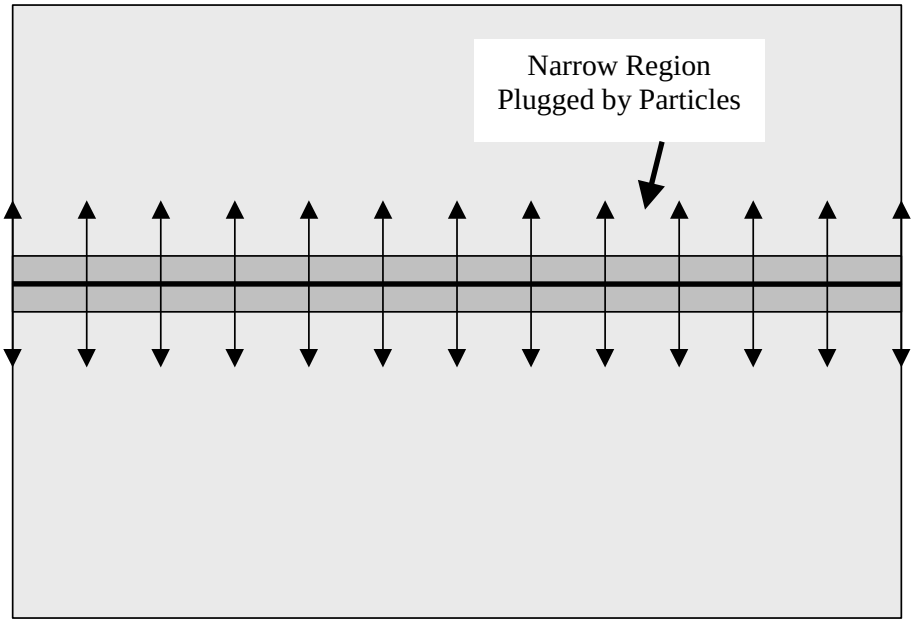

Figure 4.2: Damaged zone in a narrow region around the fracture face through which the fluid flow is almost linear

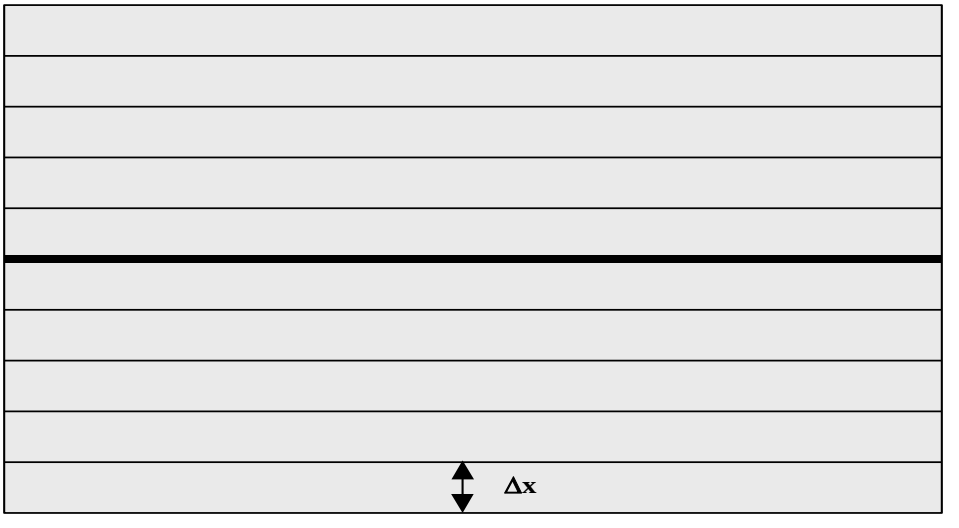

Figure 4.3: Representation of the damaged zone around the fracture as a series of linear cores

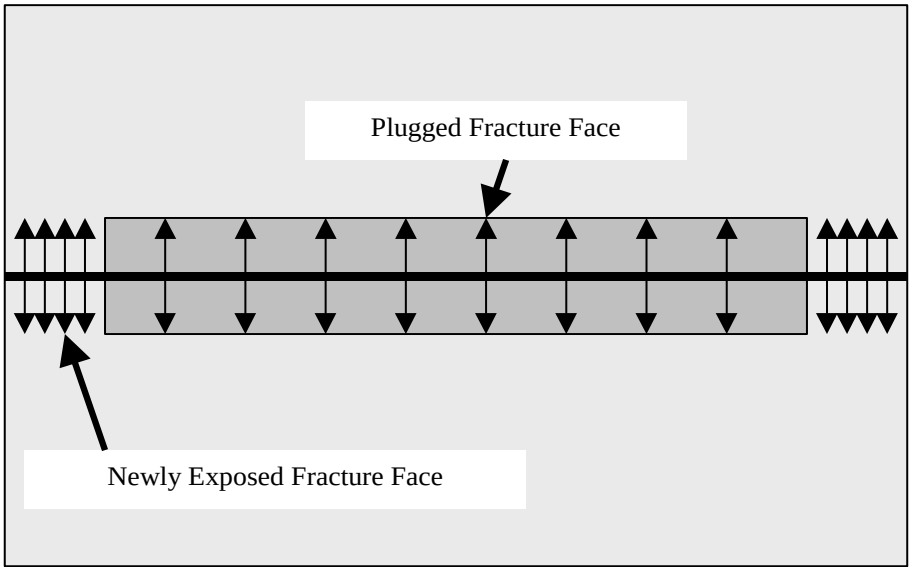

Figure 4.4: View of fracture showing plugged fracture face and higher leak-off through the newly exposed fracture face

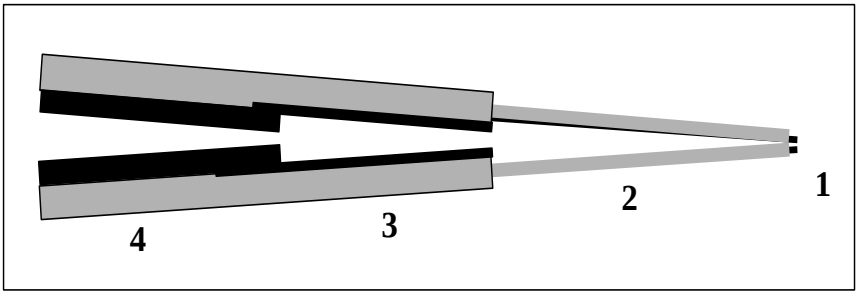

Figure 4.5: Based on the filtration model, the length of the fracture can be divided into four different regions

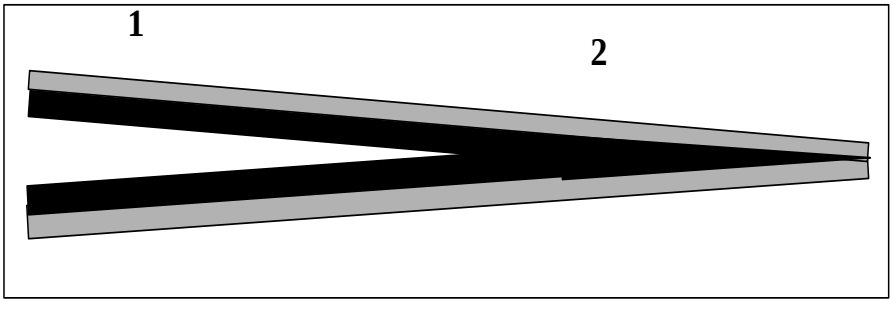

Figure 4.6: Simplified two zone fracture plugging model

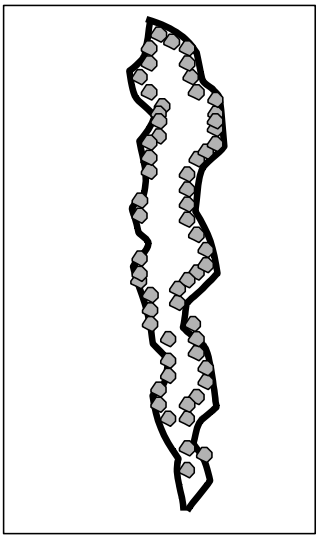

Figure 4.7: Zone 1-The filter cake thickness is small and the fracture is open to flow

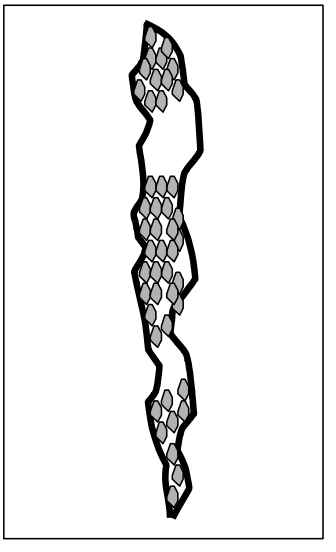

Figure 4.8: Zone 2-Relatively larger portions of the fracture filled by external cake and a few flow channels exist

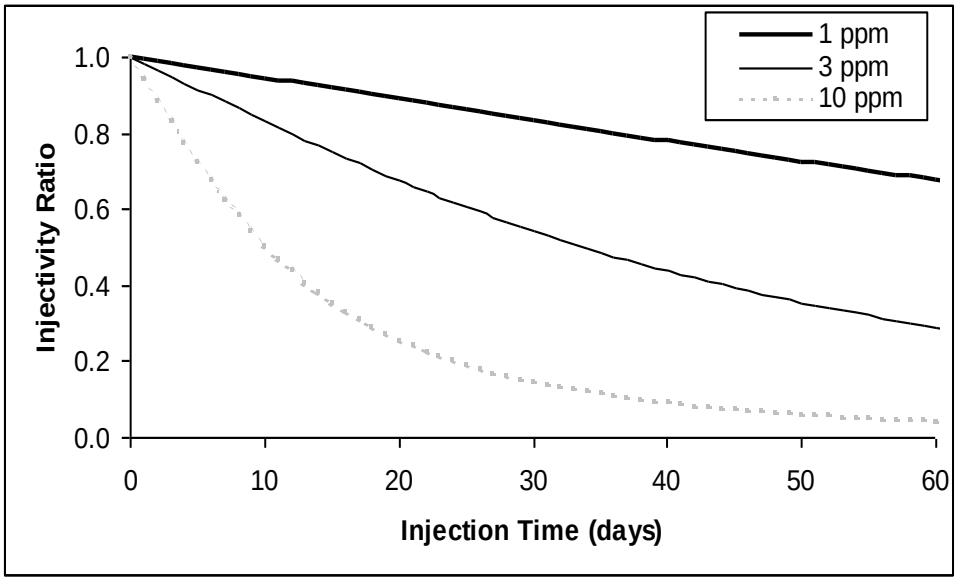

Figure 4.8a: Effect of injected particle concentration on injectivity for unfractured wells

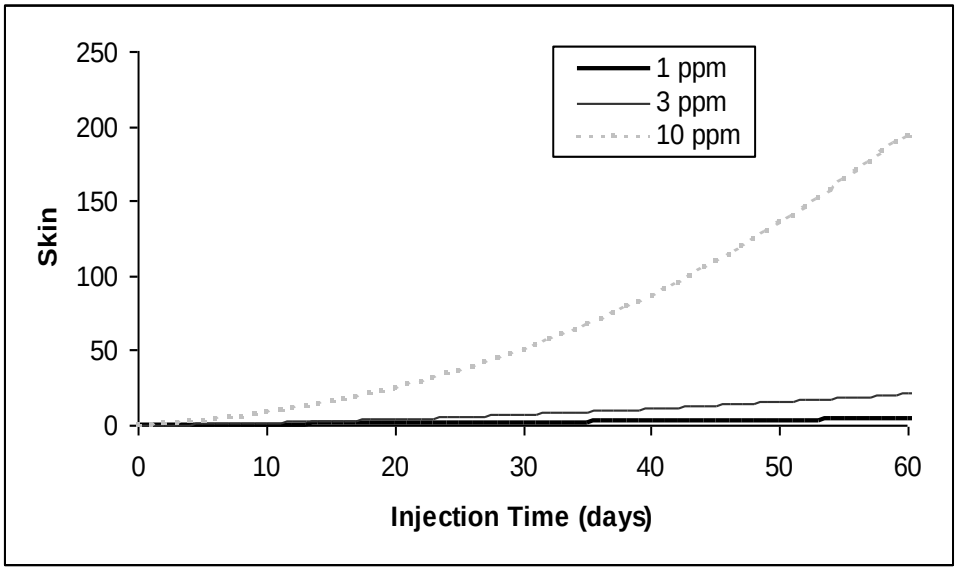

Figure 4.8b: Effect of injected particle concentration on skin for unfractured wells

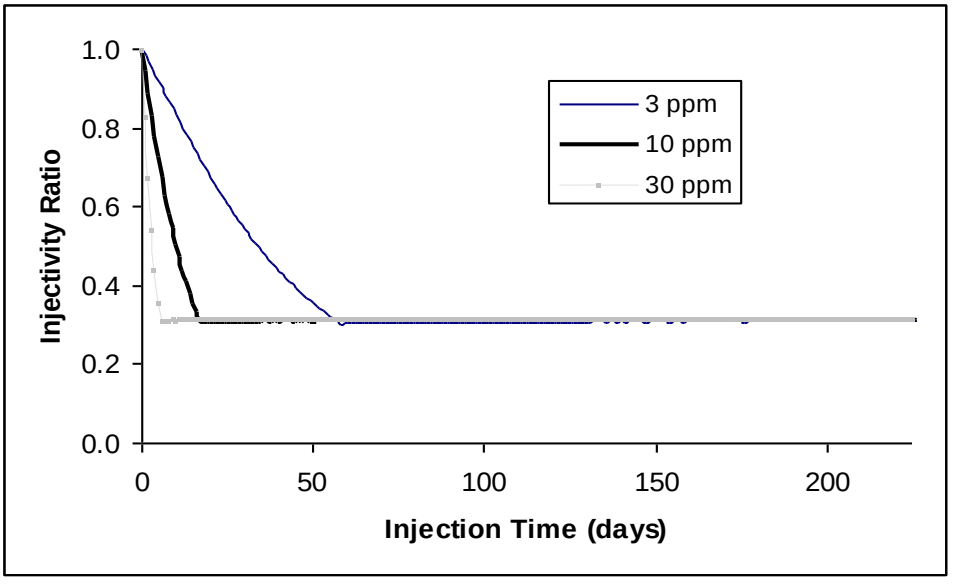

Figure 4.9a: Effect of injected particle concentration on injectivity

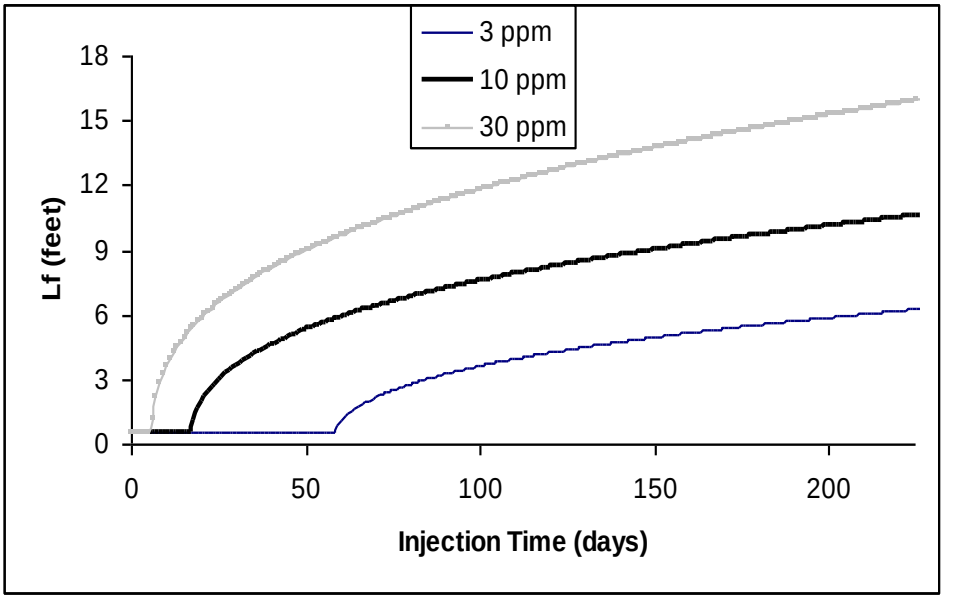

Figure 4.9b: Effect of injected particle concentration on fracture length

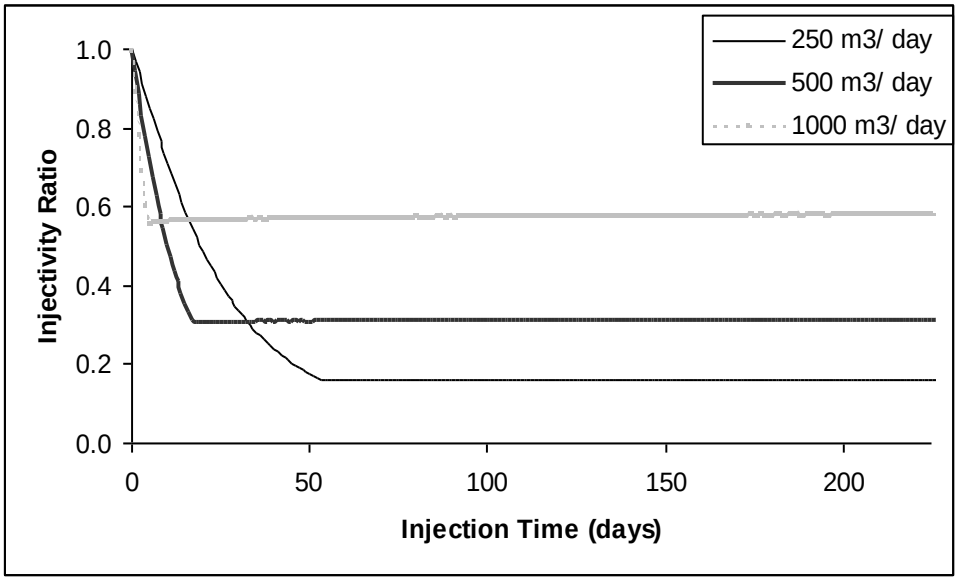

Figure 4.10a: Effect of injection rate on injectivity

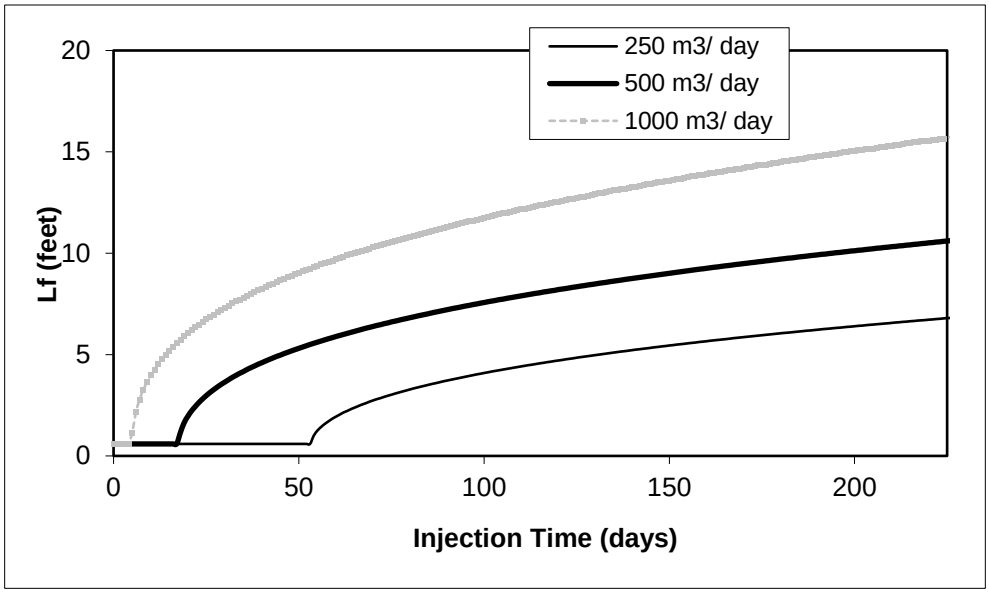

Figure 4.10b: Effect of injection rate on fracture length

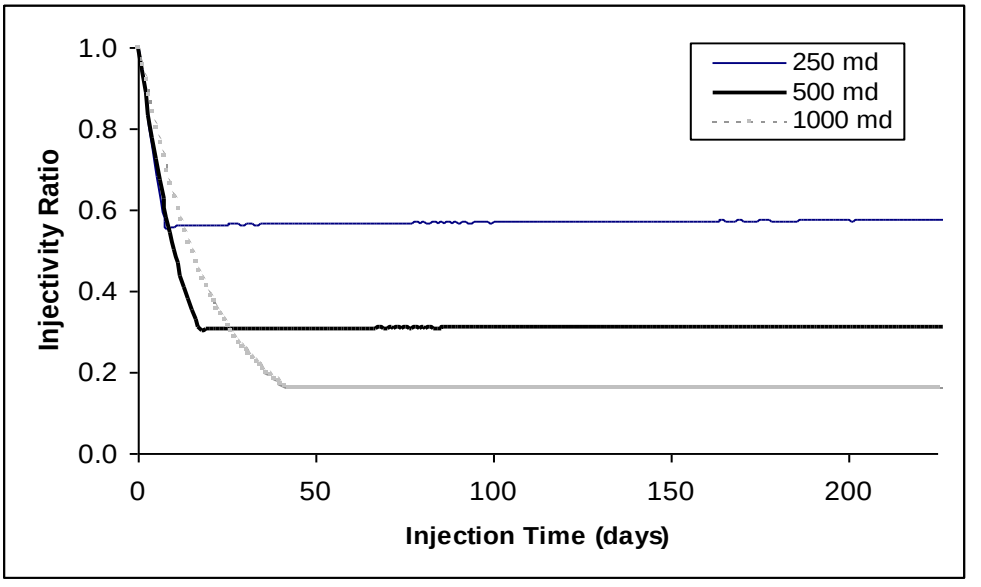

Figure 4.11a: Effect of formation permeability on injectivity

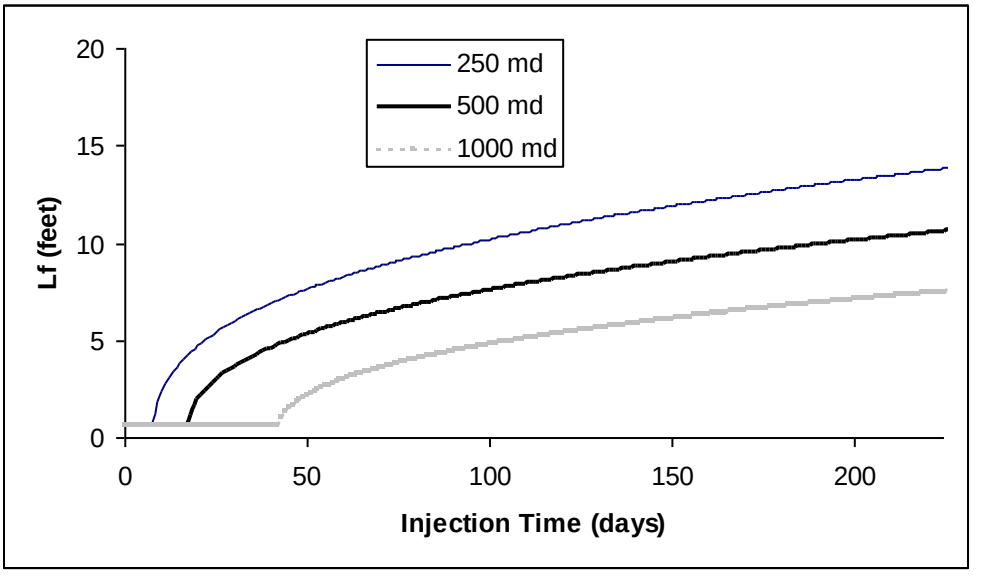

Figure 4.11b: Effect of formation permeability on fracture length

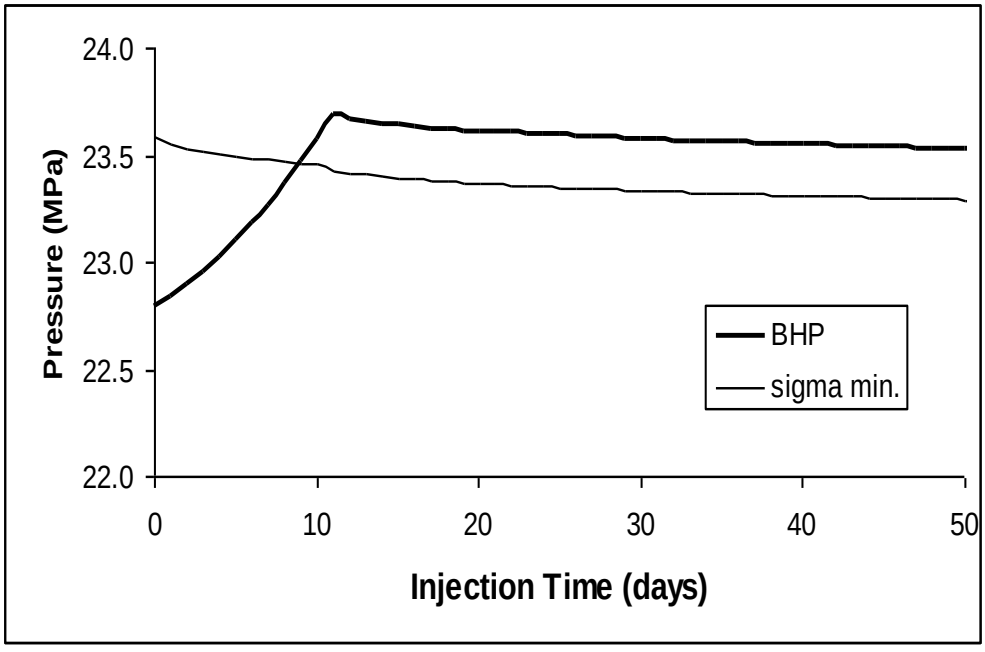

Figure 4.12: Effect of thermal stresses on minimum horizontal stress and bottomhole pressure

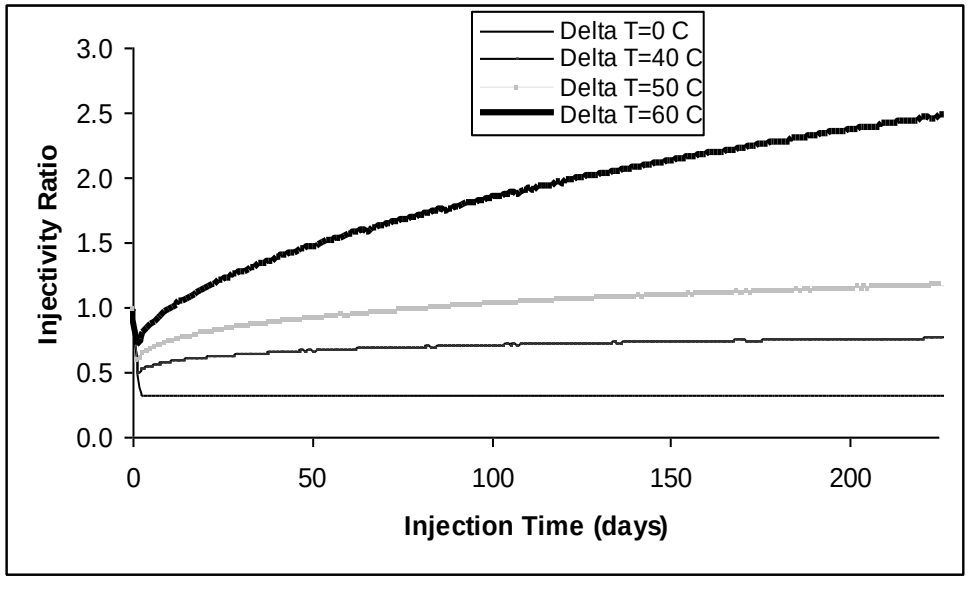

Figure 4.13a: Effect of thermal stresses on injectivity

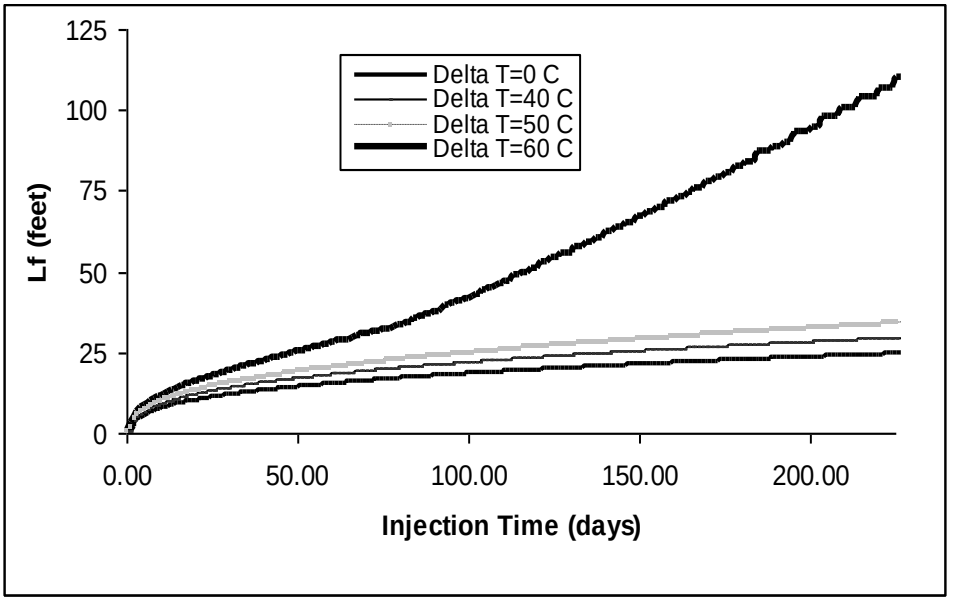

Figure 4.13b: Effect of thermal stresses on fracture length

Chapter 5: Injection in Multi-layered Reservoir

5.1 Introduction

The reservoirs into which water is injected are rarely homogeneous. The most common form of heterogeneity is layering. When the reservoir is layered, each layer can have its own fluid and rock properties. Hence, the flow into each layer and the fracturing of these layers depends on these properties. The present version of WID is designed to handle fracture propagation in non-communicating multi-layered reservoirs.

Fracture propagation in single layered reservoirs has been discussed in previous sections. This approach has been extended to the multi-layered case under the assumption that fractures in each of the layers do not communicate. Hence, the fracture mechanics for each of the layers are treated independently. However, the flow into each layer is dependent on the flow resistance for the layers, which in turn is dependent on the layer parameters. Hence the layers are decoupled for the fracture mechanics but are coupled for the flow and filtration effects.

5.2 Flow Distribution into Multiple Layers

Fracture propagation is extended to a multi-layered reservoir under the assumption that fractures in each of the layers do not communicate. Hence, the fracture mechanics for each of the layers are treated independently. However, the flow from the wellbore into each layer is distributed based on the layer total flow resistance. Hence the layers are decoupled for fracture mechanics but are coupled for the flow and filtration effects.

The flow into each layer is treated as flow in parallel. The flow resistances of each of the layers determine the flow into the layer.

$$q_{layer} = \frac{R_{tot}}{R_{layer}} q_{tot} \tag{1}$$

where qlayer is the flow into each layer, qtot is the total injection rate, Rlayer is the flow resistance of the layer and Rtot is the total flow resistance. The total flow resistance is expressed as

$$R_{tot} = \frac{1}{\sum_{1}^{Nl} \frac{1}{R_{layer}}} \tag{2}$$

where Nl is the number of layers.

Equation (1) gives flow into each layer assuming that the well is either completed open-hole or all the layers are perforated and are communicating directly with the wellbore. In that case, the layer resistance is simply the horizontal flow resistance as given by the following equation:

$$R_{hl} = \frac{\ln(r_e / r_w)}{2\pi k_{hl} h_l} \tag{3}$$

However if some of the layers aren't perforated then the following sections describe the calculation of flow resistance for each of the unperforated layers.

5.2.1 Flow into an Unperforated Layer from an Adjacent Perforated Layer

Let us discuss a simple two layer reservoir with top layer perforated and the bottom layer unperforated as shown in the figure below.

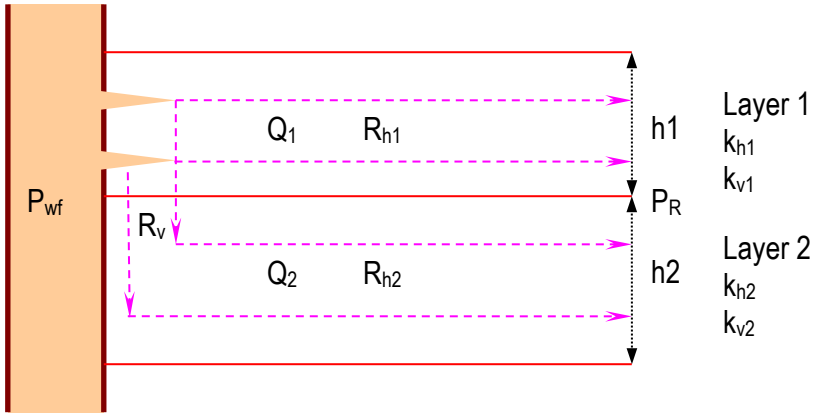

Where
1, 2 - layer numbers starting from the top layer
kh - horizontal permeability
kv - vertical permeability
h - height/thickness of the layer
Rh - horizontal flow resistance
Rv - vertical flow resistance

The flow resistance for the perforated layer is simply equal to the horizontal flow resistance by the layer as given by equation (3). For the unperforated layer the flow is modeled as shown in the figure above. The flow is distributed from the perforated layer towards the unperforated layer vertically. The vertical distributed flow later becomes horizontal as shown in the figure. The two flow resistances (Rh2 and Rv) are assumed in series which is assumed to give the flow resistance for the unperforated layer (layer 2).

The horizontal flow resistance for any of the two layers can be written in the following way (derived using Darcy's law for radial geometry) as given by equation (3).

The total vertical flow resistance (Rv) for the unperforated layer is assumed to be divided in series between the two layers as shown in the figure. The first vertical flow resistance is

by the perforated layer and the second vertical flow resistance is by the unperforated layer. The values for the two vertical flow resistances can be calculated using Darcy's law for linear geometry and is shown as below:

$$R_{V1} = \frac{h_1 / 2}{A_V k_{V1}} \tag{4}$$

$$R_{V2} = \frac{h_2 / 2}{A_V k_{V2}} \tag{5}$$

where Av is the area for linear vertical flow from perforated layer into the unperforated layer as calculated below:

$$A_V = \pi (l_p + r_w)^2 - \pi (r_w)^2 \tag{6}$$

Note lp is the length of the perforations and rw is the radius of the well.Adding the two vertical flow resistances in series gives the total vertical flow resistance (Rv); as shown below:

$$R_V = R_{V1} + R_{V2} = \frac{h_1 / 2}{A_V k_{V1}} + \frac{h_2 / 2}{A_V k_{V2}} \tag{7}$$

Adding the vertical flow resistance (Rv) to the horizontal flow resistance for the unperforated layer (Rh2) in series gives the total flow resistance of layer 2; as shown below:

$$R_2 = R_V + R_{h2} \tag{8}$$

5.2.2 Flow into an Unperforated Layer from Multiple Perforated Layer

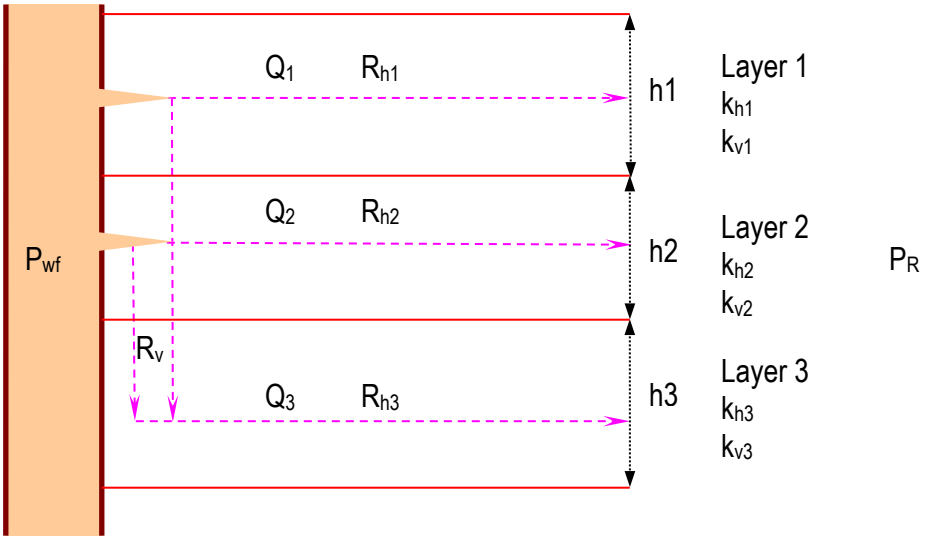

1, 2, 3 - layer numbers starting from the top layer
kh - horizontal permeability
kv - vertical permeability
h - height/thickness of the layer
Rh - horizontal flow resistance
Rv - vertical flow resistance

The horizontal flow resistance for all the layers is calculated using equation (2) as shown above. The vertical flow resistance for the unperforated layer (layer 3) is calculated using the following model. The vertical flow resistance is assumed to be in parallel between the two perforated layers and the unperforated layer. Following is the model for the flow resistance:

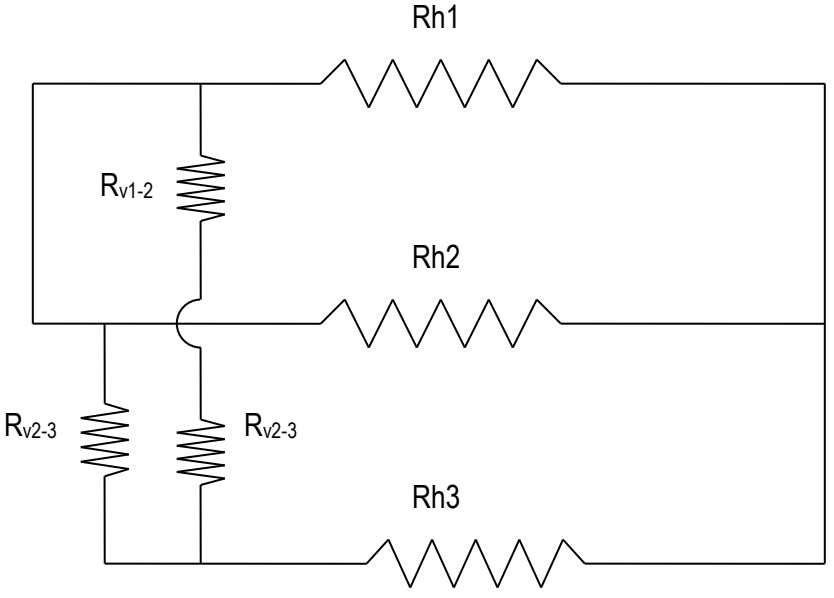

$$R_1 = R_{h1} \tag{9}$$

$$R_2 = R_{h2} \tag{10}$$

$$R_3 = R_{h3} + R_V \tag{11}$$

$$\frac{1}{R_V} = \frac{1}{R_{V2-3}} + \frac{1}{(R_{V1-2} + R_{V2-3})} \tag{12}$$

$$R_{V2-3} = \frac{h_2/2}{A_V k_{V2}} + \frac{h_3/2}{A_V k_{V3}} \tag{13}$$

$$R_{V1-2} = \frac{h_1/2}{A_V k_{V1}} + \frac{h_2/2}{A_V k_2} \tag{14}$$

Rh1, Rh2, Rh3 i.e. the horizontal flow resistance for any of the layers is calculated using equation (3).

5.2.3 Flow into Multiple Unperforated Layers from Multiple Perforated Layers

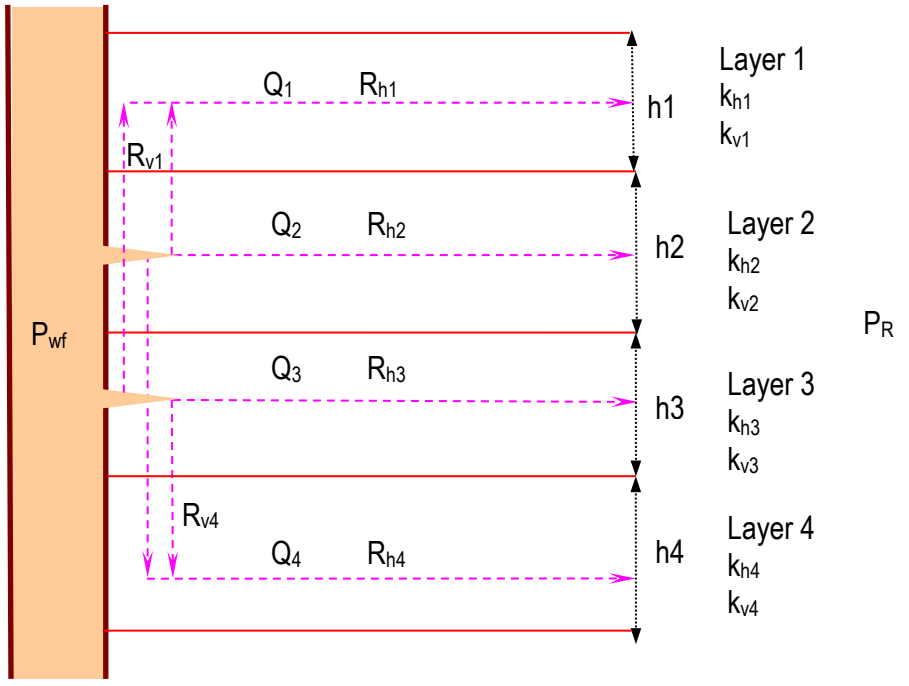

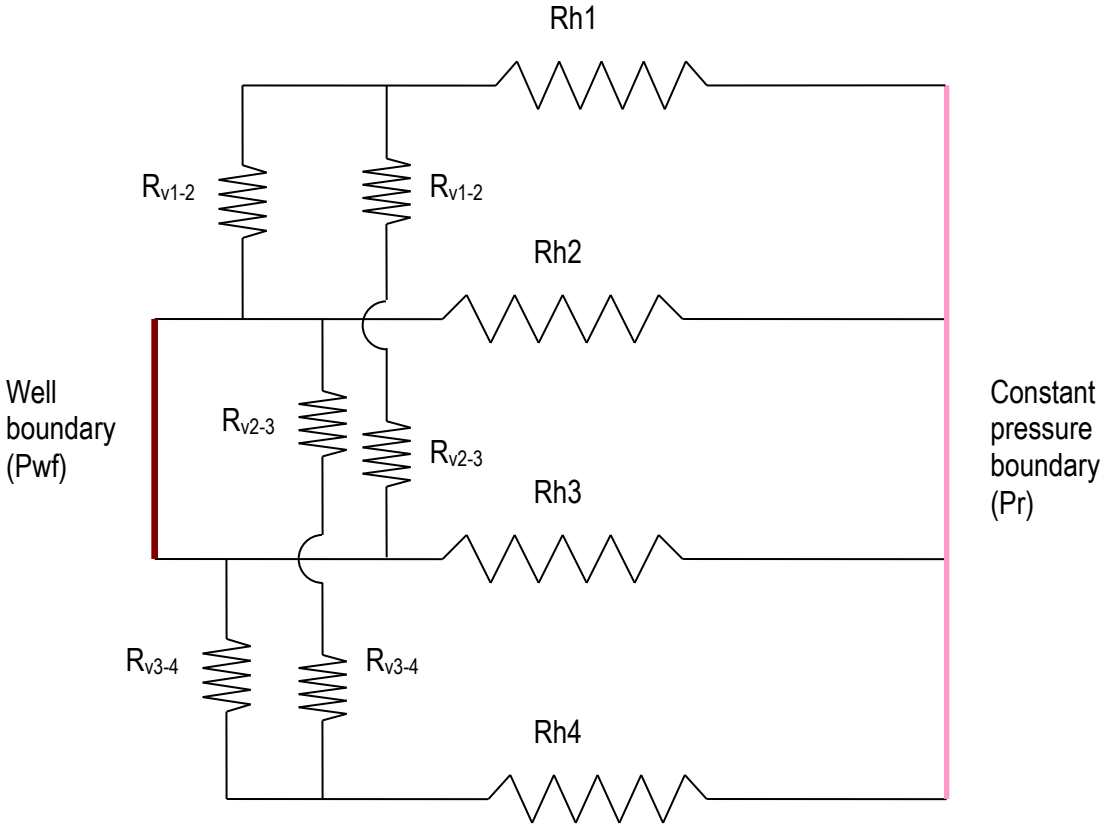

$$R_1 = R_{h1} + R_{V1} \tag{15}$$

$$R_2 = R_{h2} \tag{16}$$

$$R_3 = R_{h3} \tag{17}$$

$$R_4 = R_{h4} + R_{V4} \tag{18}$$

$$\frac{1}{R_{V1}} = \frac{1}{R_{V1-2}} + \frac{1}{(R_{V1-2} + R_{V2-3})} \tag{19}$$

$$\frac{1}{R_{V4}} = \frac{1}{R_{V2-3}} + \frac{1}{(R_{V2-3} + R_{V3-4})} \tag{20}$$

$$R_{V1-2} = \frac{h_1/2}{A_V k_{V1}} + \frac{h_2/2}{A_V k_2} \tag{21}$$

$$R_{V2-3} = \frac{h_2/2}{A_V k_{V2}} + \frac{h_3/2}{A_V k_{V3}} \tag{22}$$

$$R_{V3-4} = \frac{h_3/2}{A_V k_{V3}} + \frac{h_4/2}{A_V k_{V4}} \tag{23}$$

The horizontal flow resistance is calculated using equation (3) for all the layers.No formation damage is done in the unperforated layers; however based on the flow into each layer, the dimensions of the water flood and thermal fronts are calculated. The flow determines the filtration phenomena only in the perforated layers. The thermal and pore pressure effects are calculated separately for each layer. When the fracture criterion is satisfied for any layer (perforated or unperforated), a fracture is initiated in the layer. The new flow resistance is calculated based on the fracture length at each time step and the new flow rates are assigned to each layer. The fracture is assumed to be contained in each layer and there is no communication between fractures in different layers.

The vertical flow area changes in perforated layers for flow distribution into an unperforated layer once it is fractured. The flow area is given by the following equation:

$$A_V = \pi (l_f + r_w)^2 - \pi (r_w)^2 \tag{24}$$

The flow area considered is a cross section of a cylinder with outer radius equal to (lf + rw) and inner radius equal to rw.

5.2.4 Flow into Layered Reservoir with Shale Barriers

Most reservoirs have layers containing oil or gas (which can flow) along with shale barriers (impermeable rock) in between. Because of these impermeable shale barriers in between, not all the paying layers are in hydraulic communication with each other. We define a term called a pay block which does not have any flow barriers (mostly shales) in between. A paying block consists of group of paying (mostly sandstone or carbonate) layers containing no flow barriers in between but above and below the pay block. The flow contribution to an unperforated layer within a pay block is only available from all the perforated layers within the pay block. Below is a schematic of two paying blocks with shale barrier in between

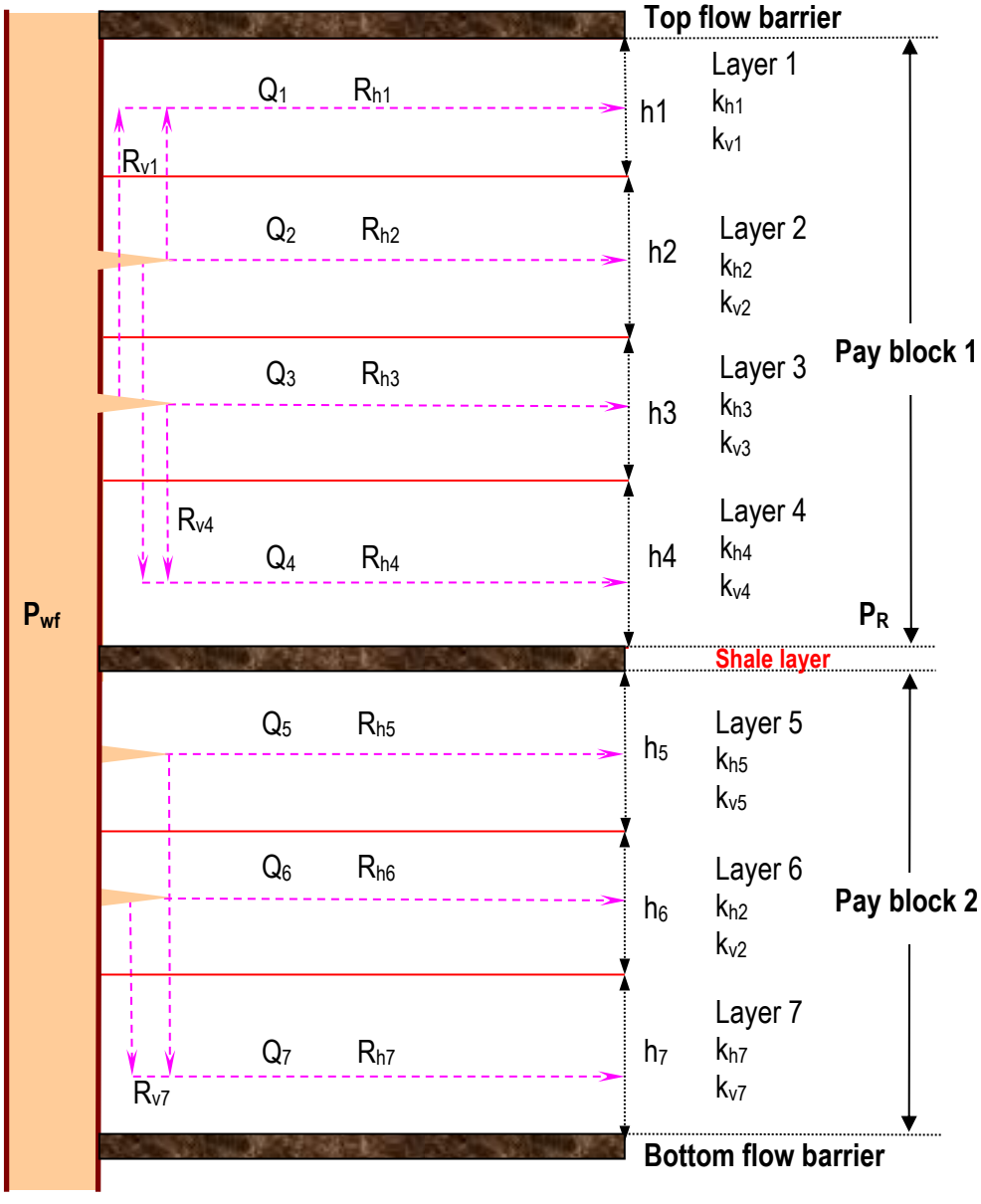
Top flow barrier
Layer 1
k_{h1}
k_{v1}
Q_1
R_{h1}
h1
R_{v1}
Layer 2
k_{h2}
k_{v2}
Q_2
R_{h2}
h2
Pay block 1
Layer 3
k_{h3}
k_{v3}
Q_3
R_{h3}
h3
R_{v4}
Layer 4
k_{h4}
k_{v4}
Q_4
R_{h4}
h4
P_{wf}
P_R
Shale layer
Layer 5
k_{h5}
k_{v5}
Q_5
R_{h5}
h_5
Layer 6
k_{h2}
k_{v2}
Q_6
R_{h6}
h_6
Pay block 2
Layer 7
k_{h7}
k_{v7}
Q_7
R_{h7}
h_7
R_{v7}
Bottom flow barrier

Chapter 6: Injectivity Decline in Horizontal Wells

6.1 Introduction

Horizontal wells are increasingly used worldwide and are especially desirable offshore for water-flooding and reservoir pressure maintenance as they allow more access to the reservoir with large injectivities. Fracture growth in these horizontal injectors can play an important role in determining the injection rates, reservoir sweep and oil recovery.

A model is developed to estimate the growth of fractures in horizontal injectors. The model considers two orientations of fracture growth: 1) longitudinal fractures i.e. fracture along the horizontal well and 2) centered transverse fractures, i.e. at the center and perpendicular to the horizontal well. Fracture growth is due to: 1) reduction of permeability around the horizontal well caused by particle deposition from injection fluids, 2) reduction in minimum horizontal stress due to cold fluid injection, and 3) injection of viscous polymer fluids. The model accounts for plugging of the horizontal well, the induced fracture and the formation around the fracture. It also calculates the thermal and pore pressure stresses to update the minimum horizontal stress around the fracture tip. It also allows injection of power-law fluids to model polymer injection in horizontal injectors.

It is shown that the injection well pressures are controlled by the minimum horizontal stress. The injection fluid quality, injection rate, and injection fluid temperature determine the rate of fracture growth in a horizontal injector. Fracture lengths are estimated for longitudinal and transverse fracture growth orientations as the lower and upper bound values.

6.2 Background: Injectivity of Horizontal Wells

In offshore locations with limited reservoir access, horizontal wells are an economic alternative to increasing reservoir access and significantly increasing the rate of injection and production from the reservoir. With the increasing limitations being placed on the overboard discharge of produced water in offshore platforms, larger volumes of treated produced water are being injected back into the ground. In onshore locations, over 91% of the produced water is reinjected. More injection wells are being utilized for waterflooding and for subsurface disposal.

There is a growing realization that a large proportion of injection wells are fractured at some point in their life. This implies that even wells that were not deliberately hydraulically fractured are likely to have fractures created due to the injection of water over extended periods of time. This is true of both vertical and horizontal wells.

In the past, models have been presented for fracture growth in vertical injection wells (Perkins et al. 1985, Saripalli et al. 1999). Fracture growth was shown to be driven by thermal stresses and by particle plugging induced by suspended solids in the injection water. As the injection pressure exceeds the fracture pressure, a fracture begins to propagate. The rate of growth of the fracture is controlled by the water quality and by the reduction in minimum horizontal stress induced by the injection of cold water. Poor water quality usually results in longer fractures and lower injectivities (higher injection pressures).

No models are currently available for describing the injectivity behavior of fractured horizontal injection wells. A great deal of attention is given to hydraulic fracturing of

horizontal wells since it's inception in the late 1980's (Wei et al. 2005). However fractures created in water injection wells differ in many ways from hydraulic fractures. The primary drivers in injection well fractures are formation plugging which causes increase in the injection pressure and thermal stresses which causes reduction in the fracture pressure. In hydraulic fracturing thermal stresses and fracture plugging play insignificant roles since the volume of fluid injected into the fracture is relatively very small (about 1000 times less than in a typical injection well). The rate of fracture propagation is also significantly different; a hydraulic fracture propagates 100's of feet in hours while an injection fracture propagates in months. Moreover the fluid used in hydraulic fracturing to carry the proppants has 100 times viscosity compared to water used in injection wells. As a result the models used for hydraulic fracturing does not or at the most in a limited way apply to injection well fracturing. Reservoir simulators could be modified to incorporate the process of particle plugging which typically occurs at the length scale of millimeters that is not captured at the reservoir grid block scale.

This paper presents a model for fracture propagation and injection well performance for horizontal injectors. It incorporates the effects of particle plugging and thermal stresses. Both longitudinal and transverse fractures are modeled. It also allows for the injection of polymers (shear thinning fluids). Results are presented to show the parameters that primarily control the fracture length and injectivity of horizontal injectors.

6.3 Model Development

We use the model proposed by Joshi (1988) as the starting point to calculate injectivity in fractured horizontal wells. In his model, the 3-dimensional flow around an unfractured horizontal wellbore is approximated by a set of two 1-dimensional flows in series. The two flow resistances in series are: 1) far field resistance or the horizontal flow resistance (R_h) between the drainage boundary and a vertical plane through the axis of the horizontal well extending through the height of the reservoir, and 2) near well-bore flow resistance which is the vertical resistance (R_v) between the wellbore and the top and bottom of the reservoir. The total initial flow resistance is,

$$R_{tot,ini} = R_H + R_V + R_{Skin,ini} \tag{1}$$

The injectivity can then be calculated as,

$$I = \frac{1}{R_{tot}} \tag{2}$$

The initial skin, if any can also be calculated as follows:

$$R_{Skin,ini} = \frac{\mu \beta_a S_{ini}}{2\pi k_H k_{rw} l_w} \tag{3}$$

The initial steady state pressure in the wellbore at a constant injection rate q will be equal to:

$$P_{wf} = P_R + R_{tot,ini} q \tag{4}$$

6.3.1 Flow Resistance for Flow into the Reservoir from a Horizontal Well with a Longitudinal Fracture

Figure 1 shows a schematic of a longitudinal fracture growing along the horizontal well. It is likely that the fracture may grow upwards more than downwards because the stress increases with depth. However, in the model presented here it is assumed that the fracture will grow symmetrically upward and downward. Appendix A discusses how asymmetric growth of the longitudinal fracture can be modeled.

An equivalent longitudinal fracture with fracture half length equal to the wellbore radius is assumed instead of the horizontal well. All the flow is assumed to go into the fracture with the fracture being a small plane source instead of the wellbore. From the fracture faces the fluid is assumed to leak-off uniformly into the matrix. Two additional flow resistances: 1) a damage flow resistance due to particle deposition and 2) a fracture flow resistance is added to the initial flow resistance given by equation (1). $R_{skin,ini}$ is excluded now because it will be bypassed by the fracture. The total flow resistance with a longitudinal fracture in the horizontal well is modeled and calculated as follows:

$$R_{tot} = R_V + R_H + R_D + R_f \tag{5}$$

R_V is the total vertical flow resistance which consists of four regions separated by the connate water front, the injection fluid front and the thermal front:

$$R_V = R_{V1} + R_{V2} + R_{V3} + R_{V4} \tag{6}$$

The flow in the upward and downward direction from the horizontal well is assumed to be elliptical and confocal with the growing longitudinal fracture. Expressions for the components of the vertical flow resistances are given in Table 1. R_H, the horizontal flow resistance is also divided into four components to account for the changes in the horizontal front locations with injection:

$$R_H = R_{H1} + R_{H2} + R_{H3} + R_{H4} \tag{7}$$

Expressions for the components of the horizontal flow resistances are given in Table 2. These resistances depend on the location of the connate water front, injection fluid front and the thermal front. The locations of these fronts are calculated from a fluid mass balance assuming incompressible flow and energy balance with no conduction to overlying and underlying

formation. All the fluid fronts are assumed to be sharp with piston-like displacement. Initially the fronts are assumed to grow radially around the horizontal well and elliptically with growing longitudinal fracture with no growth of the fronts along the horizontal well axis. Once a front reaches the layer boundary at distance h/2, it is allowed to grow in the horizontal well axis direction as well. The front doesn't grow in the vertical direction anymore but is then assumed to grow in the two horizontal directions with a fixed ratio. The ratio of the front distance in the horizontal well direction to the front distance perpendicular to the well direction equals L_w/h.

R_D in equation (5) is the damage flow resistance caused by flow from the fracture into the matrix through a filter cake (referred to as external damage) and through the matrix surrounding the fracture with reduced permeability (referred to as internal damage). It is calculated as follows:

$$R_D = R_{fd} + R_{fc} \tag{8}$$

Where R_{fd} is the flow resistance caused by the particles depositing in the surrounding matrix perpendicular to the fracture. It is calculated as the flow resistance of the matrix up to the damaged distance with reduced permeability minus the flow resistance of the matrix up to the damaged distance with the undamaged/initial permeability. R_{fc} which is the flow resistance caused by the build up of a filter cake at the fracture faces which start after the internal filtration in the surrounding formation is complete. The equations for the two resistances are provided in Table 4.

R_f, the flow resistance along the longitudinal fracture is calculated assuming a PKN model with an elliptical fracture geometry and uniform leak-off. The equations for the flow resistance and the fracture width are presented in Table 5.

Once the total flow resistance is calculated, the wellbore pressure is recalculated using Equation 4 with R_{tot} instead of $R_{tot,ini}$. The pressure at the fracture tip is calculated as follows:

$$P_{tip} = P_{wf} - \Delta P_f \tag{9}$$

A fracture propagation criterion (Perkins et al. 1985) is used to calculate the fracture propagation pressure as follows:

$$p_{frac} = \sigma_{h\min} + \sqrt{\frac{\pi UE}{(1-\nu^2)h_f}} \tag{10}$$

The minimum horizontal stress is corrected for temperature and pressure changes in the reservoir (Perkins et al. 1985):

$$\sigma_{h\min} = \sigma_{h\min,ini} + \Delta\sigma_p - \Delta\sigma_T \tag{11}$$

If $P_{tip} > P_{frac}$, the longitudinal fracture needs to grow from its initial fracture half length equal to the wellbore radius to a fracture length such that $P_{tip} = P_{frac}$. The longitudinal fracture length is iteratively computed such that $P_{tip} \sim P_{frac}$. It is achieved by a converging iterative scheme with fracture length initial minimum and maximum bounds set equal to the wellbore radius and h/2 the maximum allowed fracture length. For large fracture length guess values, P_{tip} will be lower than P_{frac}, while for small fracture length guess values, P_{tip} will be larger than P_{frac}. The right fracture length value will result in $P_{tip} \sim P_{frac.}$ This fracture length finding is performed at every time step during injection.

6.3.2 Flow Resistance for Flow into the Reservoir from a Horizontal Well with a Transverse Fracture

A transverse fracture is a fracture that grows perpendicular to the horizontal well. Figure 2 shows a schematic of a transverse fracture growing perpendicular to the horizontal well. It is assumed that the fracture is initiated from the center of the horizontal well. Furthermore it is also assumed that initially there is a transverse fracture with half-length equal the wellbore radius and height equal to the layer thickness. The transverse fracture will grow only in the horizontal direction away from

the wellbore with constant height equal to the layer height. Figure 2 also shows the front around a horizontal well with an ellipsoidal shape. The front instead of ellipsoidal is assumed to be radial around the horizontal well. The front around the transverse fracture is assumed to be elliptical as shown in the figure. The actual front around the horizontal well with the transverse fracture will be a combination of the two schematics. However, to model this 3-D flow analytically, the flood fronts around the horizontal well and the transverse fracture are assumed to be radial and elliptical.

A portion of the fluid from the horizontal well will enter into the transverse fracture and then uniformly leak-off into the adjacent formation while the remaining flow will enter the formation directly from the horizontal well. The injection fluid in the horizontal well is assumed to be distributed between the formation and the transverse fracture as per the following equations:

$$q_f = \frac{R_{tot}}{R_{f,tot}} q \; ; \qquad q_w = \frac{R_{tot}}{R_{w,tot}} q \tag{12}$$

Where $R_{f,tot}$ is the total flow resistance between the boundary and the intersecting point of the transverse fracture with the horizontal well, and $R_{w,tot}$ is the total flow resistance between the boundary and the horizontal well. The horizontal well is assumed to have no pressure drop along its length. The total flow resistance caused by the combination of the horizontal well and the transverse fracture, R_{tot} is calculated as follows:

$$R_{tot} = 1 \Big/ \left[1 \Big/ R_{f,tot} + 1 \Big/ R_{w,tot} \right] \tag{13}$$

The actual ellipsoidal flow around the horizontal well is approximated as radial flow around the horizontal well assuming no effect of the transverse fracture on the flow around the horizontal well. Similarly the flow around the transverse fracture is assumed to be elliptical. This assumption allows us to calculate the two flow resistances, $R_{f,tot}$ and $R_{w,tot}$ independently. The two resistances are then added in parallel as shown in equation 13. The thermal front, injection fluid front and the displaced connate water front around the horizontal well up to the layer height for $R_{w,tot}$ calculation assumes radial flow. Once the fluid fronts reach the top and bottom of the layer, the flood front starts to grow laterally but with fixed height equal to h. The components for $R_{f,tot}$ and $R_{w,tot}$ are shown in Figure 3.

6.3.3 Flow Resistance for Flow into the Reservoir from the Horizontal Well up to the Drainage Boundary

The flow resistance for the horizontal well flow into the matrix, $R_{w,tot}$ is calculated as follows:

$$R_{w,tot} = R_{Skin,ini} + R_{wD} + R_{wr} + R_{wh} \tag{14}$$

where $R_{skin,ini}$ is the flow resistance caused by initial skin around the horizontal well (Equation 3), R_{wD} is the flow resistance caused by the near wellbore damage and any filter cake build up at the face of the horizontal well by solids deposition from injection fluid. R_{wD}, the damage flow resistance caused by near wellbore permeability reduction and any external filter cake build up is calculated as follows:

$$R_{wD} = R_{\text{int}_w} + R_{cc_w} \quad (15)$$

Where R_{int_w} is the flow resistance of the near wellbore region around the horizontal well with reduced permeability and R_{cc_w} is the flow resistance caused by the external filter cake at the face of the horizontal wellbore. Equations for the two damage flow resistances are presented in Table 9.

R_{wr} and R_{wh} are the radial flow resistance and the horizontal elliptical flow resistance for a horizontal well. Rwr, the total flow resistance in the radial direction around the horizontal well is broken into four parts:

$$R_{wr} = R_{wr1} + R_{wr2} + R_{wr3} + R_{wr4} \quad (16)$$

Expressions for these are provided in Table 10.

Rwh, the total horizontal flow resistance also has four parts as given by Equation 7, i.e. $R_{wh} = R_H$.

6.3.4 Flow Resistance for Flow into the Reservoir from the Transverse Fracture up to the Drainage Boundary

The flow resistance, $R_{f,tot}$ is also divided into three flow resistances caused by: 1) the flow in the fracture, 2) the flow in the damage zone near the fracture, and 3) the flow resistance far away from the fracture into the reservoir up to the drainage boundary r_e:

$$R_{f,tot} = R_{fi} + R_{fD} + R_{fh} \quad (17)$$

Here R_{fi} is the resistance to fluid flow within the transverse fracture. The equations are provided in Table 5. R_{fD} is the sum of two flow resistance: 1) caused by a reduced permeability zone near the fracture (R_{fd}) and 2) caused by the filter cake at the four faces of the transverse fracture (R_{fc}). These are calculated using Equation 8 as before with the equations given in Table 4. R_{fh} is the far field flow resistance from the fracture to the drainage boundary given as:

$$R_{fh} = R_{fh1} + R_{fh2} + R_{fh3} + R_{fh4} \quad (18)$$

Expressions for the four components are given in Table 11.

Once the total flow resistance is calculated using Equation 13, Equations 9 to 11 are used to calculate the length of the transverse fracture at any time during injection.

6.4 Model Implementation

The model presented is implemented in WID 7.2, which is a single injection well simulator. The model is implemented for a multi-layered reservoir with one horizontal well in each layer. The flow in the layers is assumed to be independent of each other, i.e. the layers are treated as independent reservoirs except that they communicate at the well. Based on the total flow resistance of each of the layers, the flow distribution into each of the horizontal wells is calculated. Once the flow rate into each horizontal well in a particular layer is known, the flow resistances for that layer is calculated independently as presented earlier for a single layer with a single horizontal well. The flow distribution into the different

laterals/horizontal well sections is calculated based on layer flow resistances in parallel. After the injection rate distribution into each of the lateral/horizontal well section is known at a time step, the pressure and flow distribution within that layer through the lateral is calculated independent of the other layers. The results for multi-layered reservoir with multiple horizontal wells are useful in predicting if one or more layers will act as thief zones. Note that one layer is assumed to have one lateral and once its flow rate is known, the single layer model is used thereafter to calculate its total flow resistance, fracture growth and injectivity. Results are presented for a reservoir with a single layer a single horizontal well.

6.5 Results and Discussion

The results of the model are illustrated through an example well. Table 11 shows input parameters for this simple example. Three cases are considered: 1) injection into a vertical well, 2) injection into a horizontal well with longitudinal fracture growth and 3) injection into a horizontal well with transverse fracture growth. All the cases assume an injection rate of 8,000 bpd of water with 20 ppm of solids of size 5 μm. The reservoir/layer is 100 ft thick with k_h = 100 md, k_V = 10 md and k_{rw}^o = 0.2. The initial reservoir pressure is 2500 psi and the initial minimum horizontal stress is 4000 psi. The injection water temperature is 60 F while the reservoir is at 140 F. The cool water will reduce the minimum horizontal stress as given by equations in Table 8. The drainage boundary is assumed to be at 5000 ft maintained at constant pressure equal to the initial reservoir pressure of 2500 psi. The wellbore radius is 3 inches. The initial water saturation in the reservoir is 0.3 with remaining 0.7 as oil saturation. The residual oil saturation is 0.3. The end point relative permeability to water is assumed 0.2 while the end point relative permeability to oil is assumed to be 0.6. The formation porosity is 0.2 and any cake that will build up at the face of the well and the fracture will also have 0.2 as the porosity. The horizontal well is assumed to be 1000 ft long lying at the center of the layer. The simulations were done for an injection time of 1000 days. With these input values and other inputs shown in Table 11, WID was run to calculate the bottomhole well pressure and the fracture length as a function of injection time.

Figure 5 shows the results for the fracture length and bottom-hole pressure with injection time for the three cases of fracture growth in a vertical well and a horizontal well. The bottom-hole pressure rises very quickly in all the three cases to the fracture pressure due to particulate plugging of the formation near the wellbore. As a result a fracture is initiated within a few days or weeks in all the three cases. However, the fracture grows faster in the vertical well case as compared to the two horizontal well cases. This is mainly because the pressure drop in the reservoir is higher in a vertical well compared to a horizontal well with or without a fracture. The fracture grows up to approximately 280 ft in the vertical well case while the transverse fracture grows up to 230 ft and the longitudinal fracture grows to only 50 ft (entire height of the reservoir). The longitudinal fracture is assumed to extend across the entire length of the horizontal well (1000 ft) which gives it a much larger area for the solids to deposit. This results in a smaller thickness of the filter cake and a slower increase in bottom-hole pressure. The bottom-hole pressure for all the cases reaches a maximum and then decreases because of the reduction in minimum horizontal stress (due to thermal effects) which controls the pressure at the fracture tip and the well. This reduction in in-situ stress is directly related to the temperature difference between the injected water and the reservoir as well as the Youngs modulus of the rock. Therefore, the rate of fracture

propagation is affected by both the injection water quality and the cooling of the reservoir by the injected fluids.

Figure 6 shows the injectivities for the three cases. The initial injectivity varies from 8 bpd/psi to between 3 to 4 bpd/psi. The vertical well has the smallest initial injectivity while the horizontal well with a longitudinal fracture has the highest injectivity. Once the fracture is initiated (early in the life of the injector) the injectivities remain fairly constant because the bottomhole pressure only needs to be maintained slightly above the minimum in-situ stress (as shown in Figure 5). Figure 6 also shows the distribution of flow between the horizontal well and the transverse fracture. Initially all the flow goes to the formation via the horizontal wellbore, however with a growing transverse fracture, more and more flow goes into the transverse fracture. For the other two cases, the vertical well and the horizontal well with a longitudinal fracture, virtually all the flow goes into the fracture.

One of the important conclusions one can arrive at based on the results presented in Figures 5 and 6 is that the injectivity of vertical and horizontal wells will be comparable if injection is conducted under fracturing conditions.

Three parameters (horizontal well length, water quality and reservoir thickness) are chosen for a sensitivity on fracture length and bottom-hole pressure for the longitudinal and transverse fracture growth cases.

6.5.1 Effect of Horizontal Well Length

Four horizontal well lengths (500 ft, 1000 ft, 2000 ft, and 3000 ft) were considered to show the effect of well length on transverse and longitudinal fracture growth. Other parameter values are listed in Table 12. Figure 7 shows the transverse fracture length and the longitudinal fracture length as a function of injection time. The longer horizontal well resulted in smaller fracture growth. The transverse fracture length varied from 180 ft to 240 ft for horizontal well lengths of 3000 ft to 500 ft respectively. The longitudinal fracture length varied from 6 ft to 50 ft for horizontal well lengths of 3000 ft to 500 ft.

6.5.2 Effect of Water Quality

A water quality of 1 ppm, 20 ppm, and 100 ppm solids concentration was considered to show the effect of water quality on transverse and longitudinal fracture growth. Figure 8 shows the transverse fracture length and the longitudinal fracture length as a function of injection time. Better water quality (1 ppm) resulted in smaller fracture growth. The transverse fracture length varied from 150 ft to 250 ft for water qualities from 1 ppm to 100 ppm. The longitudinal fracture length varied from 25 ft to 50 ft for water qualities from 1 ppm to 100 ppm.

6.5.3 Effect of Reservoir Thickness

Layer thicknesses of 50 ft, 100 ft, 200 ft, and 500 ft were considered in this sensitivity study. Figure 9 shows the transverse fracture length and the longitudinal fracture length as a function of injection time. A smaller layer thickness (50 ft) resulted in the longest fracture length as expected. The transverse fracture length varied from 10 ft to 900 ft as the layer thickness was varied from 500 ft to 50 ft. The longitudinal fracture length varied from 10 ft to the entire layer height.

6.5.4 Other Factors Affecting Injector Performance and Fracture Growth

All the parameters in Table 12 affect the injectivity and fracture growth in horizontal injectors. It is not possible to show sensitivity results for all the parameters due to space limitations, however, some of the trends are summarized below. The parameters that have the largest influence on injectivity and fracture growth in horizontal injectors (other than those discussed above) are: 1) reservoir permeability, 2) injection rate, 3) reservoir pressure at the start of injection, 4) injection water temperature, 5) injection fluid mobility, 6) particle size and external cake permeability.

High reservoir permeability will result in a lower initial BHP and higher injectivity. It will also result in a smaller rate of injectivity decline. Fractures will generally be initiated later and grow at a smaller rate compared to lower permeability reservoirs. In general smaller fractures are created in injection wells completed in higher permeability reservoirs.

Higher injection rates will result in a higher initial BHP but the same injectivity. However, a higher injection rate will result in more particles entering the formation and a faster injectivity decline until the minimum horizontal stress is reached. The injectivity of the fractured injector will be higher for higher injection rates because the BHP will remain close to the minimum horizontal stress and show a very weak dependence on the injection rate.

Injecting into a reservoir with a high initial reservoir pressure affects both the BHP and the minimum horizontal stress. A reservoir with a higher initial pore pressure has a higher minimum horizontal stress. As it depletes, the minimum horizontal stress also decreases. However, with every 1 psi decrease in pore pressure, a 0.7 psi decrease in minimum horizontal stress is expected (for typical values of Poisson's ratio). Injecting into a depleted reservoir will have lower long term injectivity than a reservoir with a higher reservoir pressure. The rate of fracture growth should, however, be independent of the reservoir pressure.

Lower injection water temperatures will result in thermal fracturing, i.e. rate of fracture growth will be higher (Saripalli et al 1999; Perkins and Gonzalez 1985). In some cases, the long term injectivities can become larger than the initial injectivity if the injection water temperature is much lower than the reservoir temperature.

Complicated injectivity behavior can be expected early in the life of the injector if the mobility of the injected fluid is significantly different than the mobility of the reservoir fluids. For example, injection of water into a high viscosity oil reservoirs or polymer injection. Higher injection fluid mobility will result in a decreasing BHP with time while solids plugging of the formation will increase the BHP. If a shear thinning polymer solution is injected, it will increase the BHP as the polymer goes further from the wellbore with shear rate reducing with wellbore distance. The result will be a faster rise in BHP and faster fracture growth.

The transverse fracture growth might be undesirable compared to a longitudinal fracture if the adjacent wells are producers. A transverse fracture may result in a high permeability channel between the two wells resulting in poor sweep of the reservoir. It is almost always expected that a transverse fracture will grow longer than a longitudinal fracture under the same injection conditions. Therefore simulations

presented in this paper are needed before deciding the horizontal injector orientation, length and injection rate.

The transverse fracture growth might be undesirable compared to a longitudinal fracture if the adjacent wells are producers. A transverse fracture may result in a high permeability channel between the two wells resulting in poor sweep of the reservoir. It is almost always expected that a transverse fracture will grow longer than a longitudinal fracture under the same injection conditions. Therefore simulations presented in this paper are needed before deciding the horizontal injector orientation, length and injection rate.

6.6 Conclusions

A model for fracture growth in horizontal injectors has been developed and presented. Only two extreme fracture growth orientations are considered (longitudinal and transverse). Most likely fractures will grow with an orientation between the two; however the two extreme cases provide bounds on the range of the fracture length with the longitudinal fracture length providing a lower bound and the transverse fracture an upper bound. It is clearly shown that the rate of fracture growth depends on the injection rate, water quality, well length, reservoir thickness and permeability, temperature, fluid mobility as well as the mechanical properties of the rock. The injectivity is primarily dependent on the in-situ stresses, injection rate and the water quality.

Estimating fracture lengths and injectivity as a function of injection time is crucial to the design of horizontal wells for water or polymer flooding since it can have a significant effect on expected injection rates, reservoir sweep and time to first oil. The model presented in this paper allows us, for the first time, to explore the dependence of fracture growth and injectivity on key reservoir and injection parameters.

6.6 Nomenclature (All variables are in SI units)

a_{cool}	Major axis of the thermal front ellipse
a_{cw}	Major axis of the connate water front ellipse
a_{inj}	Major axis of the injection fluid front ellipse
b_{cool}	Minor axis of the thermal front ellipse
b_{cw}	Minor axis of the connate water front ellipse
b_{inj}	Minor axis of the injection fluid front ellipse
C	Concentration of suspended particles
C_d	Volume of solids deposited per unit bulk volume of the porous medium
C_{gr}	Specific heat of rock grains
C_o	Specific heat of oil
C_w	Specific heat of water
d	Distance of the horizontal well from the center of the layer
E	Young's modulus
h	Formation thickness / layer thickness
h_c	Filter cake thickness
h_f	Fracture height
I	Injectivity
k_H	Horizontal permeability
$k_{H,damage}$	Near well damage permeability
k_V	Vertical permeability
k_f	Initial permeability of the formation
k_p	Power law coefficient for the injected fluid at injection temperature
k_{pr}	Power law coefficient for the injected fluid at reservoir temperature
k_{ro}	End point relative permeability to oil
k_{rw}	End point relative perm. to water
k_c	Permeability of external filter cake
L_d	Length of the damage zone
L_f	fracture length from wellbore to the tip
L_w	horizontal well length
n_p	Power law exponent for the injected fluid at injection temperature
n_{pr}	Power law exponent for the injected fluid at reservoir temperature
P_{frac}	Fracture propagation pressure
P_{tip}	Pressure at frac-pack tip
P_R	Reservoir Pressure at the boundary (re)
P_{wf}	Bottomhole pressure in the well
q	Total fluid injection rate into the well
q_f	Flow rate distributed into the transverse fracture
q_w	Flow rate from the horizontal well directly into the matrix ($q-q_f$)
r_e	Drainage radius
r_w	Well radius
R	Flow resistance, $\Delta p/q$
S	Skin factor
S_{or}	Residual oil saturation
S_{wi}	Initial Water Saturation
t	Time
t^*	Transition time
T_i	Injection fluid temperature

T_R	Reservoir temperature
u	Darcy velocity
U	Rock specific surface energy (~50 J/m^2)
V_{cool}	Volume of thermal front region
V_{cw}	Volume of connate water flood region
V_{inj}	Volume of injected fluid flood region
w_{fi}	Width of the fracture without cake
w_f	Width of the fracture with cake
Wi	Total volume of water injected up to time t

6.6.1 Greek symbols

α	Coefficient of thermal expansion
β_a	Perm. anisotropy factor, $(k_H/k_V)^{0.5}$
β_p	Coefficient of pore pressure expansion
ϕ	Porosity
ϕ_c	External cake porosity
λ_f	Filtration coefficient of the formation
μ_w	Viscosity of water
μ_o	Viscosity of oil
ν	Poisson's ratio
ρ_w	Density of water
ρ_o	Density of oil
ρ_{gr}	Density of mineral grains
$\sigma_{H,min}$	Minimum horizontal stress
ΔP_1	Pressure drop between the connate water front and the drainage boundary
ΔP_2	Pressure drop between the injected fluid front and the connate water front
ΔP_3	Pressure drop between the thermal front and the injected fluid front
ΔP_4	Pressure drop from the fracture tip to the thermal front
ΔP_f	Pressure drop from the well to the fracture tip
ΔT	Temperature difference between the injected fluid and the reservoir
$\Delta\sigma_T$	Thermoelastic stress perpendicular to the fracture
$\Delta\sigma_P$	Poroelastic stress perpendicular to the fracture

6.7 References

1. Perkins, T.K. and Gonzalez, J.A. 1985. The Effect of Thermoelastic Stresses on Injection Well Fracturing. SPE Journal, February, 78-88.
2. Saripalli, K.S.; Gadde, P.B.; Bryant, S. L. and Sharma. M.M. 1999. Role of Fracture Face and Formation Plugging in Injection Well Fracturing and Injectivity Decline," presented at the 1999 SPE/EPA Exploration and Production Environmental Conference, SPE 52731, Austin, Texas, February 28- 3 March.
3. Wei, Y. and Economides, M.J. 2005. Transverse Hydraulic Fractures from a Horizontal Well. Paper SPE 94671 presented at the ATCE held in Dallas, Texas, U.S.A. 9-12 October.
4. Joshi, S.D. 1988. Augmentation of Well Productivity with Slant and Horizontal Wells. JPT, June 1988.
5. Economides, M.J. et al. 1991. Comprehensive Simulation of Horizontal-Well Performance. SPE Formation Evaluation, December.
6. Suárez-Rivera, R. et al. 2002. An Experimental Investigation of Fracture Propagation during Water Injection. Paper SPE 73740 presented at the SPE International Symposium and Exhibition on Formation Damage Control, Lafayette, Louisiana, 20–21 February.
7. Economides, M.J. and Nolte, K.G.: "Reservoir Stimulation", Second Edition, Prentice Hall, Englewood Cliffs, New Jersey 07632, 1989, Section 19-6.2, Pg. 19-22.
8. Lake, L.W. 1989. *Enhanced Oil Recovery*, published by Prentice-Hall Inc. Pg. 324.
9. Perkins, T.K. and Kern, L.R. 1961. Widths of Hydraulic Fractures. SPE 89-PA.

6.8 Appendix

A.1 Asymmetric Fracture Growth of a Longitudinal Fracture

Asymmetric fracture growth of a longitudinal fracture is modeled as follows. The horizontal well is assumed to have two different flow resistances for the flow upwards and for the flow downwards based on the length of the fracture in up and down directions. If the fracture has the same length in up and down direction then the flow resistances are equal in up and down direction. This would be the case if the minimum horizontal stress is the same in both the up and down direction. Note all the other reservoir and fluid properties above and below the horizontal well are assumed to be equal.

$$\sigma_{h\min updip} = \sigma_{h\min well} - L_{fup}\sin\theta\,(d\sigma_{h\min}/dh)$$

$$\sigma_{h\min downdip} = \sigma_{h\min well} + L_{fdown}\sin\theta\,(d\sigma_{h\min}/dh)$$

Where θ is the angle of the fracture growth with the horizontal. Note: It may or may not be the same to the layer dip depending upon the fracture orientation.

To model the fracture growth in the upward and downward direction of the horizontal well, it is assumed that there are two layers. The two layers have the same properties as that of the actual layer in which the horizontal well is. One layer has the minimum horizontal stress increasing with distance from the well and the other layer has the minimum horizontal stress decreasing with distance from the well. The flow rate into each layer is distributed according to its total resistance. At time, t = 0, the flow rate into each layer is the total initial flow rate in the horizontal well. The fracture will grow longer in the layer with decreasing minimum horizontal stress and shorter in the layer with increasing minimum horizontal stress. Therefore, the resistance of the layer with the longer fracture length will be less than the resistance of the layer with the shorter fracture length. The flow rate from the total flow rate for the two layers (twice the initial total flow rate into each layer) is then distributed according to the layer resistances as follows:

$$q_{layer} = \left(R_{tot}/R_{layer}\right)q_{tot}$$

where q_{layer} is the flow into each layer, q_{tot} is twice the total initial injection rate, Rlayer is the flow resistance of the layer and Rtot is the total flow resistance. The total flow resistance is expressed as,

$$R_{tot} = 1\Big/\sum_{1}^{N_l}\frac{1}{R_{layer}}$$

A.2 Polymer Injection

When a polymer solution is injected into the formation, it results in a change in the flow resistances. The flow resistances change because of changes in the fluid viscosity and because of suspended particles depositing on the rock grains and changing the permeability.

It is assumed that most polymer solutions can be approximated by power law rheology, with the apparent viscosity given as follows:

$$\mu = K_p(\dot{\gamma})^{n_p-1}$$

Where μ is the polymer solution viscosity, Kp is the power-law coefficient, $\dot{\gamma}$ is the shear rate, and n_p is the power-law exponent. For a Newtonian fluid np is equal to 1. For fluids whose viscosity decreases with increasing shear rate (i.e. shear thinning fluids), $0 < n_p < 1$. A typical polymer solution developed for polymer flooding can have power-law coefficient and exponent values of, $n_p = 0.5$ and $k_p = 100$ cp.sec^{np-1}.

The shear rate in a porous medium with two phases (polymer solution and the oil phase) can be calculated based on the capillary tube model as shown by Hirasaki and Pope (1974):

$$\dot{\gamma} = \left[\frac{1+3n_p}{n_p}\right]\frac{u}{\sqrt{8kk_{rw}\phi S_w}}$$

Substituting this in the above equation for the shear rate, we get the viscosity of the polymer solution as a function of Darcy velocity (u) as shown below (Ref. 8):

$$\mu = H_p(u)^{n_p-1}$$

Where,

$$H_p = K_p\left[\frac{1+3n_p}{n_p}\right]^{n_p-1}\left(8kk_{rw}\phi S_w\right)^{(1-np)/2}$$

A.3 Pressure drop along the fracture

The pressure drop from the well to the fracture tip with a uniform leak-off rate from the face of the fracture into the matrix can be calculated using equations presented by Perkins and Kern (1961):

$$\Delta P_f = 1.26\left[\frac{q\mu L_f E^3}{(1-\nu^2)^3 l_w{}^4}\right]^{0.25}$$

Where q is the total injection rate, μ is the polymer solution viscosity, Lf is the fracture length in the upward or downward direction, E is the Young's modulus of the formation, l_w is the horizontal well length, and ΔPf is the pressure drop from the wellbore to the fracture tip. Perkins and Gonzalez (1985) presented and used the above equation in their model to calculate the total pressure drop between the well and the fracture tip. If no leak-off is assumed, the coefficient value changes from 1.26 to 1.50 resulting in a larger pressure drop (see Appendix A for a derivation).

A uniform leak-off rate from the fracture faces results in the following flow rate in the fracture:

$$q_x = q(1-x/L_f)$$

It is assumed that all the flow that enters the fracture leaks-off from the two fracture faces and that the flow rate is zero at the fracture tip. This is an approximation resulting from our assumption of constant leakoff.

For turbulent flow of a power-law fluid in a fracture with no leak-off:

$$\Delta P_f = \left[\frac{16}{3\pi}\frac{(2n_p+1)^{n_p}(n_p+1)q^{n_p}k_pL_fE^{2n_p+1}}{n_p{}^{n_p}2^{2n_p-1}(1-\nu^2)^{2n_p+1}l_w{}^{3n_p+1}}\right]^{\frac{1}{2n_p+2}}$$

Where k and n are the power-law coefficient and exponent. Here q is the total injection rate in the well which is equal to twice the flow rate entering each fracture wing. Considering uniform leak-off with flow distribution in the fracture given by q_x, the total pressure drop can be shown to be equal to:

$$\Delta P_f = \left[\frac{16}{3\pi}\frac{(2n_p+1)^{n_p}q^{n_p}k_pL_fE^{2n_p+1}}{n_p{}^{n_p}2^{2n_p-1}(1-\nu^2)^{2n_p+1}l_w{}^{3n_p+1}}\right]^{\frac{1}{2n_p+2}}$$

The decrease in the pressure drop because of a uniform leak-off assumption for a shear thinning fluid is less as compared to a Newtonian fluid. This is because np<1 for a shear thinning fluid and np=1 for a Newtonian fluid.

For the fracture growth model in a horizontal well, an equivalent fracture is assumed to represent the horizontal well. The equivalent fracture length is calculated by equating the horizontal wellbore surface area and the equivalent four fracture faces area.

$$A_f = 4 l_f l_w$$

Where Af is the total fracture face area, lf is the distance from the wellbore to the fracture tip, and lw is the horizontal well length. The horizontal wellbore surface area is equal to:

$$A_w = 2\pi r_w l_w$$

Equating the above two equations, we can calculate the equivalent well fracture length given as:

$$l_f = \pi r_w / 2$$

The equivalent fracture now represents the horizontal wellbore and it is assumed that all the flow enters the fracture and then leaks-off into the formation. The flow is linear in the fracture with uniform leak-off into the matrix.

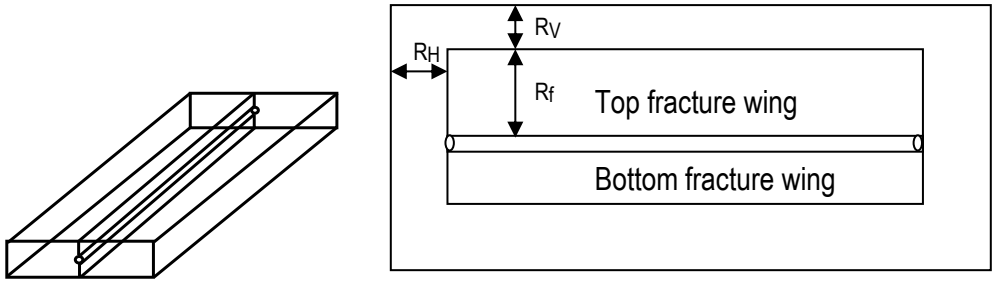

Figure 1: A schematic of a horizontal well with a longitudinal fracture. The upward wing could be longer than the downward wing as shown in the right schematic.

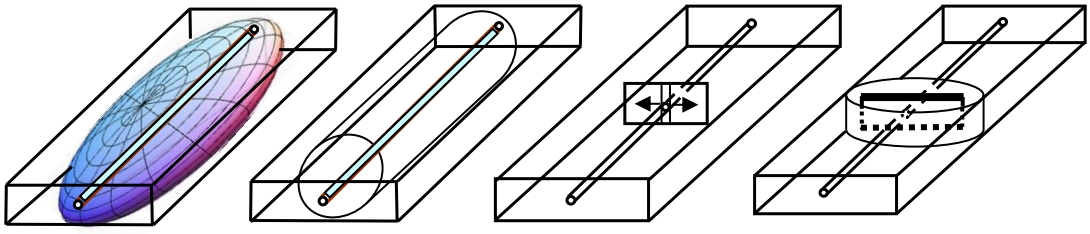

Figure 2: A schematic of a horizontal well with ellipsoidal and approximated cylindrical flow. The right two figures show a transverse fracture with elliptical flow around.

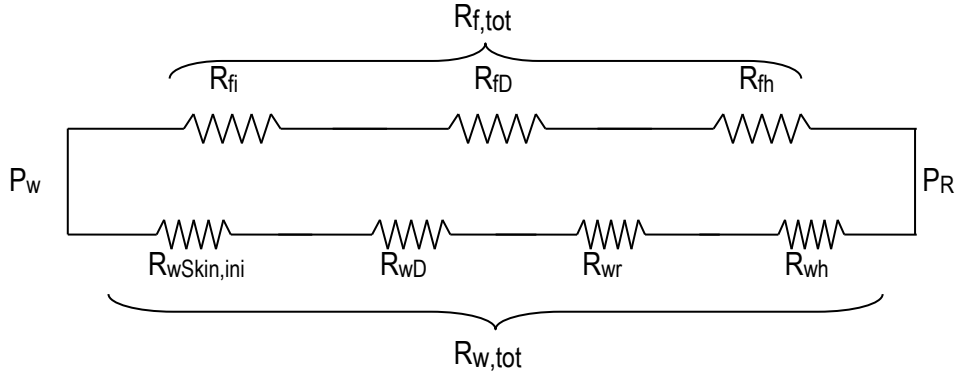

Figure 3: The flow resistances in a horizontal well with a transverse fracture. The horizontal well flow resistance is added in parallel to the transverse fracture flow resistance.

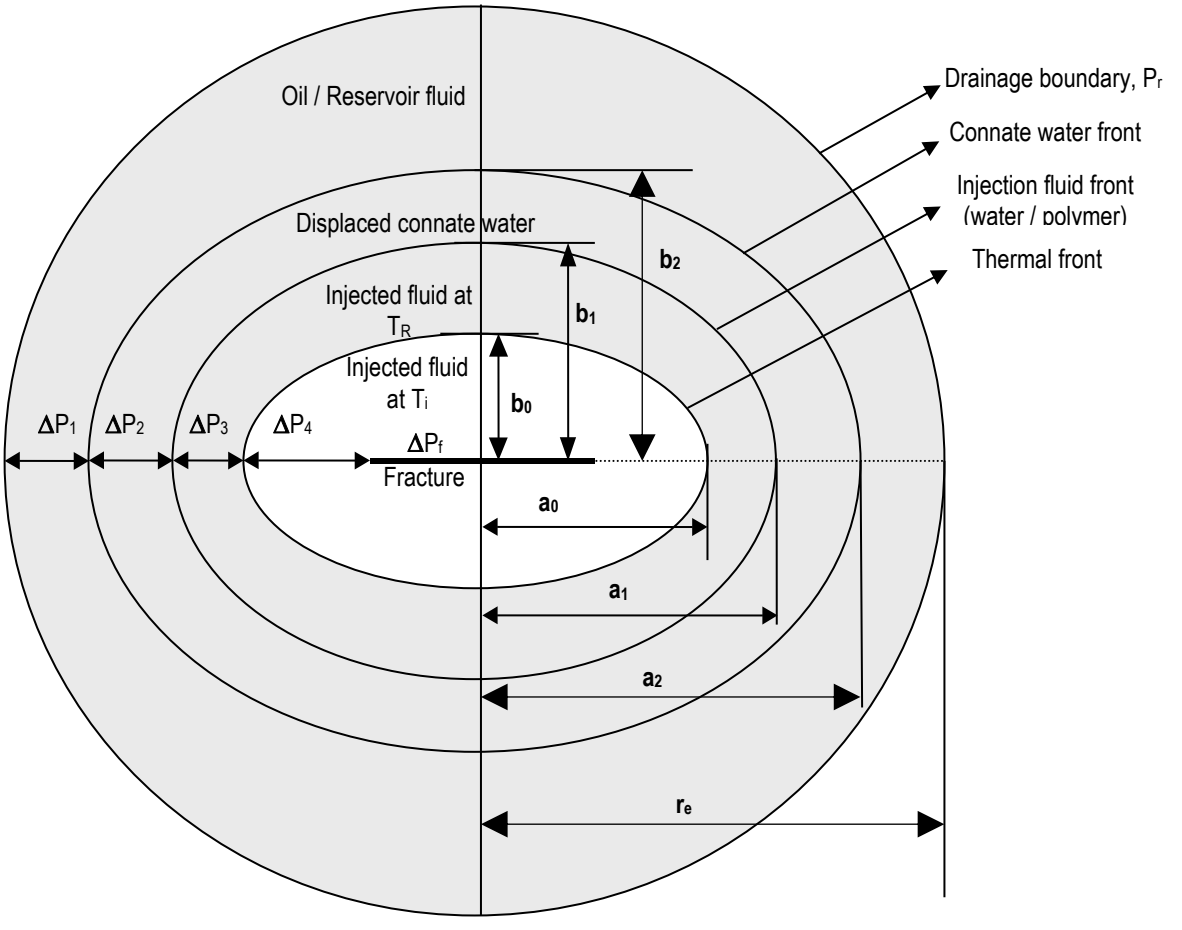

Figure 4: The elliptical fluid regions and fronts around a fractured injection well.

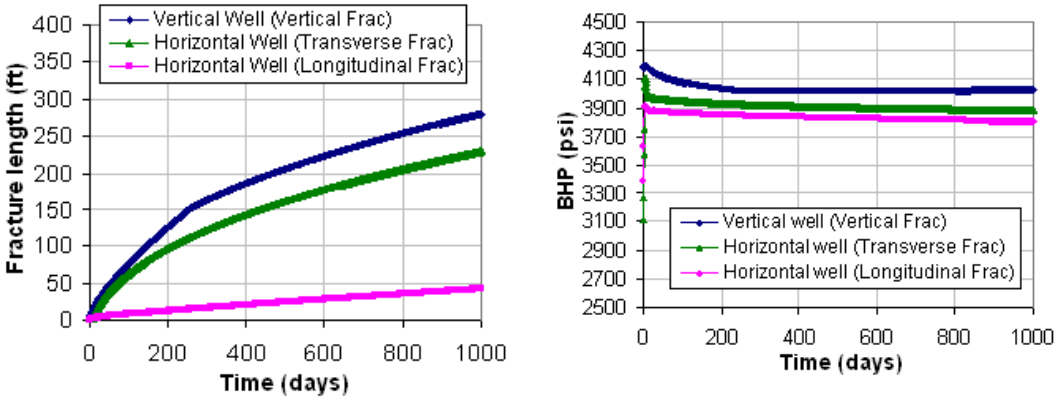

Figure 5: Comparison of the growth of the fracture and the bottomhole pressure between a vertical injection well, a horizontal well with a longitudinal fracture orientation, and a horizontal well with a transverse fracture orientation.

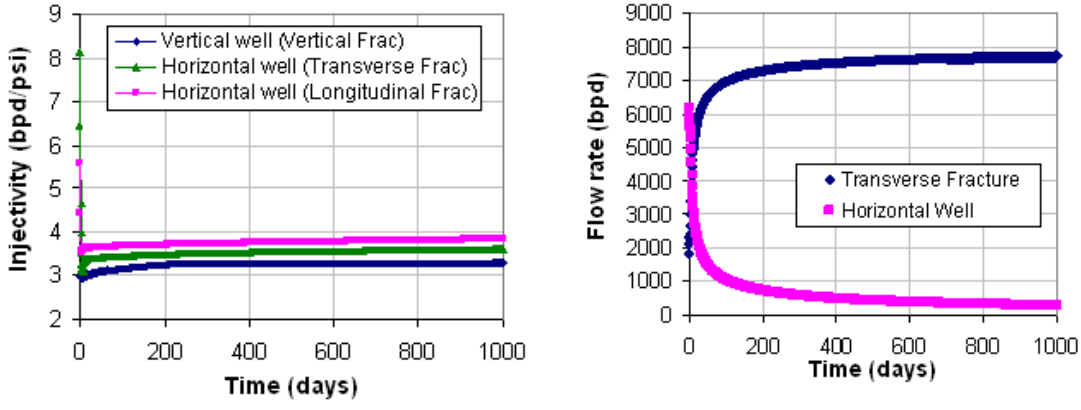

Figure 6: Injectivity in a vertical injector getting fractured, a horizontal well with a longitudinal fracture, and a horizontal well with a transverse fracture. The figure on the right shows the flow distribution between a horizontal well with a transverse fracture. In case of longitudinal fracture growth and a vertical fracture growth in a vertical well, all the flow is assumed to go into the fracture.

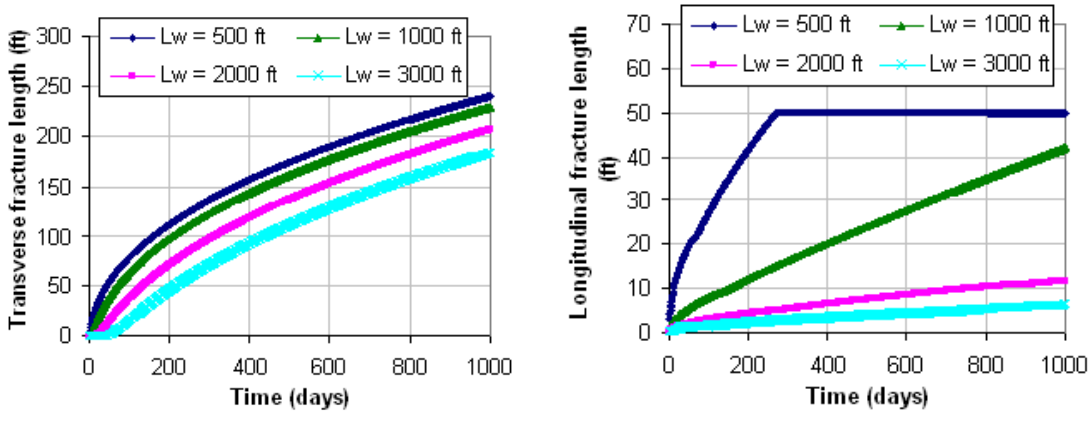

Figure 7: Effect of horizontal well length on the transverse fracture length and the longitudinal fracture length.

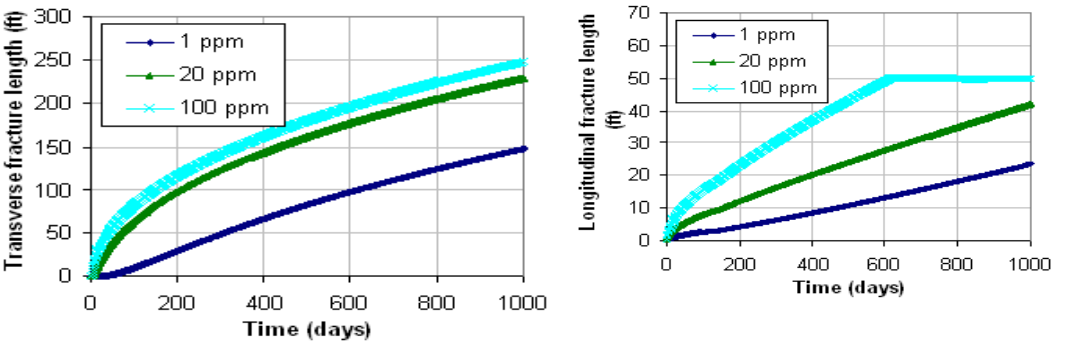

Figure 8: Effect of water quality on the transverse fracture length and the longitudinal fracture length.

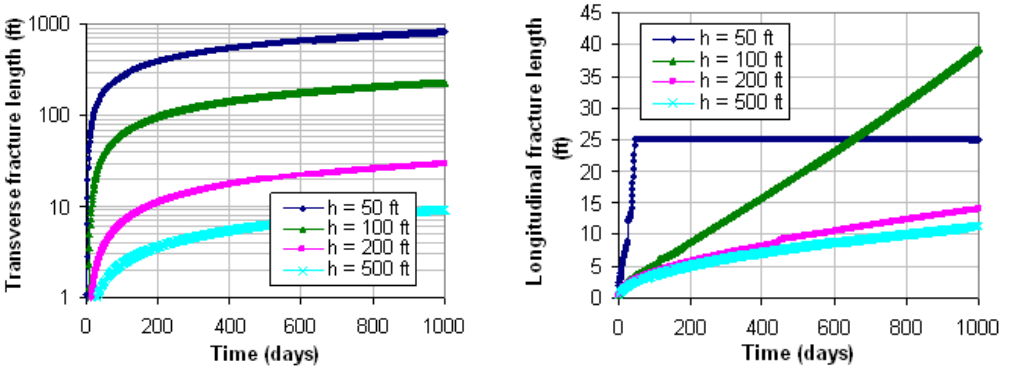

Figure 9: Effect of layer thickness on the transverse fracture length and the longitudinal fracture length.

Table 1: Near well / vertical flow resistance for a horizontal well with a longitudinal fracture.

The vertical flow resistance between the vertical bounds of the layer and the displaced connate water front ellipse:

$$R_{V1} = \frac{\mu_o \beta_a}{2\pi k_H k_{ro} L_w} \ln\left[\left[\left\{\frac{\beta_a h}{(\beta_a+1)}\right\}^2 + \beta_a{}^2 d^2\right] \Big/ \left[\frac{\beta_a h (a_{cw}+b_{cw})/2}{(\beta_a+1)}\right]\right]$$. Until

$$(a_{cw}+b_{cw}) < h \text{ else = 0}$$

The vertical flow resistance between the displaced connate water front ellipse and the injected fluid ellipse:

$$R_{V2} = \frac{\mu_w \beta_a}{2\pi k_H k_{rw} L_w} \ln\left[\frac{(a_{cw}+b_{cw})}{(a_{inj}+b_{inj})}\right]$$ Until $(a_{inj}+b_{inj}) < h$ else = 0

The vertical flow resistance between the injection fluid ellipse and the thermal ellipse:

$$R_{V3} = \frac{q^{n_{pr}-1} H_{pR} \beta_a}{(2\pi l_w)^{n_{pr}} k_H k_{rw}} \frac{\left[\left[(a_{inj}+b_{inj})/2\right]^{1-n_{pr}} - \left[(a_{cool}+b_{cool})/2\right]^{1-n_{pr}}\right]}{(1-n_{pr})}$$

Until $(a_{cool}+b_{cool}) < h$ else = 0

The vertical flow resistance between the thermal ellipse and the fracture tip is:

$$R_{V4} = \frac{q^{n_p-1} H_p \beta_a}{(2\pi l_w)^{n_p} k_H k_{rw}} \frac{\left[\left[(a_{cool}+b_{cool})/2\right]^{1-n_p} - (L_f/2)^{1-n_p}\right]}{(1-n_p)}$$

Note: The front axes (major and minor) values are calculated using Table 6. If the sum of axes is found > h, then the sum is replaced by h. H_{PR} and H_P are provided in Table 3.

Table 2: Far field horizontal flow resistance for a horizontal well.

The horizontal flow resistance between the constant pressure drainage boundary and the connate water front is:

$$R_{H1} = \frac{\mu_o}{2\pi k_H k_{ro} h} \ln\left(\frac{a+\sqrt{a^2-(L_w/2)^2}}{a_{cw}+b_{cw}}\right)$$ Until

$$(a_{cw}+b_{cw}) < a+\sqrt{a^2-(L_w/2)^2} \text{ else = 0}$$

The horizontal flow resistance between the displaced connate water front ellipse and the injected fluid ellipse:

$$R_{H2} = \frac{\mu_w}{2\pi k_H k_{rw} h} \ln\left(\frac{a_{cw}+b_{cw}}{a_{inj}+b_{inj}}\right)$$

The horizontal flow resistance between the injection fluid ellipse and the thermal ellipse:

$$R_{H3} = \frac{q_w{}^{n_{pr}-1} H_{pR}}{(2\pi h)^{n_{pr}} k_H k_{rw}} \frac{\left[\left[a_{inj}+b_{inj})/2\right]^{1-n_{pr}} - \left[(a_{cool}+b_{cool})/2\right]^{1-n_{pr}}\right]}{(1-n_{pr})}$$

The horizontal flow resistance between the thermal ellipse and the ends of the horizontal well:

$$R_{H4} = \frac{q_w^{\,n_p-1} H_p}{(2\pi h)^{n_p} k_H k_{rw}} \frac{\left[\left[(a_{cool}+b_{cool})/2\right]^{1-n_p} - (L_w/4)^{1-n_p}\right]}{(1-n_p)}$$

Note: The axes values are calculated using Table 7. The sum of major and minor axes of all the horizontal fronts can be maximum = $a+\sqrt{a^2-(L_w/2)^2}$ and minimum = $L_w/2$. a and β_a are provided in Table 3.

Table 3: Some terms used in Table 1 and 2.

$$H_{pR} = K_{pR}\left[\frac{1+3n_{pR}}{n_{pR}}\right]^{n_{pR}-1}\left(\frac{8k_H k_{rw}\phi(1-S_{or})}{\beta_a}\right)^{\frac{(1-n_{pR})}{2}};$$

$$H_p = K_p\left[\frac{1+3n_p}{n_p}\right]^{n_p-1}\left(\frac{8k_H k_{rw}\phi(1-S_{or})}{\beta_a}\right)^{\frac{(1-n_p)}{2}}$$

$$a = \frac{L_w}{2}\left(\frac{1}{2}+\sqrt{\frac{1}{4}+\frac{1}{(0.5L_w/r_e)^4}}\right)^{0.5};\ \beta_a = \sqrt{\frac{k_H}{k_V}}$$

Table 4: Flow resistance for the damage in and around the fracture (cake and reduced near well perm).

$$R_{fd} = \frac{q^{n_p-1}}{(4l_f h_f)^{n_p} k_{rw}}\left[\int_0^{L_d}\frac{H_{pD}dx}{k_{Hdamage}(x)} - \frac{H_p L_d}{k_H}\right];$$

$$H_{pD} = K_p\left[\frac{1+3n_p}{n_p}\right]^{n_p-1}\left(8k_{Hdamage}(x)k_{rw}\phi\right)^{\frac{(1-n_p)}{2}}$$

$$R_{fc} = \frac{q^{n_p-1}H_p}{(4l_f h_f)^{n_p}}\frac{h_c}{k_c};\ H_p = K_p\left[\frac{1+3n_p}{n_p}\right]^{n_p-1}\left(8k_c\phi_c\right)^{\frac{(1-n_p)}{2}}$$

Note: The fracture height h_f is equal to the thickness of the layer for transverse fracture and length of the horizontal well for longitudinal fracture. The flow rate q is equal to q_f for damaged transverse fracture.

Table 5: Flow resistance for flow with in the fracture.

$$R_{fi} = \left[\frac{16}{3\pi} \frac{(2n_p+1)^{n_p}(n_p+1)k_p L_f E^{2n_p+1}}{{n_p}^{n_p} 2^{2n_p-1}(1-\nu^2)^{2n_p+1} {h_f}^{3n_p+1}} \right]^{\frac{1}{2n_p+2}} q^{-\left[\frac{n_p+2}{2n_p+2}\right]};$$

$$w_{fi} = \frac{2(1-\upsilon^2)h_f}{E} q * R_{fi}$$

For $h_c > 0$ $\quad R_f = \frac{w_f E}{2(1-\upsilon^2)h_f} \frac{1}{q}; w_f = w_{fi} + 2h_c$

Note: The fracture height h_f is equal to the thickness of the layer for transverse fracture and length of the horizontal well for longitudinal fracture. The flow rate q is equal to q_f for the transverse fracture.

Table 6: Distance of elliptical and radial fronts.

$$a=\frac{L_f}{2}\left(\sqrt{X_1}+\frac{1}{\sqrt{X_1}}\right);b=\frac{L_f}{2}\left(\sqrt{X_1}-\frac{1}{\sqrt{X_1}}\right);X_1=\frac{2V}{\pi {L_f}^2 h_f}+\frac{1}{2}\sqrt{\left(\frac{4V}{\pi {L_f}^2 h_f}\right)^2+4};r=\sqrt{{r_w}^2+\frac{V}{\pi l_w}}$$

$$V_{cw}=\frac{\int qdt}{\phi(1-S_{or}-S_{wi})};V_{inj}=\frac{\int qdt}{\phi(1-S_{or})};V_{cool}=\frac{\rho_w C_w\int qdt}{\rho_{gr}C_{gr}(1-\phi)+\rho_w C_w\phi(1-S_{or})+\rho_o C_o\phi S_{or}}$$

Note: a, b, r, and V are in general form; for specific front, its volume will be used to calculate it's a, b or r. The fracture height is equal to the thickness of the layer for transverse fracture and length of the horizontal well for longitudinal fracture growth. The flow rate for the front calculation in case of horizontal well with a transverse fracture will be q_w and q_f.

Table 7: Fronts major and minor axes in the horizontal directions.

$a=0.5\sqrt{L_w V/h^2}$; $b=0.5\sqrt{V/L_w}$; if $a\geq L_w/2$ and $b\geq h/2$ else

$a=L_w/2$ and $b=h/2$ .....

Note: a, b, and V are in general form; for specific front, its volume will be used to calculate it's a and b in the horizontal direction along the horizontal well. The fracture height is equal to the thickness of the layer for transverse fracture and length of the horizontal well for longitudinal fracture growth.

Table 8: Change in minimum horizontal stress due to thermal and pore pressure changes.

$$\frac{(1-\nu)}{E\beta_p\Delta p}\Delta\sigma_{1p}=\frac{(b_{cool}/a_{cool})}{1+b_{cool}/a_{cool}}+\left(\frac{1}{1+b_{cool}/a_{cool}}\right)\left[1+0.5\left\{1.45\left(\frac{L_f}{2b_{cool}}\right)^{0.9}+0.35\left(\frac{L_f}{2b_{cool}}\right)^2\right\}\left\{1+\left(\frac{b_{cool}}{a_{cool}}\right)^{0.774}\right\}\right]^{-1}$$

$$\beta_p=\frac{1-2\nu}{E}-\frac{c_{gr}}{3};$$

For Longitudinal fracture case: $\Delta p=q\left[R_{V1}+R_{H1}+R_{V2}+R_{H2}+R_{V3}+R_{H3}+(R_{V4}+R_{H4})/2\right]$;

For Transverse fracture case: $\Delta p=q(R_{fh1}+R_{fh2}+R_{fh3}+R_{fh4}/2)$;

$\Delta T=T_R-T_i$

$$\frac{(1-\nu)}{E\alpha\Delta T}\Delta\sigma_{1T}=\frac{(b_{cool}/a_{cool})}{1+b_{cool}/a_{cool}}+\left(\frac{1}{1+b_{cool}/a_{cool}}\right)\left[1+0.5\left\{1.45\left(\frac{L_f}{2b_{cool}}\right)^{0.9}+0.35\left(\frac{L_f}{2b_{cool}}\right)^2\right\}\left\{1+\left(\frac{b_{cool}}{a_{cool}}\right)^{0.774}\right\}\right]^{-1}$$

Table 9: Damage flow resistance for the horizontal well with a transverse fracture growth case.

$$R_{\text{int}_w} = \frac{{q_w}^{n_p-1}\beta_a}{(2\pi l_w)^{n_p} k_{rw}} \int_{r_w}^{r_d} \frac{H_{pD}dr}{k_{Hdamage}(r)\, r^{n_p}};$$

$$H_{pD} = K_p \left[\frac{1+3n_p}{n_p}\right]^{n_p-1} \left(8k_{Hdamage}(x)k_{rw}\phi(1-S_{or})/\beta_a\right)^{\frac{(1-n_p)}{2}}$$

$$R_{cc_w} = \frac{{q_w}^{n_p-1}H_p}{(2\pi l_w)^{n_p} k_c} \frac{\left[{r_w}^{1-n_p} - {r_c}^{1-n_p}\right]}{(1-n_p)};$$

$$H_p = K_p \left[\frac{1+3n_p}{n_p}\right]^{n_p-1} \left(8k_c\phi_c\right)^{\frac{(1-n_p)}{2}}$$

Table 10: Radial and far field horizontal flow resistance for a horizontal well with transverse fracture growth case.

R_{wr1} is the radial flow resistance between the connate water front and the boundary of the layer:

$$R_{wr1} = \frac{\mu_o\beta_a}{2\pi k_H k_{ro} L_w} \ln\left[\left[\left\{\frac{\beta_a h}{(\beta_a+1)}\right\}^2 + {\beta_a}^2 d^2\right] \Big/ \left[\frac{\beta_a h r_{cw}}{(\beta_a+1)}\right]\right]$$

R_{wr2} is the radial flow resistance between the injected fluid front and the displaced connate water front:

$$R_{wr2} = \frac{\mu_w\beta_a}{2\pi k_H k_{rw} L_w} \ln\left[\frac{r_{cw}}{r_{inj}}\right]$$

R_{wr3} is the radial flow resistance between the thermal front and the injected fluid front:

$$R_{wr3} = \frac{{q_w}^{n_{pR}-1}H_{pR}\beta_a}{(2\pi l_w)^{n_{pR}} k_H k_{rw}} \frac{({r_{inj}}^{1-n_{pR}} - {r_{cool}}^{1-n_{pR}})}{(1-n_{pR})}$$

R_{wr4} is the radial flow resistance between the horizontal well and the thermal front:

$$R_{wr4} = \frac{{q_w}^{n_p-1}H_p\beta_a}{(2\pi l_w)^{n_p} k_H k_{rw}} \frac{({r_{cool}}^{1-n_p} - {r_d}^{1-n_p})}{(1-n_p)}$$

$$R_{whi} = R_{Hi} \quad \text{where i goes from 1 to 4}$$

Table 11: Flow resistance for the transverse fracture in a horizontal well

The flow resistance between the constant pressure boundary and the connate water front is:

$$R_{fh1} = \frac{\mu_o}{2\pi k_H k_{ro} h} \ln\left(\frac{2r_e}{a_{cw} + b_{cw}}\right)$$

The flow resistance between the connate water front and the injection fluid front is:

$$R_{fh2} = \frac{\mu_w}{2\pi k_H k_{rw} h} \ln\left(\frac{a_{cw} + b_{cw}}{a_{inj} + b_{inj}}\right)$$

The flow resistance between the injected fluid front and the thermal front ellipse is:

$$R_{fh3} = \frac{{q_f}^{n_{pR}-1} H_p}{(2\pi h)^{n_{pR}} k_H k_{rw}} \frac{\left[\left[(a_{inj} + b_{inj})/2\right]^{1-n_{pR}} - \left[(a_{cool} + b_{cool})/2\right]^{1-n_{pR}}\right]}{(1-n_{pR})} \quad \text{.....}$$

The flow resistance between the thermal ellipse and the transverse fracture is:

$$R_{fh4} = \frac{{q_f}^{n_p-1} H_p}{(2\pi h)^{n_p} k_H k_{rw}} \frac{\left[\left[(a_{cool} + b_{cool})/2\right]^{1-n_p} - (L_f/2)^{1-n_p}\right]}{(1-n_p)}$$

Table 12: Input parameters for simulation of water injection into vertical and horizontal wells.

$k_{formation}$	100 md	S_{wi}	0.3
r_e	5000 ft	S_{or}	0.3
r_w	3 inch	k_{rw}^o	0.2
Q_T	8000 bpd	k_{ro}^o	0.6
dp	5 micron	μ_w	1.1 cp (60 F) 0.49 cp (140 F)
c_0	20 ppm	μ_o	1 cp
h	100 ft	ϕ_f	0.2
P_R	2500 psi	ϕ_c	0.2
σ_{hmin}	4000 psi	k_c	0.01 md
ν	0.2	$d_{formation\ grains}$	141 microns
E	1.45 * 10^6 psi	$\lambda_{f\ vwell}$	1056 1/m (calc. by the program)
T_w	60 F	$\lambda_{f\ hwell}$	4004 1/m (calc. by the program)
T_R	140 F	L_w	1000 ft

Chapter 7: Injection into Frac-Packed Wells

7.1 Introduction

Description of the material
A model is presented for predicting the injectivity of water injection wells with frac-packed completions. The model estimates the plugging of the frac-pack by solids in the injected water. The model considers changes in the minimum horizontal stress due to cold water injection and pore pressure increase to calculate the critical pressure that leads to widening of the frac-pack.

Application
Frac-packs are increasingly being used for sand control in injection wells in poorly consolidated reservoirs. This completion allows for large injection rates and longer injector life. Many of the large off-shore developments in the Gulf of Mexico and around the world rely on these completions for water flooding and pressure maintenance. The performance of these injectors is crucial to the economics of the project since well intervention later in the life of the field is expensive and undesirable.

Results, Observations, and Conclusions
Injectivity is shown to depend on the solids content in the injected water, injection rate, injection water temperature, size of proppants in the frac-pack, width and length of the frac-pack, and the minimum horizontal stress. In case of wide frac-packs with large proppants, the plugging of the frac-pack is expected to be gradual while in case of narrow frac-packs with small proppants, significant plugging is expected with a rapid rise in the bottom-hole pressure due to a sharp permeability decline in the frac-pack. In both cases, after years of injection, we believe that the frac-packs will widen which will alleviate the injectivity decline thereafter.

Significant New Contributions
A model for water injection into frac-packed wells is presented for the first time. It estimates the plugging of the frac-pack and the formation around it, thermal stresses caused by cold water injection and frac-pack widening.

Background and Problem Description

All injected fluids contain suspended particles, which can potentially plug the formation around a well. This reduces the permeability in the near-wellbore region and causes a rise in the injection pressure to maintain a constant injection rate. When the injection pressure exceeds fracture pressure, fractures are initiated. Subsequently, the face of the fracture gets plugged with continued injection, and the pressure at the fracture tip exceeds the fracture propagation pressure and the fracture extends in length (Suárez-Rivera, et al. 2002, and Saripalli, et al. 1999). The particle plugging and fracture propagation are coupled. In addition, if the injected fluid is colder than the reservoir, thermal stresses are induced, which lower the fracture propagation pressure significantly and may cause thermally induced fractures.
There are no models and little field data (McCarty, et al. 2006) published on the injection performance of frac-packed wells. Frac-packing is widely used in production wells but

recently many water injectors have used frac-pack completion technology as well. Some of the advantages of frac-packing in water injectors are:

1. It provides a resilient and robust long term completion with minimum intervention required, especially in sub-sea wells.
2. It provides sand control if the formation is poorly consolidated.
3. It minimizes plugging of the injection well by providing a larger permeability and flow area in comparision to perforated completions or gravel pack completions.
4. Larger injection rates are possible.

McCarty et al. (2006) have documented the utilization of frac-pack completion technology for water injectors in sand control environments. They observed no sand control failures in frac-packed injectors for more than five years.

7.2 Model Formulation

In developing the model the following assumptions are made:

1. The reservoir is layered and isotropic. No vertical flow is allowed within and between the layers.
2. The frac-packed reservoir has a set of hydraulic fractures packed with proppant which are contained within each injection layer with communication with other layers only at the wellbore.
3. Both the injected fluid and the reservoir fluids are incompressible i.e. remain at constant density.
4. Darcy's law (Reynold's number < =1) is assumed both in the reservoir and the frac-pack.
5. Fluid is injected at a constant rate into the well which then distributes into the frac-pack and the formation.
6. The displacement of fluids in the reservoir is piston-like. The oil saturation becomes residual in the waterflooded region while remains at the initial oil saturation ahead of the water-flood front.
7. Heat conduction to overlying and underlying formations is neglected. This is a good assumption since the process is convection dominated and the contact area between the fracture and the layers above and below is small.
8. The gravel size in the frac-pack and the grains in the formation are represented by a mean size.
9. An equi-pressure elliptical boundary encloses the frac-pack who's major and minor axes are obtained from solutions presented by Prats (1960). The equi-pressure ellipse axes remain constant with continued injection.

The full model includes the following basic elements:

- A model for pressure profile and flow distribution in and around a frac-packed well.
- A model for particle deposition and permeability decline in the frac-pack and the adjacent formation due to deposition of solids, bacteria, and/or oil particles in the injected water on the formation grains and proppant in the frac-pack.
    - A model for changes in minimum horizontal stress induced by changes in temperature and pore pressure from the injection water.
    - A model for estimating the widening of the existing frac-pack.

- Finally these models are coupled together explicitly for estimating the change in injectivity of the frac-pack with time.

7.2.1 Pressure Profile and Flow Distribution around a Frac-Packed Well

A model for pressure profile and flow distribution in and around a frac-packed well is formulated using a resistor model with bilinear flow bounded by an equi-pressure ellipse.

Prats (1960) presented a steady state solution for pressure distribution around a fractured well. Equi-pressure lines were determined by a parameter, "a", and a dimensionless length defined as r_e/L_{fp}. The parameter "a" was defined as:

$$a = \frac{\pi k_f L_{fp}}{2 k_{fp} w_{fp}} \quad \text{..... (1)}$$

Where k_f is the formation permeability, L_{fp} is the length of the frac-pack (distance from the wellbore to the frac-pack tip), k_{fp} is the permeability of the frac-pack, and w_{fp} is the average width of the frac-pack. Figure 2 shows the equi-pressure lines around the frac-pack for five values of "a" (0, 0.1, 1, 10, and infinity) and for r_e/L_{fp} = 2.4. The extreme values for "a" are (a=0) which mimics an infinitely conductive fracture and (a=infinity) which mimics a fracture with zero permeability. A typical value of "a" will be less than 1 for frac-packs in low permeability formations. However, in highly permeable formations, the value of "a" could be significantly larger. The pressure distribution for a>100 will be nearly the same as that for radial flow. For (a=0), there is no pressure drop in the fracture and the equi-pressure lines away from the fracture are confocal ellipses (with foci = $-L_{fp}$ and L_{fp}). For infinite a, the equi-pressure lines are circles concentric with the well axis (similar to radial flow in a well with no fracture).

7.2.1.1 Comparison of Bilinear Model with Prats Solutions

Figure 3 shows a comparison between Prats solution and the bilinear model for fluid flow around a frac-pack for four values of "a" (0, 0.1, 1, and 10). The difference in the total pressure drop in the fracture obtained from Prats solution and our bilinear flow model for (a = 0, 0.1, and 1) was found to be < 5% of the total pressure drop in the reservoir. For a = 10, the error was 14%. Therefore, up to a = 1, the assumption of bilinear flow is quite accurate and up to a = 10, is a reasonable engineering approximation; while above that the flow is essentially radial. The equi-pressure ellipse axes values for the different "a" values were obtained by keeping r_e/L_{fp} = 2.4 as nearly no dependence on this dimensionless number was found by Kyle et al. (2009). So, even in cases with other r_e/L_{fp} ratios, the minor axis of the equi-pressure is still interpolated from Figure 2.

7.2.2 Filtration and Permeability Decline Model

Equation 2 is a 1-D mass balance of particles in a porous medium with injection of an incompressible fluid with suspended particles.

$$\phi \frac{dC}{dt} + \frac{dC_d}{dt} + u \frac{dC}{dx} = 0 \quad \text{..... (2)}$$

Where, C is the volume of suspended particles per unit volume of fluid injected, u is the fluid volumetric rate per unit area, ϕ is the porosity of the porous medium, and C_d is the volume of particles deposited per unit volume of the porous medium. We assume Iwasaki's (1937) empirical model for particle deposition as shown in equation 3.

$$\frac{dC_d}{dt} = \lambda C u \quad \text{..... (3)}$$

Where, λ is the filtration coefficient obtained from a semi-analytical model presented by (Rajgopalan, and Tien, 1976). Assuming that the suspended particles concentration becomes steady inside the porous medium, the solution for suspended particle concentration can be easily shown to be exponential with distance for 1-D linear flow and constant injection rate.

Figure 1 shows the assumed bilinear flow around the frac-pack up to an equi-pressure ellipse. This is an approximation to the actual flow which is between bilinear and radial. The errors are discussed in Section 1.1 for different values of "a". With the bilinear flow assumption, flow from the wellbore divides into two: 1) flow going into the frac-pack, and 2) flow going into the formation but in a direction perpendicular to the frac-pack. The flow going into the frac-pack gets further divided into: 1) flow perpendicular to the frac-pack into the adjacent formation often termed as leak-off, and 2) flow continuing into the frac-pack.

The bilinear flow assumption allows us to obtain the suspended and deposited particle concentrations in the formation and the frac-pack from two 1-D solutions.

Equations 4 and 5 show the suspended particle concentration in the frac-pack and in the formation. It is also assumed that the superficial velocities in the formation and the frac-pack do not change significantly with distance from the well. This is required since in deriving the solution presented in Equations 4 and 5, linear flow with constant superficial velocities is assumed.

$$C_x\big|_{fracpack} = C_0 \exp(-\lambda_g x) \quad \text{..... (4)}$$

$$C_y\big|_{well-formation} = C_0 \exp(-\lambda_f y) \quad \text{..... (5)}$$

Where C_0 is the concentration of suspended particles in the well, λ_g is the filtration coefficient of the frac-pack, x is the distance in the frac-pack from the wellbore boundary, y is the distance in the formation perpendicular to the frac-pack, and λ_f is the filtration coefficient of the formation.

However, since there is also leak-off from the frac-pack into the formation, there will be particles entering and depositing near the frac-pack faces as well. The concentration of particles in the frac-pack then becomes the inlet boundary condition for the particles entering the adjacent formation. The solution for the concentration profile in the adjacent formation, at a distance y from the frac-pack and perpendicular to the frac-pack (which is at a distance x from the wellbore face) is:

$$C_y\big|_{fp-formation} = C_x\big|_{fracpack} \exp(-\lambda_f y) \quad \text{..... (6)}$$

Where C_x is given by Equation 4. Figure 4 shows a schematic of the concentration profile of the suspended particles in the frac-pack and the formation adjacent to it. It also shows a schematic of filtration of particles in a porous medium with an internal and external filter cake. Since the frac-pack is filled with proppant which have larger pore throat radii than the formation sand, it has a very low filtration coefficient. This means that the particle trapping capacity of the frac-pack is much smaller than the formation sand and injected particles can travel relatively far along the length of the frac-pack. The filtration coefficient for the formation, however, will be large because of the smaller formation grain size. Therefore, the particles will be trapped within a relatively short distance (inches) in the formation adjacent to the well and the frac-pack.

7.2.2.1 Permeability Reduction Model

The deposited particles reduce the permeability of the proppant pack and the formation. The corresponding reduction in permeability is calculated from an empirical equation proposed by (Pang and Sharma, 1994). They postulated that the permeability reduction because of particle deposition can be split into 3 parts: reduced porosity, increased surface area and increased tortuosity and can be calculated as follows:

$$k / k_0 = k_{dp} k_{ds} k_{dt} \quad \text{..... (7)}$$

Where k is the permeability of the near formation/frac-pack at any time, k_0 the initial permeability respectively and

$$k_{dp} = \frac{\phi^3 (1-\phi_0^2)}{\phi_0^3 (1-\phi^2)}$$

$$k_{ds} = \left(\frac{1 + C_d /(1-\phi_0)}{1 + C_d /(1-\phi_0)(d_g / d_p)} \right)^2$$

$$k_{dt} = \frac{1}{1+\beta C_d} \quad \text{..... (8)}$$

Where ϕ is the reduced porosity, ϕ_0 is the initial porosity, d_g is the grain diameter, d_p is the particle diameter, k_{dp} is the decline associated with decrease in porosity, k_{ds} is the decline associated with increase in surface area and k_{dt} is the decline associated with increased tortuosity. All three fractions have values between 0 and 1. In the above

relation the empirical parameter β represents a damage factor, which accounts for the change in tortuosity as trapped particles deposit in the pores. It can be better estimated by fitting experimental data. We have however assumed its value to be equal to 0 for simplicity.

The reduced porosity at any time t is calculated to be equal to $\phi = \phi_0 - C_d$. The deposited particle concentration in the frac-pack and the formation with time is shown in Appendix A. When the porosity at the formation-wellbore interface, formation-frac-pack interface or at the frac-pack-wellbore interface reaches a critical porosity (defined as the product of initial porosity and the filter cake porosity) no more particles can enter through that interface and an external filter cake starts to form. The time when the external cake begins to form is called the transition time (Sharma and Wennberg, 1997).

7.2.3 Flow Resistance Model for Bilinear Flow

Figure 5 shows discretization of half of the 2-D horizontal plane area between the well and the equi-pressure boundary around the frac-pack. The frac-pack is discretized into equal segments along the length of the pack. The formation near the well and the frac-pack is discretized into equal but much smaller segments for capturing permeability decline which occurs in the formation adjacent to the wellbore and the frac-pack. The pressure difference between the equi-pressure ellipse around the frac-pack and the wellbore is calculated using a flow resistance model. The flow resistance is defined as the ratio of differential pressure (analogous to the voltage difference across a conductor) to the flow rate (analogous to the current) across a permeable medium.

$$R = \frac{\Delta P}{q} \quad \text{.....} \quad (9)$$

The flow is assumed to be bilinear up to the equi-pressure ellipse. Since the flow is assumed bilinear, the flow resistance can be easily calculated by using Darcy's equation for linear flow in equation 9:

$$R(x) = \frac{\mu(x)}{k_{eff}(x)} \frac{dx}{A} \quad \text{.....} \quad (10)$$

Where A is the cross-sectional area, $\mu(x)$ is the viscosity of the injected fluid, and K_{eff} (x) is its effective permeability. Note that the Reynold's number for typical flow-rates in the frac-pack can be in the order of ~100. This implies that non-Darcy flow in the frac-pack can be important and will result in an additional flow resistance along the frac-pack. To include non-Darcy effects the Forcheimer equation should be used to calculate the flow resistance in the frac-pack.

7.2.3.1 Flow Resistance along the Frac-pack

The flow resistance of a segment of the frac-pack between x and x+Δx distance from the wellbore face is:

$$R_{fp}\Big|_i = \frac{\mu_w(T_w)}{k_{fp}(i,t)} \frac{\Delta x}{2w(i,t)h} \quad \text{..... (11)}$$

Where the product 2w(i, t)*h is the area of the ith frac-pack segment for flow in the frac-pack. Note that the factor 2 is used to include the two sides of the frac-pack. Δx is the length of the frac-pack segment, and $k_{fp}(i, t)$ is the permeability of the ith frac-pack segment which is calculated using Equations 7 and 8 with C_d obtained from equation A.1 shown in the Appendix. The flow resistance caused by an external filter cake which is formed after the internal filtration in the frac-pack is completed is given by:

$$R_{fp}\Big|_{cake} = \frac{\mu_w(T_w)}{k_c} \frac{h_{cfp}}{2w(0,t)h} \quad \text{.....} \quad \text{(12)}$$

Where h_{cfp} and k_c are the thickness and permeability of the external filter cake formed at the interface between the wellbore and the frac-pack (assuming the frac-pack has not widened yet and that no channel has been formed). The widening of the frac-pack and the creation of a channel is discussed in Section 5. The thickness of the external filter cake is obtained from equation A.2 in the Appendix. w(0, t) is the width of frac-pack at the wellbore and is equal to the initial assumed width of the frac-pack. If the frac-pack widens, then the particle concentration upto the channel tip is assumed to be equal to C_0 the same as the injected particle concentration in the well.

7.2.3.2 Flow Resistance Perpendicular to the Frac-pack

The water in the frac-pack flows from one segment to the next and a part of it leaks-off into the formation. Particles are trapped in the frac-pack based on the filtration coefficient for the frac-pack. Particles deposit on the formation grains adjacent to the frac-pack. These particles however get trapped within a few inches from the frac-pack-formation interface. These particles reduce the formation porosity and permeability. After internal filtration is complete in the formation adjacent to a particular frac-pack segment, an external filter cake at the formation-frac-pack interface begins to form. When the thickness of the external cake in the first frac-pack segment (closest to the wellbore) becomes larger than the frac-pack width, the frac-pack segment starts to widen to accommodate the filter cake.

The flow resistance to leak-off is caused by 1) an external filter cake at the frac-pack face, 2) a zone of reduced permeability of the formation near the frac-pack face, and 3) undamaged formation up to the equi-pressure ellipse around the frac-pack. The undamaged zone can further have three zones based on the fluid mobilities: 1) a zone at injected water temperature with injected water as the mobile phase, 2) a zone at reservoir temperature with water as the mobile phase, and 3) a zone at reservoir temperature with both water and oil as the mobile phases (unflooded zone). The flow resistance perpendicular to the ith frac-pack segment up to the equi-pressure ellipse is:

$$R_{fpo}\Big|_i = \frac{\mu_w(T_w)h_{co}(i)}{k_{co}(4h\Delta x)} + \frac{1}{(4h\Delta x)} \sum_{j=1}^{Ns} \frac{\mu_w(T_w)\Delta y}{k_f(i,j,t)} +$$

$$\frac{1}{(4h\Delta x)}\frac{\mu_w(T_w)b_c\left[1-\left(\frac{i}{Ns+1}\right)^2\right]^{0.5}}{k_{rw}{}^{o}k_f}+$$

$$\frac{1}{(4h\Delta x)}\frac{\mu_w(T_R)\left\{(b_{wf}-b_c)\left[1-\left(\frac{i}{Ns+1}\right)^2\right]^{0.5}\right\}}{k_{rw}{}^{o}k_f}+$$

$$\frac{1}{(4h\Delta x)}\frac{\mu_o(T_R)\left\{(b_{fp}-b_{wf})\left[1-\left(\frac{i}{Ns+1}\right)^2\right]^{0.5}\right\}}{k_{ro}{}^{o}k_f} \quad (13)$$

The subscript i goes from 1 to Ns+1, i.e. up to the equi-pressure ellipse which is one segment ahead of the frac-pack tip. In the above equation, it is assumed that $b_{wf}<b_{fp}$, i.e. both the thermal and waterflood fronts are inside the equi-pressure ellipse around the frac-pack. If $b_{wf}>=b_{fp}$, i.e. the waterflood front has crossed the equi-pressure ellipse boundary around the frac-pack then the last term is zero, and in the second last term instead of b_{wf}, b_{fp} is used. If $b_c>=b_{fp}$, i.e. the cooled front has also crossed the equi-pressure ellipse around the frac-pack then, the last two terms are zero, and in the third last term instead of b_c, b_{fp} is used.

The product $4h*\Delta x$ is the area of frac-pack segments for flow perpendicular to the 4 faces of the frac-pack, hco and kco are the thickness and the permeability of the external cake formed at the face of the ith segment of the frac-pack and is non-zero only after the internal filtration is complete, otherwise it is set to zero. The thickness of any external filter cake formed at the interface between the frac-pack and the formation is calculated using equation A.4 in the appendix.

The second term is the flow resistance in the reduced permeability zone also known as the damage zone which has Ns discretized segments and total damage length equal to $Ns*\Delta y$. The k (i, j, t) is calculated at a jth segment perpendicular to the frac-pack's ith segment at time t using equations 7 and 8 for reduced permeability with C_d obtained from equation A.3 in the appendix

The third term is the flow resistance between the damage zone and the thermal front assuming that the thermal front is within the equi-pressure ellipse enclosing the frac-pack. We also assume that the damage length is negligible compared to the thermal front length from the frac-pack. The thermal zone is occupied by injected water with viscosity at injected water temperature $\mu_w(T_w)$, b_c is the minor axis of the thermal front, $k_{rw}{}^{o}$ is the relative permeability of water at residual oil saturation. k_f is the undamaged formation permeability.

The fourth term is the flow resistance between the thermal front and the waterflood front assuming both the fronts are inside the equi-pressure ellipse just enclosing the

frac-pack. The injected water viscosity in this zone is based on the reservoir temperature $\mu_w(T_R)$, and b_{wf} is the minor axis of the waterflood front.

The fifth term is the flow resistance between the waterflood front and the equi-pressure ellipse just enclosing the frac-pack assuming the waterflood front hasn't crossed the equi-pressure ellipse. The flowing phase is the reservoir fluid in this zone assuming it to be oil with viscosity $\mu_o(T_R)$, b_{fp} is the minor axis of the equi-pressure ellipse, and $k_{ro}{}^o$ is the relative permeability of oil at residual water saturation.

7.2.3.3 Flow Resistance between the Wellbore and the Equi- pressure Ellipse

The flow resistance from the wellbore to the equi-pressure ellipse in the direction perpendicular to the frac-pack is given by equation 14. It is similar to equation 13 with a few changes:

$$R_w = \frac{\mu_w(T_w)h_{cw}}{k_{cw}(2\pi r_w h)} + \frac{1}{(2\pi r_w h)}\sum_{j=1}^{Ns}\frac{\mu_w(T_w)\Delta y}{k_f(0,j,t)} + \frac{1}{(2\pi r_w h)}\frac{\mu_w(T_w)b_c}{k_{rw}{}^o k_f} + \frac{1}{(2\pi r_w h)}\frac{\mu_w(T_R)(b_{wf}-b_c)}{k_{rw}{}^o k_f} + \frac{1}{(2\pi r_w h)}\frac{\mu_o(T_R)(b_{fp}-b_{wf})}{k_{ro}{}^o k_f} \quad \text{..... (14)}$$

Where, $(2\pi r_w h)$ is the cross-sectional area of the wellbore for flow in the direction perpendicular to the frac-pack (assuming that the width of the frac-pack is negligible compared to the area of the wellbore).

Note: Equation 14 has been modified in WID 7.2. The third, fourth and fifth terms are calculated based on radial flow instead of linear flow. This now makes the model applicable to Prats' "a"> 10 as well; i.e. the model is applicable to any value of "a" now.

The rest of the terms are similar in meaning as defined for equation 13. The first term is the flow resistance caused by the external filter cake after the internal filtration is complete, with hcw and kcw as the thickness and the permeability of the external cake formed at the wellbore face after the transition time. The thickness is calculated by equation A.6 in the appendix and the permeability assumed is ~0.001 md. The second term is the flow resistance caused by the near wellbore permeability reduction up to the damage length equal to Ns*Δy, with $\mu_w(T_w)$ as the viscosity of the injected water at the injected water temperature. k_f (0, j, t) is the permeability of the formation near the wellbore in the perpendicular direction to the frac-pack and is calculated using equations 7 and 8 with C_d obtained from equation A.5 in the appendix.

The third, fourth and fifth term are the same as in equation 13. These terms become zero after the thermal front has crossed the equi-pressure ellipse; otherwise they need to be used as described for equation 13.As injection proceeds, the flow resistances

are calculated at each time step for the different flow resistances as given by equations 11, 12, 13, and 14. The flow resistances would mostly increase because of permeability reduction and formation of an external filter cake but may also reduce if a very less mobile fluid (viscous oil) is displaced by a more mobile fluid. The first segment (closest to the wellbore) in the frac-pack and the formation will have the largest deposition rate compared to other flow resistors and an external filter cake will form at this interface when the porosity reaches the critical porosity.

7.2.3.4 Total Flow Resistance up to the Equi-pressure Ellipse

Figure 5 shows flow resistors in the discretized frac-pack and the formation up to the equi-pressure ellipse around the frac-pack. The flow resistance between the wellbore and the equi-pressure ellipse can be viewed as two flow resistances in parallel: 1) An equivalent flow resistance offered by the frac-pack and its adjacent formation up to the equi-pressure ellipse, and 2) flow resistance offered by the formation adjacent to the wellbore. To calculate the equivalent flow resistance of the frac-pack and its adjacent formation (R_{eqfp}) which excludes the flow resistance by the formation adjacent to the wellbore is calculated as follows:

$$R_{eqfp}\Big|_{i=Ns+1} = R_{fpo}\Big|_{i=Ns+1} \quad \text{..... (15)}$$

$$\frac{1}{R_{eqfp}\Big|_{i=Ns}} = \frac{1}{R_{eqfp}\Big|_{Ns+1} + R_{fp}\Big|_{N_S}} + \frac{1}{R_{fpo}\Big|_{Ns}} \quad (16)$$

We iterate equation 16 by reducing i by 1 each time until i=1. Then we add any external filter cake flow resistance if formed at the interface between the wellbore and the frac-pack to get the total flow resistance of the frac-pack up to the equi-pressure ellipse as shown below:

$$R_{eqfp} = R_{eqfp}\Big|_{i=1} + R_{fp}\Big|_{cake} \quad \text{..... (17)}$$

The total flow resistance (R_T) between the wellbore and the equi-pressure ellipse is calculated by adding the well flow resistance (R_w) and the frac-pack flow resistance (R_{eqfp}) in parallel as shown below:

$$\frac{1}{R_T} = \frac{1}{R_w} + \frac{1}{R_{eqfp}} \quad \text{..... (18)}$$

7.2.3.5 Flow Distribution around the Wellbore and the Frac- pack

The flow rate perpendicular to the well-bore (Q_w) into the formation is calculated as follows:

$$Q_w = Q_T * \frac{R_T}{R_w} \quad \text{..... (19)}$$

While the flow-rate into the frac-pack (Q_{fp}) from the well-bore is calculated as follows:

$$Q_{fp} = Q_T * \frac{R_T}{R_{eqfp}} \quad \text{..... (20)}$$

Where, Q_T is the total injection rate into the well and R_T is the total flow resistance up to the equi-pressure ellipse from the wellbore (through both the formation and the frac-pack). The sum of the two flow rates (Q_w and Q_{fp}) must sum to Q_T. The flow rate perpendicular to the frac-pack (leak-off) from the ith segment but from all the four faces of the frac-pack is calculated as follows:

$$Q_{fpo}\Big|_i = Q_{fp}\Big|_i * \frac{R_{eqfp}\Big|_i}{R_{fpo}\Big|_i} \quad \text{..... (21)}$$

Where $Q_{fpo}\Big|_i$ is the total flow rate perpendicular to the ith segment of the frac-pack at a distance i*Δx from the wellbore and $Q_{fp}\Big|_i$ is the total flow rate entering into the ith segment of the frac-pack at a distance i*Δx from the wellbore. Note the flow rates include both the frac-pack wings and all the 4 faces. In equation 21, $Q_{fp}\Big|_i$ with i = 0, i.e. the total flow rate entering into both sides of the first frac-pack segment from the wellbore is calculated using equation 20. The subscript i then goes from 1 to Ns+1 to calculate all $Q_{fp}\Big|_i$ and $Q_{fpo}\Big|_i$. $Q_{fpo}\Big|_i$ with i = Ns+1, is the total flow rate leaking-off at the two frac-pack tips. The flow rate entering the ith +1 segment of the frac-pack is the flow rate entering into the ith segment minus the flow rate leaking-off perpendicular to the ith segment as shown below:

$$Q_{fp}\Big|_{i+1} = Q_{fp}\Big|_i - Q_{fpo}\Big|_i \quad \text{..... (22)}$$

7.2.4. Pressure Distribution in the Reservoir and the Frac-pack

Beyond the damage zone, three distinct regions in the reservoir around the frac-pack are modeled:

1. Cool injection zone: The region closest to the wellbore and the frac-pack which could be cooler than the reservoir, with only injection water as mobile and oil at residual saturation (S_w=1-S_{or} and S_o=S_{or}) and temperature equal to the injected water temperature.
2. Warm injection zone: The region ahead of the cooled zone with both injection water and connate water as mobile but oil at residual saturation S_w=1-S_{or} and S_o=S_{or} but temperature at the initial reservoir temperature.

3. Oil zone: The region ahead of the waterflood front where both oil and water are mobile with S_{wi} and S_o equal to the initial fluid saturations and temperature equal to the initial reservoir temperature.

It is assumed that each of these three regions would grow confocally with the frac-pack. Note that there is also a region very close to the frac-pack and the wellbore with reduced permeability (damage zone) because of injected particle deposition.

The ΔP between the well and the equi-pressure ellipse around the frac-pack is calculated as follows:

$$\Delta P_{ep} = Q_T * R_T \quad \text{..... (23)}$$

Where Q_T is the total injection rate into the well and R_T is total flow resistance from the well upto the equi-pressure ellipse around the frac-pack.

The bottomhole pressure in the well is calculated as follows:

$$P_{wf} = P_R + \Delta P_1 + \Delta P_2 + \Delta P_3 + \Delta P_{ep} \quad \text{..... (24)}$$

Where ΔP_{ep} is the pressure difference between the well and the equi-pressure ellipse enclosing the frac-pack. ΔP_1, ΔP_2 and ΔP_3 are pressure differences between the reservoir boundary and the waterflood front, waterflood front and thermal front and thermal front and the equi-pressure ellipse (the three regions). Note ΔP_1, ΔP_2 and ΔP_3 are zero until they cross the equi-pressure ellipse around the frac-pack. The pressure drops across each of these regions are obtained from equations 25-29. The following three cases will arise:

1) At first both the waterflood front and the thermal front will be within the equi-pressure ellipse around the frac-pack, i.e. the minor axis of the waterflood front, $b_{wf} < b_{fp}$, the minor axis of the equi-pressure ellipse. In this case the approximate pressure difference between the reservoir boundary and the equi-pressure ellipse is calculated as follows:

$$\Delta P_1 = \frac{q\mu_o}{2\pi k k_{ro}{}^o h} \ln\left(\frac{2r_e}{a_{wf} + b_{fp}}\right) \quad \text{..... (25)}$$

With ΔP_2 and ΔP_3 equal to zero.

2) The waterflood front has crossed the equi-pressure ellipse, i.e. bwf > bfp but not the thermal front, i.e. $b_c < b_{fp}$. For this case, ΔP_1 and ΔP_2 are calculated as follows:

$$\Delta P_1 = \frac{q\mu_o}{2\pi k k_{ro}{}^o h} \ln\left(\frac{2r_e}{a_{wf} + b_{wf}}\right) \quad \text{..... (26)}$$

$$\Delta P_2 = \frac{q\mu_w}{2\pi k k_{rw}{}^o h} \ln\left(\frac{a_{wf} + b_{wf}}{a_c + b_{fp}}\right) \quad \text{..... (27)}$$

ΔP_3 is equal to zero.

3) Both the waterflood front and the cooled front have crossed the equi-pressure ellipse i.e. both b_{wf} and b_c are > $b_{fp.}$ For this case, ΔP_1 is the same as equation 26, while ΔP_2, and ΔP_3 are calculated as follows:

$$\Delta P_2 = \frac{q\mu_{wr}}{2\pi k k_{rw}{}^{o} h} \ln\left(\frac{a_{wf} + b_{wf}}{a_c + b_c}\right) \text{..... (28)}$$

$$\Delta P_3 = \frac{q\mu_{w}}{2\pi k k_{rw}{}^{o} h} \ln\left(\frac{a_c + b_c}{l_{fp} + b_{fp}}\right) \text{..... (29)}$$

The pressure at the frac-pack tip can be calculated as follows:

$$P_{tip} = P_R + \Delta P_1 + \Delta P_2 + \Delta P_3 + R_{fpo}\Big|_{Ns+1} * Q_{fpo}\Big|_{Ns+1} \text{... (30)}$$

Where ΔP_2 and ΔP_3 values would depend upon the front's location as described before.

The pressure at any point in the frac-pack can also be calculated as follows:

$$P_{fp}\Big|_i = P_{tip} + \sum_{i=i}^{Ns} R_{fp}\Big|_i * Q_{fp}\Big|_i \text{..... (31)}$$

Figure 6 shows confocal ellipses with the waterflood and thermal fronts. This confocal assumption for the fronts is true only for "a" = 0, for as "a" increases the flow becomes slightly radial and for the extreme case of a = infinity, the flow is completely radial. However, for simplicity the fronts are assumed confocal and no error quantification is attempted.

7.2.5. Frac-Pack Widening and Channeling

Figure 7 shows the rise in bottomhole for a range of filtration coefficients for the frac-pack. For small filtration coefficients, the rise in BHP is gradual while for large filtration coefficients, the rise in BHP is steep. The figure also shows decreasing fracture propagation pressure due to cold water injection.

The width of a fracture as a function of net pressure within it is given by Schechter (1992):

$$w(x,t) = \frac{2\,[P_{fp}(x,t) - \sigma_{h\min}(t)](1-\upsilon^2)h}{E} \text{..... (32)}$$

Where P_{fp} is the fluid pressure in the frac-pack, ν is the Poisson's ratio, E is the Young's modulus, h is the frac-pack height, and σ_{hmin} is the minimum horizontal stress perpendicular to the frac-pack. By rearranging equation 32, the critical pressure at which widening of the frac-pack will take place can be calculated as follows:

$$P_{fp}{}^{*}(x,t) = \sigma_{h\min}(t) + \frac{w_{fpi}E}{2(1-\upsilon^2)h} \quad \text{..... (33)}$$

Where w_{fpi} is the initial frac-pack width.

Because of particle deposition in the frac-pack with continued water injection, the pressure in the frac-pack will rise and cause it to widen. The widening of the frac-pack will result in the creation of a high permeability channel through the proppant pack. The length of the channel (distance up to which the widening has taken place) would be up to the point where the pressure is just equal to the critical pressure for widening. The permeability of the channel is calculated using slot equation. The slot width is the additional width of the frac-pack segment compared to the initial width as is calculated as follows:

$$w(x,t) - w_{fpi} = \frac{2[P_{fp}(x,t) - P_{fp}{}^{*}(x,t)](1-\upsilon^2)h}{E}$$

$$K_c(x,t) = \frac{[w(x,t) - w_{fpi}]^2}{12} \quad \text{..... (34)}$$

The flow in the frac-pack would occur through both the proppants and the channel in parallel and the effective segment permeability will is calculated as follows:

$$K_{eff}(x,t) = \frac{k_{fp}(x,t)w_{fpi} + k_c(x,t)[w(x,t) - w_{fpi}]}{w(x,t)} \quad \text{..... (35)}$$

With increasing pressure in the frac-pack, the width of the channel will increase and so will the effective permeability of the frac-pack segment will alleviate. Note no external filter cake at the face of the frac-pack segment is accounted in equation 35. In case of a developing filter cake at the face of the frac-pack segment, the filter cake permeability will be added in parallel as well. Note that the width and the effective permeability of a frac-pack segment needs to satisfy Darcy's flow assumption as follows:

$$\frac{P_{fp}(x,t) - P_{fp}(x+\Delta x,t)}{\Delta x} = \frac{\mu_w Q_{fp}(x,t)}{k_{eff}(x,t)2w(x,t)h}$$

$$P_{fp}(x,t) = \frac{\mu_w Q_{fp}(x,t)}{k_{eff}(x,t)2w(x,t)h}\Delta x + P_{fp}(x+\Delta x,t) \quad \text{..... (36)}$$

There will be an equilibrium channel/slot width at which the rate of pressure increase because of plugged segment will be equal to the rate of pressure decline because of creation of a large permeability channel, i.e. for segments in which the pressure is above the critical pressure, the pressure, width, and the effective permeability need to satisfy equations 32, 35, and 36. The flow rate from the previous time step and the pressure in the frac-pack segments ahead of the channel are used in equation 36 for solving for the segment width, pressure and segment effective permeability at the channel tip (where the pressure just becomes larger than the critical pressure for widening). After the channel tip segment's unknowns are found; the pressures, widths

and permeabilities are calculated for all the widened segments up to the wellbore marching backwards. Figure 8 shows a schematic of the widened frac-pack with pressures, widths and the permeabilities of the frac-pack segments. The channel length will increase with a minimum length equal to the frac-pack segment length. Figure 9 shows a plot of channel/slot permeability and slot width as a function of pressure above the critical pressure.

7.2.6. Frac-Pack Lengthening

The frac-pack will extend in length if the pressure at the tip becomes larger than the fracture propagation pressure obtained from Perkins, T.K. and Gonzalez, J.A. (1985):

$$P_{fracture} = \sigma_{h,\min} + \sqrt{\frac{\pi UE}{(1-\nu^2)h}} \quad \text{..... (37)}$$

Where $P_{fracture}$ is the fracture propagation pressure needed at the tip of the frac-pack for frac-pack extension, σ_{hmin} is the earth's minimum stress perpendicular to the frac-pack faces, and U is the specific surface energy. A different fracture propagation criterion (such as stress intensity factor) can be used instead if desired.

The extension of the frac-pack can occur either because of a) large reduction in the minimum horizontal stress because of injection of cold water (discussed in Appendix B), or due to rapid plugging and channeling in the frac-pack. Whether the frac-pack will grow in length will depend on the pressure at the tip of the frac-pack, which is controlled by the plugging and widening of the proppant pack.

7.3 Model Implementation and Results

The model presented in the paper is implemented in WID 7.2, which is a single-well water injection simulator. The well injectivity, I is used as the performance indicator for water injection wells and is defined as:

$$I = \frac{Q_T}{P_{wf} - P_R} \quad \text{..... (38)}$$

Where Q_T is the total injection rate at the well, P_{wf} is the bottomhole flowing pressure and P_R is average reservoir pressure at a circular boundary (re).

The model is implemented for injecting into a multi-layered reservoir. The layers can be perforated or frac-packed. The layers are assumed to be non-communicating along the length of the reservoir except at the boundaries. Based on the total flow resistance of each of the layers, the flow distribution into each of the layers is calculated and the frac-packs in the layers are then treated independently as shown in the paper. The flow distribution between the layers is calculated based on resistances in parallel. After the injection rate distribution in the layers is known at a time step, the pressure and flow distribution within the layer in and around its frac-pack is calculated independent of the other layers. The results are useful in predicting if one or more layers will act as thief zones.

An Example

Table 1 shows input parameters for two simple case studies with injection into a frac-packed well and an initially unfractured well. The cases consisted of an injection rate of 5,000 bpd of water with 5 ppm of solids into a single layered reservoir with k_h = 100 md and k_{rw}^o = 0.2. In the case of a frac-packed well, the length of the frac-pack is assumed 200 ft, initial width 0.2 inch, proppants 1.5 mm in diameter and frac-pack permeability 500 Darcy. The "a" value for the case was found to be 0.75 which is within the range where bi-linear flow is a very good approximation. The injection water temperature was set equal to the reservoir temperature for simplicity, i.e. no thermal stresses were considered. Figures 12-17 show the results for injection into the frac-packed well case. The Reynolds number in the frac-pack was found to be 216 which suggest that Non-Darcy effect would also play a role.

Figure 10 shows how the pressure profile in the frac-pack varies with injection time. A relatively small pressure drop of 273 psi is found along the frac-pack from the wellbore to the frac-pack tip on day 0 since the frac-pack is very conductive (500 Darcy) and clean (particle deposition hasn't started). Note steady state is assumed in calculating this number by the model. As injection proceeds, the pressure in the frac-pack near the wellbore rises because of particle deposition in the frac-pack. The filtration coefficient for the frac-pack is estimated to be ~0.1 1/m. The actual value could be smaller than the estimated value becasue of large flow velocities in the frac-pack as compared to the deep bed filtration experiments used to validate their model. No correction for the high flow velocities in the frac-pack is attempted. With the estimated ~ 0.1 1/m value of filtration coefficient, the rate of frac-pack plugging is calculated by the model. Figure 11 shows the permeability profile in the frac-pack with injection time. As shown, the frac-pack permeability is decreased from 500 Darcy to 20 Darcy in the frac-pack near the wellbore face in just 50 days because of continued deposition of particles. As a result the pressure in the frac-pack reaches the critical pressure for widening within 70 days, as shown in Figure 12. The widening of the frac-pack results in a channel within the frac-pack which doesn't allow the permeability of the frac-pack to reduce further (as seen in Figure 11). The permeability of the frac-pack is high before the channel tip, lowest at the channel tip and higher again in front of the channel tip. With time, as the pressure at the channel tip rises above the critical pressure, the frac-pack widens-up there and the high permeability channel advances.

Figure 13 and 14 show the flow rate in the frac-pack and the flow rate perpendicular to the frac-pack (leak-off). The flow rate in the frac-pack is found to be linearly decreasing as part of it leaks off into the formation. The leak-off rate is found to be nearly constant along the frac-pack length, except near the tip where it is found to be large. A part of this finding is in agreement with Suarez et al. (2002) experimental investigation of fracture propagation during water injection. The high leak-off rate is found and believed to be true when the frac-pack faces get damaged (with build up a filter cake) which results in the continuation of the flow along the frac-pack as it is the path of least resistance. As the flow continues and reaches near the tip, it has to leak-off in the formation which explains a higher leak-off rate near the frac-pack tip. However for frac-packs with no damage, the authors are not sure if the flow at the tip would be higher than other places, though the model still shows higher leak-off rates. Therefore in clean frac-packs with no damage, the model results are not yet verified by the authors.

Figure 15 shows the bottomhole pressure, pressure at the frac-pack tip and the fracture propagation pressure with time. The bottomhole pressure rises sharply because of plugging of the frac-pack and the formation and within 70 days the pressure at the well-frac-pack interface reaches the critical pressure for widening. After that the BHP becomes fairly constant because of the creation of a high permeability channel as a result of widening of the frac-pack making the BHP nearly equal to the critical pressure for widening. The fracture propagation pressure remains fairly constant except for a small rise because of pore pressure increase. The pressure at the frac-pack tip also increases gradually because only a very low concentration of injected particles reaches the tip. The pressure at the tip does not exceed the fracture propagation pressure and, therefore, the frac-pack does not extend in length.

A case of water injection into an initially unfractured well (open-hole or perforated completion) was run for comparison with the frac-packed well. The results for injection into the unfractured well case show fracture growth within the first day because of poor initial injectivity of the well. The fracture keeps growing because of plugging caused by continued injection of water containing 5 ppm solids. The fracture is found to grow up to a length of 74 ft in 1000 days. Figure 16 shows this growth of fracture in the unfrac-packed well with time in comparison to the growth of the channel in the frac-packed well case. A similar channel length of 60 ft was found which can be thought of a fracture with in the frac-pack refered as the channel. Figure 17 shows the injectivity of the two cases with time. The initial injectivity of the frac-packed well (~6 bpd/psi) is much larger than the initial injectivity of the un-fractured well (~2 bpd/psi). However, because of plugging of the frac-pack the injectivity of the two wells becomes approximately the same after 70 days of injection.

This result shown in Figure 17 may suggest that the additional cost of frac-packing wells may not be justified. However, this argument does not consider several other factors such as 1) sand control needed in poorly consolidated formations such as in the Gulf of Mexico. The gravel in the wellbore might flow into a growing fracture (Saripalli, et al. 1999). The loss of wellbore gravel into a growing fracture may result in a situation where sand production and wellbore fill-up may occur in wells which are not frac-packed. These factors need to be considered before final completion decisions are made.

7.4 Conclusions

A model for water injection into frac-packed wells is presented. This model can be used to compute the injectivity of frac-packed wells with time. Injector performance is shown to depend on the solids content in the injected water, proppant size in the frac-pack, width and length of the frac-pack, injection rate, injection water temperature and the minimum horizontal stress. In cases with wide and conductive frac-packs, the plugging of the frac-pack is found to be gradual and the bottom-hole pressure to rise slowly. However, in cases with narrow and less conductive frac-packs, significant plugging might occur, with a rapid rise in the bottom-hole pressure. After long periods of injection with injection water with a few ppm of solids, some widening of the frac-pack is expected and for short frac-packs some lengthening will occur. The widening of the frac-pack results in a high permeability channel which alleviates the injectivity decline and stops the bottomhole pressure to rise steeply further. The plugging almost always is expected to play a significant role during

long injection periods; however thermal stresses can only play a role when large temperature gradients are introduced in the formation via very low temperature injection water. We believe that most of the frac-packs will widen-up with in few years of injection and may even extend in length. Therefore, simulations from similar kinds of models are needed to pre-estimate the injectivity of designed frac-packs for sustaining long periods of injection.

7.5 Nomenclature (All variables are in SI units)

a_c	Major axis of the thermal front ellipse
a_{wf}	Major axis of the waterflood ellipse
A	Cross-sectional area
b_c	Minor axis of the thermal front ellipse
b_{wf}	Minor axis of the waterflood ellipse
b_{fp}	Minor axis of the equipressure ellipse around the frac-pack
C	Concentration of suspended particles
C_d	Volume of solids deposited per unit bulk volume of the porous medium
C_{gr}	Specific heat of mineral grains
C_o	Specific heat of oil
C_w	Specific heat of water
E	Young's modulus
h	Formation thickness / frac-pack height
h_c	Filter cake thickness
I	Injectivity index
k	Permeability at time t
k_{eff}	Effective permeability
k_o	Permeability at time t
k_f	Initial permeability of the formation
k_{fp}	Initial permeability of the frac-pack
k_{ro}^o	End point relative permeability of oil
k_{rw}^o	End point relative permeability of water
k_c	Permeability of external filter cake
k_{dp}	k reduction because of decreased porosity
k_{ds}	k reduction because of increased surface
k_{dt}	k reduction because of increased tortuosity
L_{fp}	Initial frac-pack length from wellbore face to the tip
P_{fp}	Pressure in the frac-pack
$P_{fracture}$	Fracture propagation pressure
P_{tip}	Pressure at frac-pack tip
P_R	Reservoir Pressure at the boundary (re)
P_{wf}	Bottomhole flowing pressure in the well
Q_T	Total water injection rate at the well
Q_{fp}	Flow rate in the frac-pack
Q_{fpo}	Flow rate perpendicular to the frac-pack
r_w	Well radius
S	Specific surface area
S_{or}	Residual oil saturation
S_{wi}	Initial Water Saturation
t	Time
t^*	Transition time
T_w	Injection water temperature
T_R	Reservoir temperature
u	Darcy velocity
U	Rock specific surface energy (~50 J/m^2)
V_c	Volume of cooled zone
V_{wf}	Volume of waterflooded region

w_{fp}	Width of the frac-pack
Wi	Total volume of water injected upto time t

Greek symbols

β	Damage factor
ϕ	Porosity
ϕ_{fp}	Porosity of a frac-pack segment
ϕ^*	Critical porosity
λ_g	Filtration coefficient of the frac-pack
λ_f	Filtration coefficient of the formation
μ_w	Viscosity of water
μ_o	Viscosity of oil
ν	Poisson's ratio
ρ_w	Density of water
ρ_o	Density of oil
ρ_{gr}	Density of mineral grains
$\sigma_{H,min}$	Minimum horizontal stress
ΔP_1	Pressure drop between the waterflood front and the drainage boundary
ΔP_2	Pressure drop between the thermal front and the waterflood front
ΔP_3	Pressure drop from the fracture to the thermal front
ΔP_{ep}	Pressure drop from the wellbore to the equi-pressure ellipse around the frac-pack
ΔT	Temperature difference between the injected and reservoir fluids
$\Delta\sigma_{1T}$	Thermoelastic stresses perpendicular to the frac-pack
$\Delta\sigma_{1P}$	Poroelastic stresses perpendicular to the frac-pack

7.6 References

1. Friehauf, K.E. et al. 2009. A Simple and Accurate Model for Productivity of Hydraulically Fractured Wells. Paper SPE 119264 to be presented at the SPE HFTC, The Woodlands, Texas, USA, 19-21 January.
2. Iwasaki, I. 1937. Some notes on sand filtration. Paper J. Am. Waterworks Assoc., 29 (10), 1591-1602.
3. McCarty, R.A. et al. 2006. The Resiliency of Frac-Packed Subsea Injection Wells. Paper SPE 102990 presented at the SPE ATCE, San Antonio, Texas, USA, 24-27 September.
4. Pang, S., and Sharma, M.M. 1994. A Model for Predicting Injectivity Decline in Water-Injection Wells. Paper SPE 28489 presented at the SPE ATCE, New Orleans, LA, USA.
5. Perkins, T.K., and Gonzalez, J.A. 1985. The Effect of Thermoelastic Stresses on Injection Well Fracturing. SPE Journal, February, 78-88.
6. Prats, M. 1960. Effect of Vertical Fractures on Reservoir Behavior – Incompressible Fluid Case. Paper SPE 1575-G presented at 35th Annual Fall Meeting, Denver, October 2-5.
7. Rajgopalan, R., and Tien, C. 1976. Trajectory Analysis of Deep-Bed Filtration with Sphere- in-Cell Porous Media Model. AICHE Journal, Vol. 22, No. 3.
8. Saripalli, K.P., et al. 1999. Role of Fracture Face and Formation Plugging in Injection Well Fracturing and Injectivity Decline. Paper SPE 52731 presented at the SPE/EPA Exploration and Production Environmental Conference, Austin, February 28 – March 3.
9. Schechter, R. S. 1992 *Oil Well Stimulation*. Prentice-Hall.
10. Sharma, M.M., and Wennberg, K.E. 1997. Determination of the Dynamic Filtration Coefficient and transition time for Water Injection Wells. Paper SPE 38181 presented at the European Formation Damage Conference, The Hague.
11. Suárez-Rivera, R. et al. 2002. An Experimental Investigation of Fracture Propagation during Water Injection. Paper SPE 73740 presented at the SPE International Symposium and Exhibition on Formation Damage Control, Lafayette, Louisiana, 20–21 February.

7.7 Appendix

A.1 Particle deposition in the frac-pack

The flow rate in the frac-pack in a given layer can change in case of injection into multiple layers or when the total injection rate is changed. The total current flow-rate entering into both halves of the frac-pack is used to calculate the deposition rate of particles in the frac-pack in a time step. The cumulative deposition of particles (at distance x from the wellbore face) up to time t is calculated by summing the deposition volume as shown below:

$$C_d(x,t)\big|_{fp} = \lambda_g(x) C_0 \exp(-\lambda_g(x)x) \int_0^t \frac{Q_{fp}(x)}{2w_{fp}(x,t)h}\,dt$$

Until $C_d(0,t^*)\big|_{fp} = \phi_{fp} - \phi_{fp}{}^*$ ..... (A.1)

Where ϕ_{fp} is the initial frac-pack porosity and $\phi_{fp}{}^*$ is the critical frac-pack porosity (product of ϕ_{fp} and the external filter cake porosity). After the frac-pack porosity reaches the critical porosity, the internal filtration stops and external filter cake starts to form. After this transition time, the external filter cake thickness formed at the face of the frac-pack is calculated as follows:

$$h_c(0,t)\big|_{fp} = \frac{C_0 \int_0^t \frac{Q_{fp}(0,t)}{2w_{fp}(0,t)h}\,dt}{(1-\phi_{fp})(1-\phi_c)} \quad t > t_{fp}{}^* \text{ ..... (A.2)}$$

A.2 Particle deposition in the formation adjacent to the frac-pack

The deposited particle concentration in the formation perpendicular to the frac-pack (with distance y from the face of the frac-pack and distance x from the face of wellbore as shown in Figure 4) is calculated as follows:

$$C_d(x,y,t)\big|_{fpo} = \int_0^t \lambda_f \frac{Q_{fpo}(x,t)}{4h\Delta x} C_0 \exp(-\lambda_g x)\exp(-\lambda_f y)\,dt \text{ Until}$$

$$C_d(x,0,t^*)\big|_{fpo} = \phi_f - \phi_f{}^* \text{ ..... (A.3)}$$

Where ϕ_f is the initial porosity of the formation and $\phi_f{}^*$ is the critical porosity of the formation after which internal filtration stops and external filtration starts. It is interesting to note that the transition time will be minimum for x = 0, i.e. at the interface between the frac-pack and the formation which is closest to the wellbore. This means that internal filtration will continue into the formation from frac-pack segments ahead. This suggests a larger skin at the face of the frac-pack near the well-bore

than away from the well-bore in the frac-pack. The thickness of the external filter cake at the face of the frac-pack at a distance x from the wellbore is calculated as follows:

$$h_c(x,t)\big|_{fpo} = \frac{C_0 \int_0^t Q_{fpo}(x)dt}{(1-\phi_c)4h\Delta x} \quad t > t\big|^*_{fpo} \text{ ..... (A.4)}$$

A.3 Particle deposition in the formation adjacent to the wellbore

The flow from the well to the formation adjacent is modeled linear rather than radial as shown in figure 4. An equivalent wellbore in a rectangular shape is assumed as shown in figure 1 (on the right side). The length of the rectangle is taken equal to πr_w. The deposition volume of the injected solids at a distance y from the wellbore and time t is calculated as follows:

$$C_d(y,t)\big|_w = \lambda_f C_0 \exp(-\lambda_f y) \int_0^t \frac{Q_w dt}{2\pi r_w h}$$

Until $C_d(0,t^*)\big|_w = \phi_f - \phi_f{}^*$ ..... (A.5)

Where ϕ_f is the formation initial porosity and ϕ_f^* is the formation critical matrix porosity after which external filtration starts. The external filter cake thickness formed at the wellbore face after the transition time is calculated as:

$$h_c(0,t)\big|_w = \frac{C_0 \int_0^t Q_w dt}{(1-\phi_c)2\pi r_w h} \quad t > t\big|^*_w \text{ ..... (A.6)}$$

B. Model for Minimum Horizontal Stress

The initial minimum horizontal stress magnitude and direction is assumed to be known before water injection with the direction of the stress to be perpendicular to the frac-pack faces. The stress direction is assumed to remain the same with continued injection. However the stress magnitude is changed because of water injection which can cause thermal and pore pressure stresses.

To model injection of cold water into the reservoir, it is assumed that from the wellbore up to a zone (known as the cooled zone) the temperature is equal to the injected water temperature and ahead of this zone the temperature is equal to the reservoir temperature. This step change approximation (from T_{wi} to T_R) marks the cooled/thermal front. It is also assumed that no thermal energy is lost to the overlying and the underlying formations.

$$V_c = \frac{\rho_w C_w W_i}{\rho_{gr} C_{gr}(1-\phi) + \rho_w C_w \phi(1-S_{or}) + \rho_o C_o \phi S_{or}} \text{ .. (B.1)}$$

V_c is the volume of cooled zone, W_i is the total volume of injected water upto time t, ρ_w, ρ_o and ρ_{gr} are the densities of water, oil and rock grains, C_w, C_o and C_{gr} are specific heat of the water, oil and rock grains, ϕ is the formation porosity and S_{or} is the residual oil saturation.

With equal frac-pack length along both sides of the wellbore, the flow geometry will be close to elliptical. As an approximation, the cooled zone is assumed to be confocal with the frac-pack at any given time.

The reduction in temperature of the reservoir rock causes contraction, which results in reduction of the in-situ stresses both in the region of reduced temperature and in the surrounding rock, which is at the initial temperature.

The average reduction in stress $\Delta\sigma_{1T}$ inside the cooled zone and perpendicular to the major axes of the frac-pack is given by (Perkins, T.K., and Gonzalez, J.A. 1985):

$$\Delta\sigma_{1T} = \frac{E\alpha\Delta T}{(1-\nu)}\left[\frac{(b_c/a_c)}{(1+b_c/a_c)} + \left\{(1+b_c/a_c)\left\{1+\frac{1}{2}\left\{1.45\left(\frac{h}{2b_c}\right)^{0.9}+0.35\left(\frac{h}{2b_c}\right)^{2}\right\}\left\{1+\left(\frac{b_c}{a_c}\right)^{0.774}\right\}\right\}\right\}^{-1}\right] \quad \text{(B.2)}$$

Where, h is the thickness of the formation, a_c and b_c are the major and minor axes of the cooled ellipse (calculated from equation C.1), α is the linear coefficient of thermal expansion of the reservoir rock and E is the Young's modulus of the reservoir rock.

Pore pressure changes also cause stress changes in the rock. Lubinski (Perkins, T.K., and Gonzalez, J.A. 1985) has shown that for a non-deformable pore structure, i.e. assuming the porosity and permeability of the rock to be independent of the pressure, the stress-strain relationships for thermal phenomena and the pore pressure phenomena are analogous. The linear coefficient of pore pressure expansion β is analogous to the linear coefficient of thermal expansion α and is calculated as follows:

$$\beta = \frac{1-2\nu}{E} - \frac{c_{gr}}{3} \quad \text{..... (B.3)}$$

Where, ν is the Poisson's ratio and c_{gr} is the compressibility of rock grains. To calculate $\Delta\sigma_{1P}$, which is the change in rock stress because of pore pressure changes, α is replaced by β and ΔT is replaced by ΔP in the right hand side of equation 24. The ΔP is taken equal to the average pressure inside the equi-pressure ellipse minus the initial reservoir pressure.

The change in the minimum horizontal stress because of thermal and pore pressure effects is then,

$$\sigma'_{H\min} = \sigma_{H\min} + \Delta\sigma_{1T} + \Delta\sigma_{1p} \quad \text{..... (B.4)}$$

Note that $\Delta\sigma_{1T}$ would be negative and $\Delta\sigma_{1P}$ would be positive for cold water injection and for a rise in pore pressure.

C. Thermal and Waterflood Fronts

The waterflood front and the thermal front are assumed to move confocally with the frac-pack. The two foci of the confocal ellipses are the frac-pack half lengths ($-L_{fp}$, L_{fp}) with thermal front axes given by (Perkins, T.K., and Gonzalez, J.A. 1985):

$$a_c = \frac{L_{fp}}{2}\left(\sqrt{F} + \frac{1}{\sqrt{F}}\right)$$

$$b_c = \frac{L_{fp}}{2}\left(\sqrt{F} - \frac{1}{\sqrt{F}}\right)$$

Where $F = \frac{2V_c}{\pi L_{fp}{}^2 h} + 0.5\sqrt{\left(\frac{4V_c}{\pi L_{fp}{}^2 h}\right)^2 + 4}$ ..... (C.1)

The volume of waterflooded region which is equal to the volume of mobile oil displaced region (and which includes injection water plus the connate water flooded regions) can be calculated as shown:

$$V_{wf} = \frac{W_i}{\phi(1 - S_{or} - S_{wi})}$$ ..... (C.2)

The major axis (a_{wf}) and minor axis (b_{wf}) of the waterflooded confocal ellipse is also calculated by equation C.1 by replacing V_c by V_{wf} given by C.2.

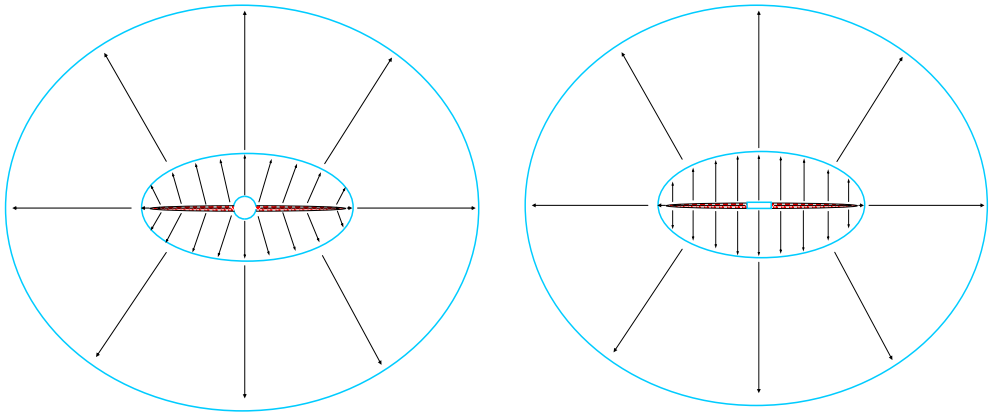

Figure 1: On the left: Top view of equi-pressure lines (in blue) and flow direction (in black) around a frac-packed injector.
On the right: Equivalent rectangular wellbore with bilinear flow assumption inside the inner equi-pressure ellipse

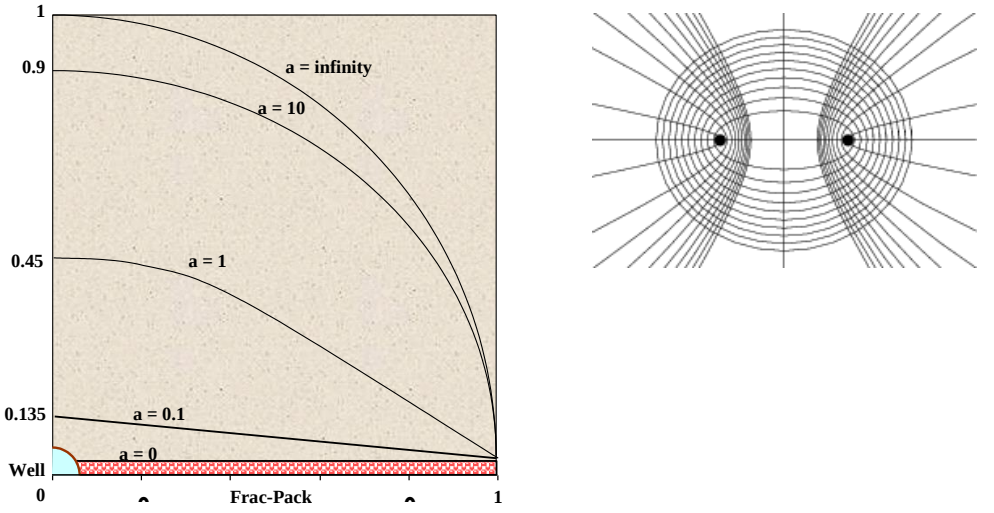

Figure 2: Equi-pressure lines just around the frac-pack for five values of "a" (0, 0.1, 1, 10, and infinity) and r_e/L_{fp} = 2.4.

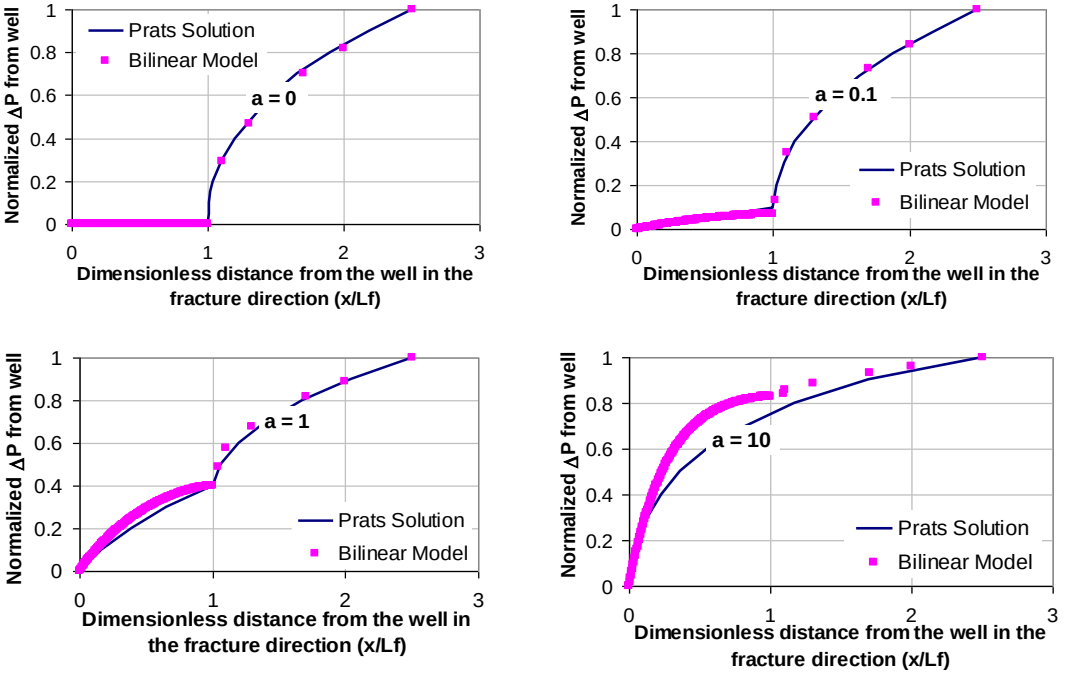

Figure 3: Comparison of results obtained from Prats elliptical model for fractured wells [2] and bilinear model.

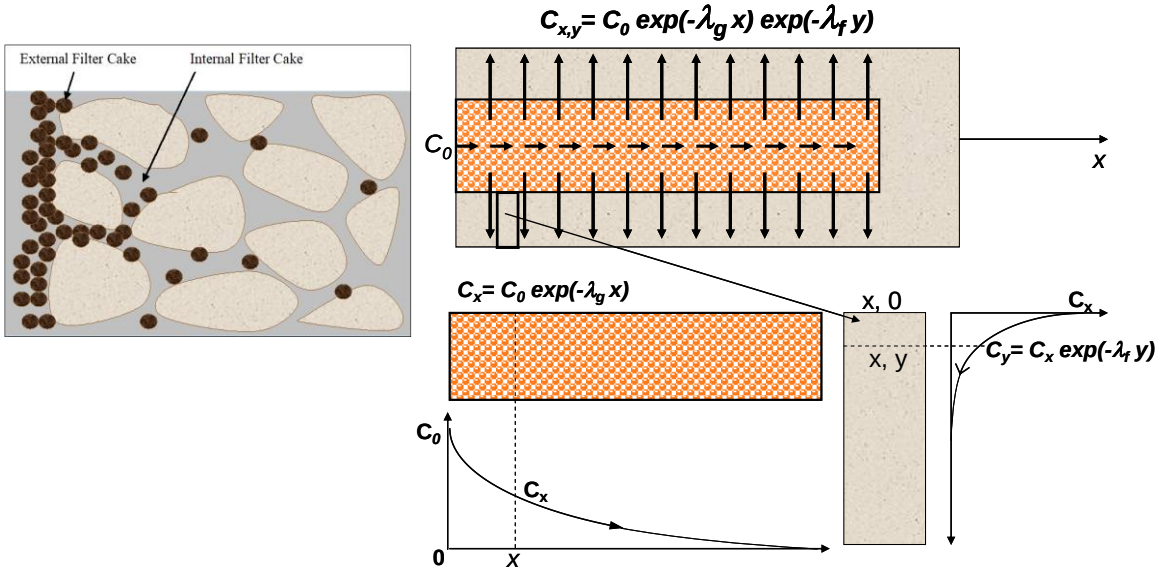

Figure 4: On the left: A schematic of particles plugging the formation and forming an internal and external filter cake.
On the right: Concentration profile of suspended particles in the frac-pack and adjacent formation.

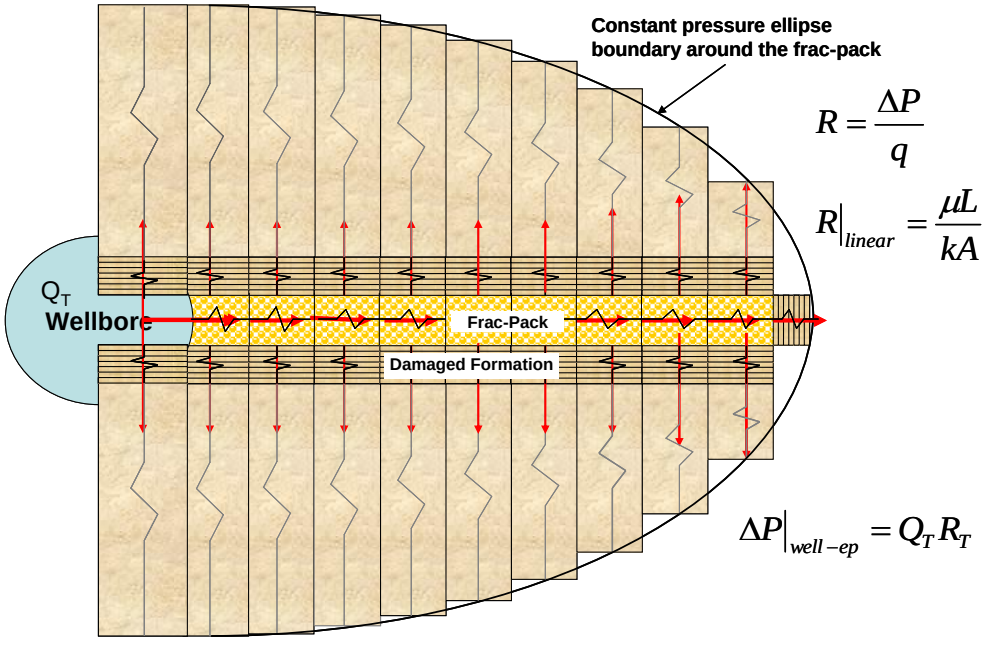

Figure 5: Discretized Frac-pack and the reservoir within the equi-pressure ellipse and bilinear flow resistors.

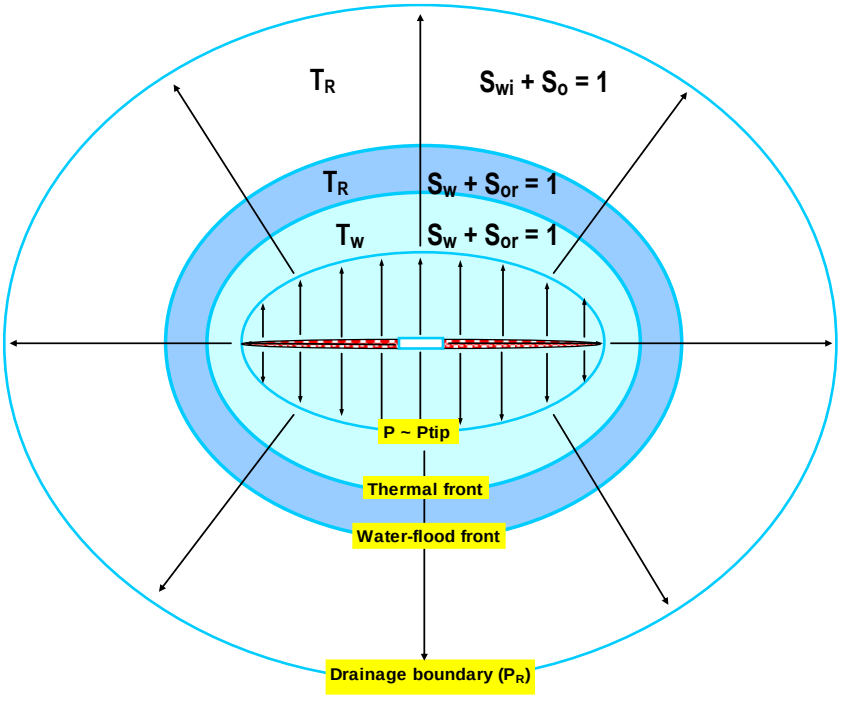

Figure 6: A schematic of thermal and waterflood front as confocal ellipses after they have crossed the equi-pressure ellipse.

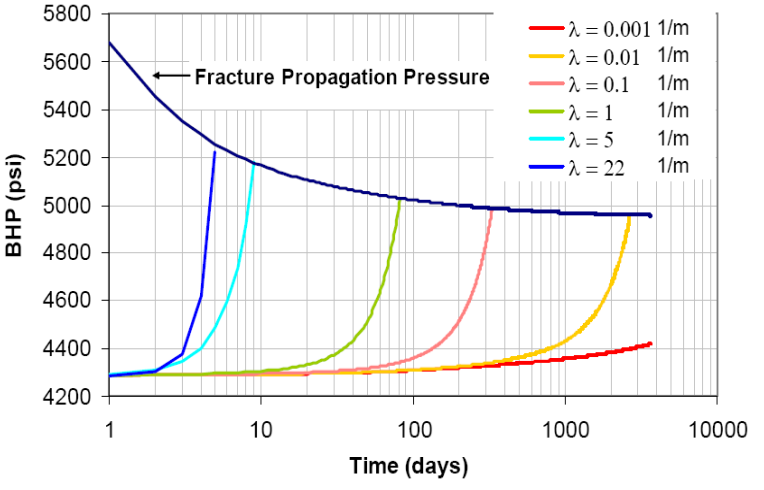

Figure 7: Rise in bottom-hole pressure as a function of different filtration coeffs for the frac-pack.

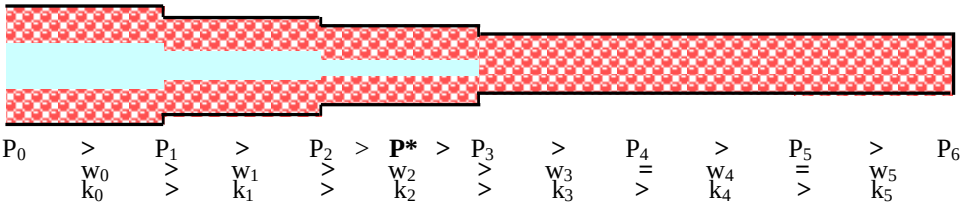

Figure 8: A top view of the widened frac-pack with a high permeability channel.

$$K_c(x,t) = \frac{[w(x,t) - w_{fpi}]^2}{12} \qquad w(x,t) - w_{fpi} = \frac{2[P_{fp}(x,t) - P_{fp}^{*}(x,t)](1-\upsilon^2)h}{E}$$

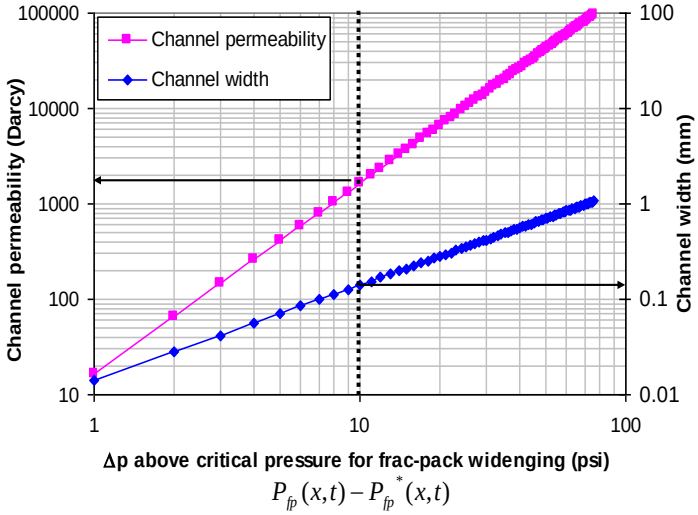

Figure 9: Channel width and permeability as a function of pressure in the frac-pack above the critical pressure.

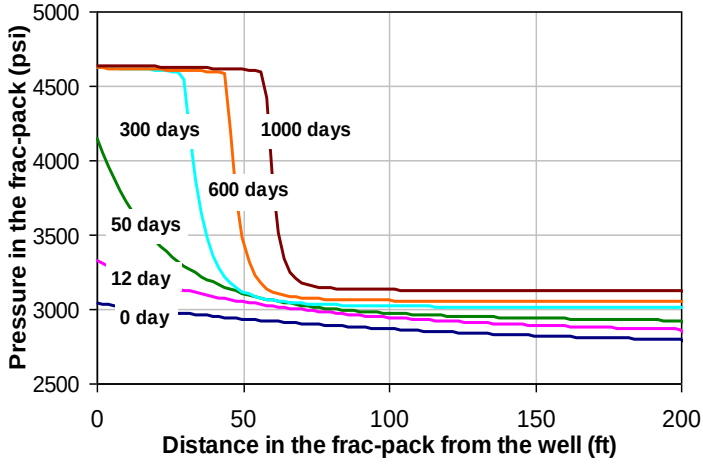

Figure 10: Frac-pack pressure profile with injection time.

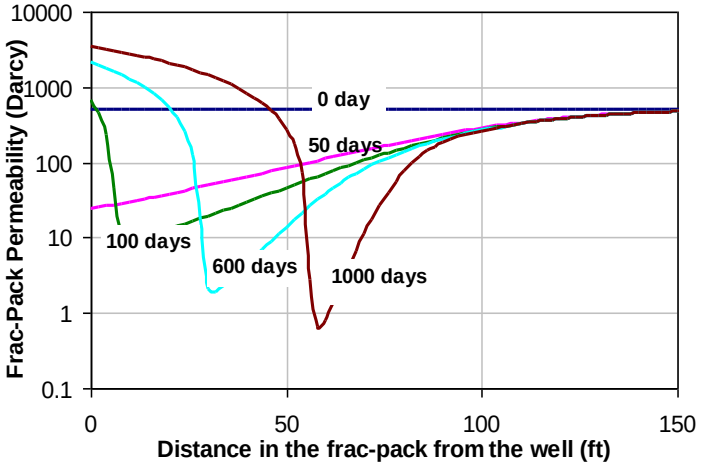

Figure 11: Frac-pack permeability with injection time.

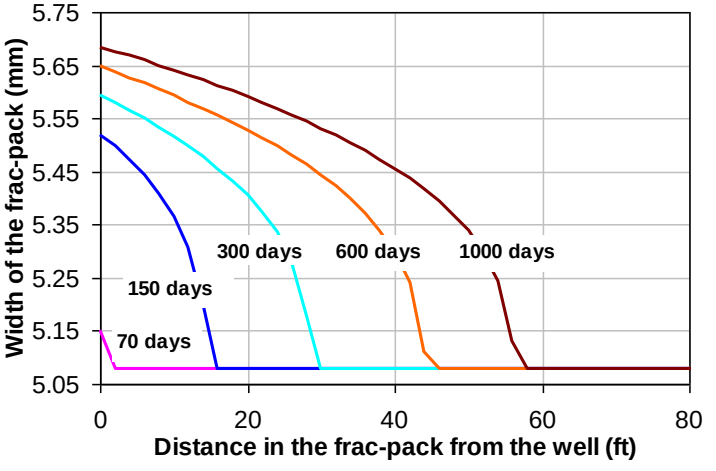

Figure 12: Frac-pack width profile with injection time.

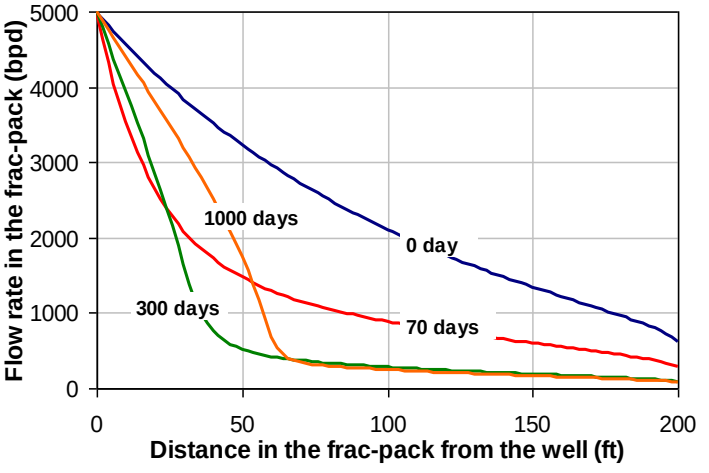

Figure 13: Flow rate in the frac-pack with injection time.

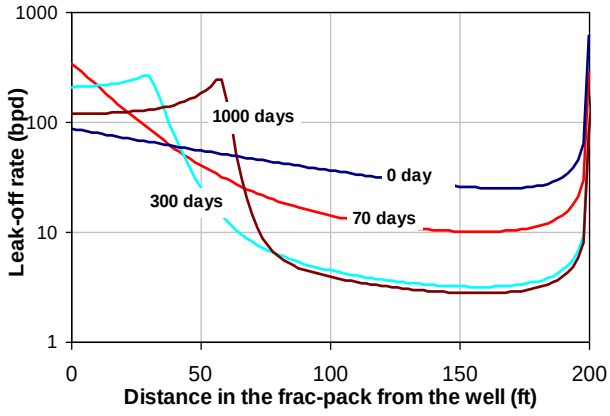

Figure 14: Flow rate perpendicular to the frac-pack (leak-off rate) with injection time.

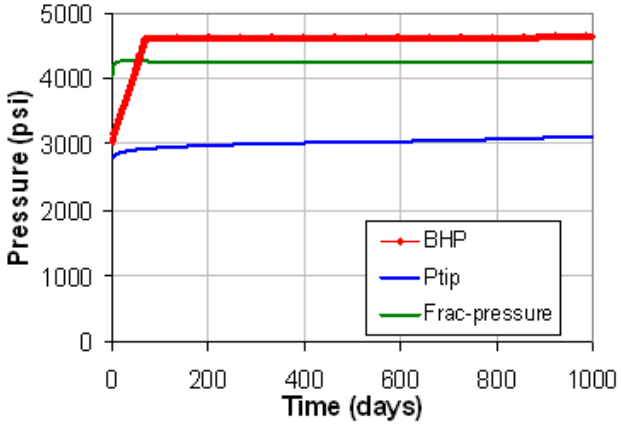

Figure 15: Bottomhole pressure, pressure at the frac-pack tip and fracture propagation pressure with injection time.

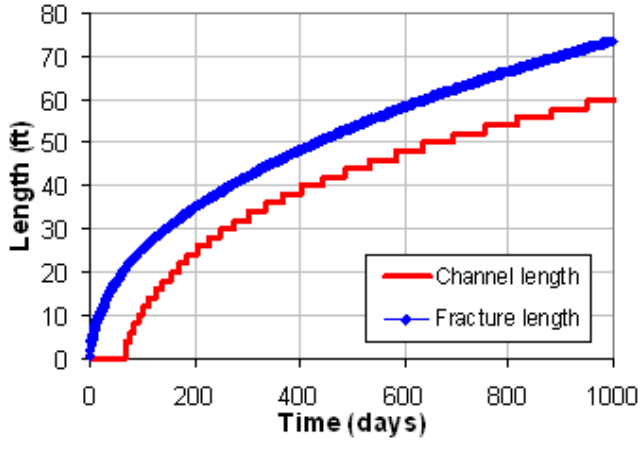

Figure 16: Comparison showing growth of a fracture in an initially unfractured injector vs. growth of a channel in a frac-packed injector with injection time.

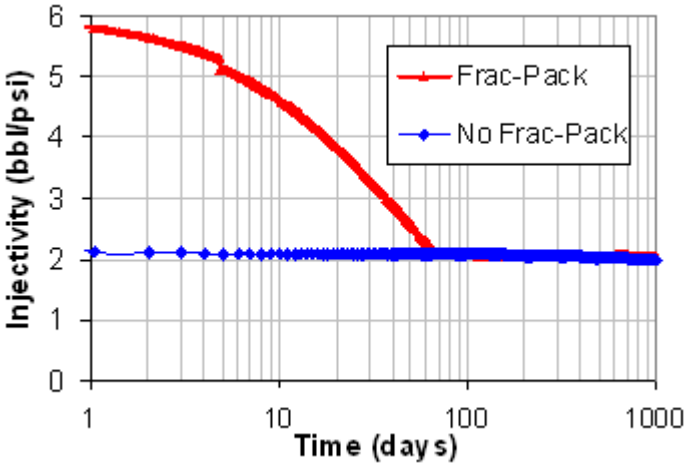

Figure 17: Comparison of injectivity ratio of an unfractured injector with a frac-packed injector. The frac-packed injector has large injectivity ratio initially as compared to the unfractured injector, but later the injectivities become equal.

Table 1: Input parameters for simulation of water injection into a frac-packed and an unfractured well.

$k_{formation}$	100 md	S_{wi}	0.52
r_e	500 m	S_{or}	0.248
r_w	3.6 inch	K_{rw}^o	0.2
Q_T	5000 bpd	K_{ro}^o	0.3
dp	5 micron	μ_w	1 cp
c_0	5 ppm	μ_o	1 cp
h	100 ft	ϕ_f	0.1
P_R	2200 psi	ϕ_{fp}	0.38
σ_{hmin}	4000 psi	ϕ_c	0.2
ν	0.2	k_c	0.001 md
E	$4.35 * 10^6$ psi	$d_{formation\ grains}$	200 microns
$T_R = T_w$	25 ^oC	$d_{gravels}$	1500 microns
k_{fp}	500 Darcy	λ_{fp}	~ 0.1 1/m (calculated by the program)
L_{fp}	200 ft	λ_f	~ 1000 1/m (calc. by the program)
w_{fp}	5.08 mm		

Chapter 8: Pressure Transient Model in WID

8.1 A Simple Model for Estimating Pressure in an Injection Well with 2-phase Flow.

The early pressure solution at the well and in the reservoir for single-phase flow between the well and the reservoir is well-known through the solution of the diffusivity equation. This pressure solution is applied as a standard in well-testing to estimate reservoir permeability, skin, and drainage radius of the reservoir. However so far this method has been applied mostly in production wells which has mostly single phase flow; however to apply this diagnostic method to injection wells need pressure solution of the diffusivity equation with 2-phase flow as in the case of injection wells (water injected into an oil reservoir).

We extend the single phase pressure solution for the diffusivity equation to 2-phase flow as an approximate method to apply it to injection well pressure build-up testing.

$$P(r_w,t) = P_R + \frac{162.6qB}{h}\left[\frac{\mu}{k}\right]_{eff}\left[\log t + \log\left[\frac{1}{\phi c_t r_w^{\,2}}\right]\left[\frac{k}{\mu}\right]_{eff} - 3.23\right]$$

The effective mobility is calculated instead of a single-phase mobility as a function of the injection water front and temperature front as shown below.

$$\left[\frac{\mu}{k}\right]_{eff} = \frac{\frac{(\mu_w)_{T_w}}{kk_{rw}}\ln\left[\frac{r_c}{r_w}\right] + \frac{(\mu_w)_{T_R}}{kk_{rw}}\ln\left[\frac{r_{wf}}{r_c}\right] + \frac{(\mu_o)_{T_R}}{kk_{ro}}\ln\left[\frac{r_e}{r_{wf}}\right]}{\ln(r_e/r_w)}$$

8.2 Comparison of Analytical Model Results with CMG

Below are plots showing a comparison of the above approximate method in calculating the early well pressure with CMG-IMEX (a industry standard black-oil reservoir simulator). Mobility ratios of 0.375 (low viscosity oil), 1, 3.75, and 9.5 (viscous oil displacement or low injection water temperature) were used as four different cases covering the range of injection scenarios for effective water-flooding.

Kory relative permeability model was used for flow of both oil and water as a function of their saturations. Three values 1, 2, and 3 for the Kory's exponent were considered as to cover the possible rock types. We can clearly see that the steady state results were completely off from both the approximate model and the CMG-IMEX results at early time. However the approximate method provided reasonable early time pressure values with CMG-IMEX pressure values as quite correct reference values. At late time the CMG-IMEX

pressure values took off because the reservoir model used in CMG was a closed reservoir with no flow boundaries. A closed reservoir will result in a wellbore pressure rise abruptly once the pressure transient reaches the boundaries where as in an unclosed or infinite acting reservoir the pressure will rise close to the solution presented above.

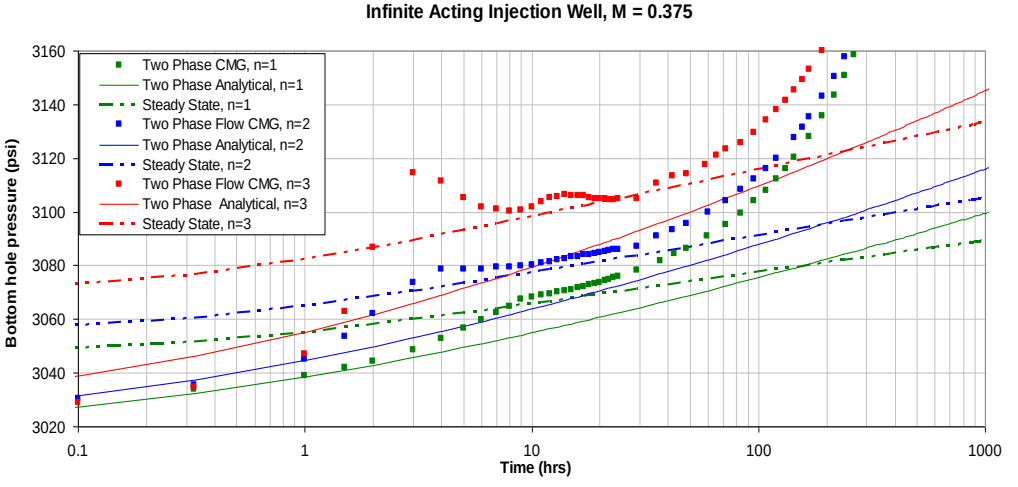

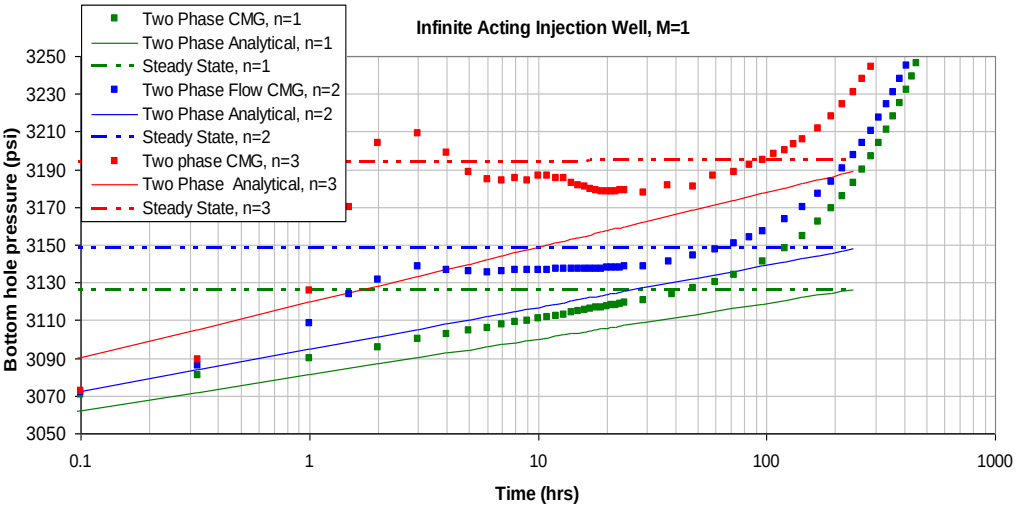

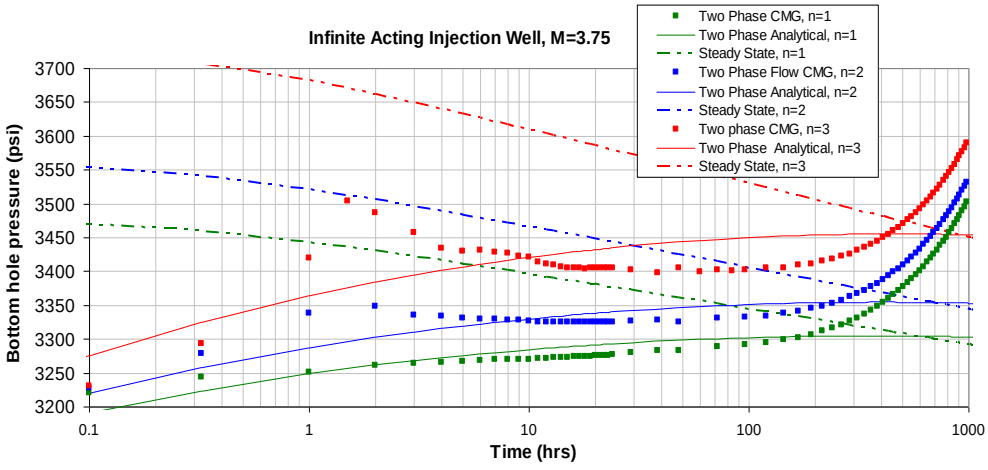

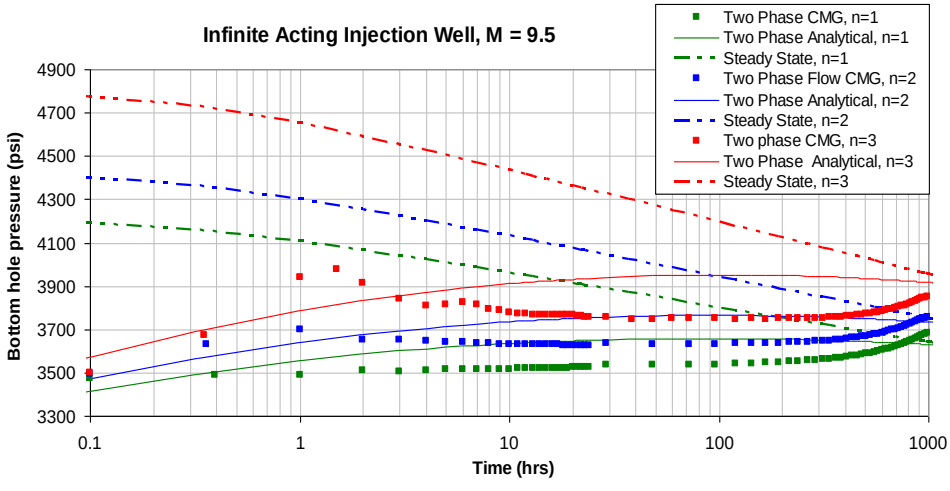

The above plots comparing early well pressure results obtained from CMG, the analytical model and steady stated model (WID 7.2) for mobility ratios between 0.375 and 9.5 suggest that steady state well pressure (WID 7.2) and more accurately estimated well pressure (CMG) vary greatly at early time. Therefore WID 7.2 early pressure model was modified to the analytical model presented above to estimate closely the early time pressure in an injection well. The analytical model agrees well with CMG results at M = 3.75 but yields larger pressure estimates at smaller mobility ratios and lower pressure estimates at higher mobility ratios.

8.3 Comparison of WID Early Pressure Model with CMG

Note: The grid size (ΔX) near the wellbore is 3 ft.

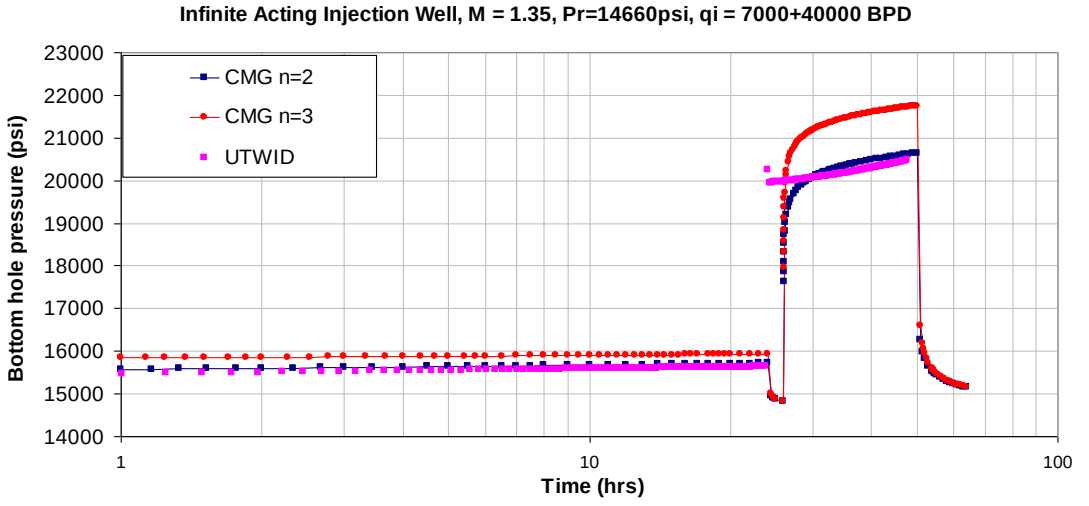

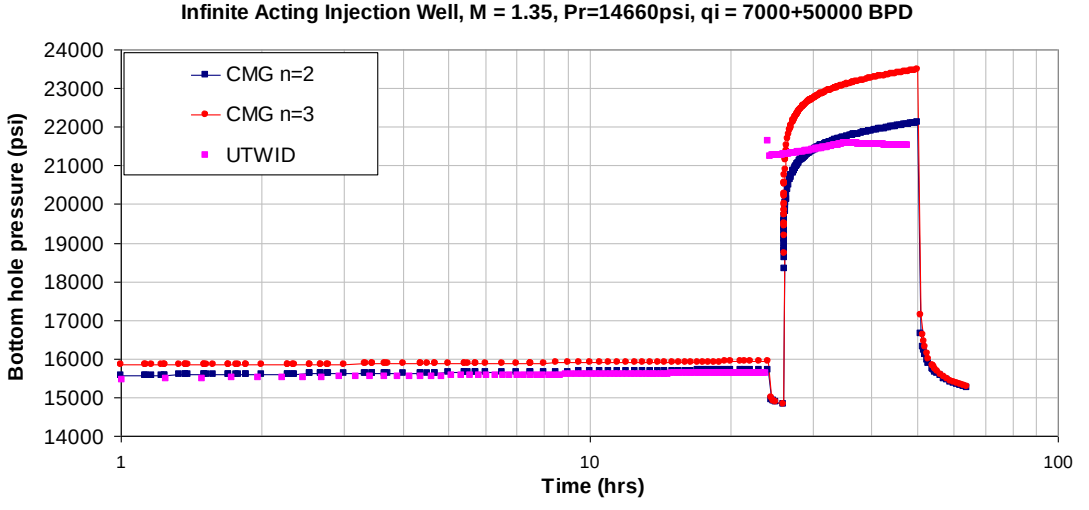

The differences between CMG and WID 7.2 pressure estimate seem reasonable and therefore WID 7.2 uses now the analytical model presented to estimate the early pressure in an injection well. We see that WID pressure results flatten at 35 hrs and 21600 psi approximately because of a creation of a fracture. This is not modeled in CMG simulations and therefore the pressure results from CMG continue to go up.

8.4 A Simple Model for Estimating BHP for a Fractured Injector

The early time pressure in the fractured well can be estimated using Gringarten's infinite conductivity fracture model in an infinite acting reservoir. The fracture is assumed to be infinitely conductive with no wellbore storage and skin.

$$P_{wf}(t_{Dxf}) = P_R + \left(\frac{141.2q(\mu/k)_{eff}}{h}\right)P_D(t_{Dxf})$$

$$P_D(t_{Dxf}) = \frac{1}{2}\sqrt{\pi t_{Dxf}}\left[erf\left(\frac{0.134}{\sqrt{t_{Dxf}}}\right) + erf\left(\frac{0.866}{\sqrt{t_{Dxf}}}\right)\right] + 0.067E_1\left(\frac{0.018}{t_{Dxf}}\right) + 0.433E_1\left(\frac{0.750}{t_{Dxf}}\right)$$

Where $$t_{Dxf} = \frac{0.0002637t}{\phi(\mu/k)_{eff}(c_t)_{eff}\,x_f{}^2}$$

The effective mobility at time t for the entire reservoir is approximated as:

$$\left[\frac{\mu}{k}\right]_{eff} = \frac{\frac{(\mu_w)_{T_w}}{kk_{rw}}\ln\left[\frac{(a_c+b_c)}{x_f}\right] + \frac{(\mu_w)_{T_R}}{kk_{rw}}\ln\left[\frac{(a_w+b_w)}{(a_c+b_c)}\right] + \frac{(\mu_o)_{T_R}}{kk_{ro}}\ln\left[\frac{2r_e}{(a_w+b_w)}\right]}{\ln(2r_e/x_f)}$$

The effective total compressibility at time t for the entire reservoir is approximated as:

$$(c_t)_{eff} = \frac{c_{tcool}(a_cb_c) + c_{tcw}(a_wb_w - a_cb_c) + c_{ti}(r_e{}^2 - a_wb_w)}{r_e{}^2}$$

An average c_t for the reservoir is calculated based on the volume of the different regions with different S_w and S_o as a function of time:

$$c_{tcool} = c_f(T_{wi}) + (1-S_{or})c_w(T_{wi}) + S_{or}c_o(T_{wi})$$

$$c_{tcw} = c_f(T_R) + (1-S_{or})c_w(T_R) + S_{or}c_o(T_R)$$

$$c_{ti} = c_f(T_R) + S_{wi}c_w(T_R) + (1-S_{wi})c_o(T_R)$$

This is based on the definition of the total compressibility for a single phase flow in a two phase system:

$$c_t = c_f + S_wc_w + S_oc_o$$

Note the units in the above equations are field units:

t	hrs
μ	cp
k	md
h	ft
c_t	1/psi
x_f	ft
P	psi
q	bpd (bottomhole rate)
r	ft
ϕ	fraction

8.5 Superposition for Variable Injection Rates

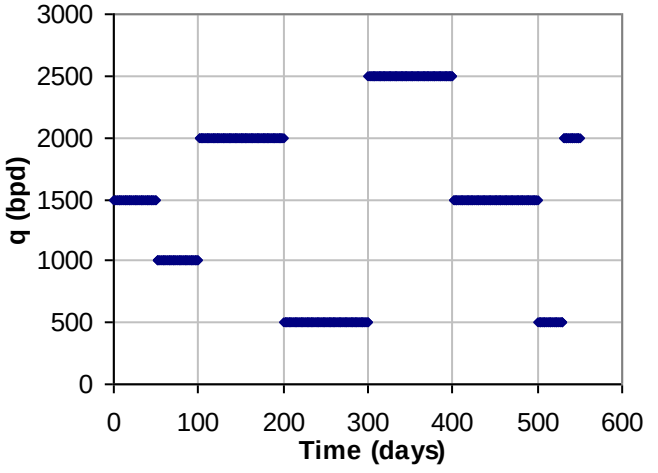

Figure above shows a variable injection rate history for a typical injection well. The injection starts at time 0; the rate remains constant at q_1 until time t_1, then changes to q_2 until time t_2, etc. The last rate is denoted as q_N until injection time t_N which is also the end of injection. We can calculate the pressure at the well (or at any other point for which we know P_D) at any injection time by using the principle of superposition as follows:

$$P_{wf}(t) = P_R + \frac{141.2q}{h}(\mu/k)_{eff}\left[q_1 P_D(t_D) + (q_2 - q_1)P_D([t-t_1]_D)\right.$$
$$\left. +(q_3 - q_2)P_D([t-t_2]_D + \ldots + (q_N - q_{N-1})P_D([t-t_{N-1}]_D)\right]$$

To account for non-unit mobility during injection, the approximate model for effective mobility is used in the above equation. The solution for PD for a fractured well with in a constant pressure boundary is approximated as follows:

$$P_D(t_D) = \min\left[P_{D\infty}(t_D), P_{DSS}(t_D)\right]$$

Where $P_{D\infty}(t_D)$ is the solution for wellbore pressure in an infinite reservoir while $P_{DSS}(t_D)$ is the solution for wellbore pressure in a finite reservoir with a constant pressure boundary. $P_{D\infty}(t_D)$ is calculated using Gringarten's solution as presented in section 5.5 while $P_{DSS}(t_D)$ is calculated as follows:

$$P_{DSS}(t_D) = \frac{h}{141.2q\left(\mu/k\right)_{eff}}\Delta P_{SS}$$

Where ΔP_{SS} is calculated in WID as a function of time t using piston like fronts and Darcy's law. Note that the ideal state pressure drop in WID could be different in different layers because the flow rate in each layer is calculated based on the actual total pressure drop in a layer.

The details of the equations and a better write-up can be found in the following SPE paper:

Suri, A., and Sharma M.M. 2010. Estimation of Fracture Lengths and Injection Profile by History Matching Injection Well Pressures in a Multi-layered Reservoir. SPE Western Regional Meeting 27-29 May 2010 Anaheim, California, USA.

Chapter 9: Injection Modeling with Fracture Closure

9.1 Injection Well Modeling with Fracture Closure

A new feature added to WID 7.2 is the inclusion of the possibility that the propagating injection induced fracture will close if the pressure at the fracture tip becomes lower than the minimum horizontal stress during injection because of either a pump shut down or a large decrease in injection rate.

If an injection well was un-fractured initially, and was fractured during subsequent water injection, then, during a shut down the fracture may remain propped open due to the solids that have accumulated in the fracture or close completely (with the solids being absorbed within the rock matrix). If the injection rate is decreased significantly, the induced fracture may close partially to yield a shorter fracture length such that it honors the condition that the fracture tip pressure is equal to the minimum horizontal stress. The pressure at the tip is dependent mainly on the injection rate and if that is reduced the fracture will tend to close.

9.2 Algorithm for Injection Well Modeling with Fracture Closure

The cumulative solids around the shorter or closed fracture are estimated using a simple model based on the injection history. It is assumed that the solids around a fracture are distributed uniformly every time the fracture length changes. The algorithm (with equations) that was used to calculate fracture opening and closure and account for the cumulative solids around the fracture if the fracture closes to some reduced length at any time is presented below:

$$t_{\max}1 = 0$$

$$t_{\max}2 = 0$$

Do while ($t_{max2} < t$)

$$t_{\max}2 = \max loc\left[l_f\left(t_{\max}1+1 : t\right)\right]$$

$$C_s(l_f, t) = \int_{t_{\max}1}^{t_{\max}2} \min\left(q(t)c(t)dt \frac{l_f}{l_f(t_{\max}2)}, q(t)c(t)dt \right)$$

$$t_{\max}1 = t_{\max}2$$

End Do

Where q(t) is the injection rate at time t,
c(t) is the injected solids concentration in the injection fluid at time t,

$L_f(t)$ is the fracture length at time t,
And $C_s(lf, t)$ is the cumulative solids just around the fracture at time t.

This modeling of fracture closure with reduced fracture length at any time t was essential to estimate more accurately the filter cake thickness in the fracture. The filter cake thickness value is the dominant parameter in estimating the pressure at the fracture tip and the bottomhole well pressure. The pressure at the fracture tip is needed to accurately know the fracture length and the bottomhole well pressure is needed to history match the well.

9.3 An Example of Injection Well Modeling with Fracture Closure

The figure below shows an example injection well in which the fracture length in changing with injection time. We can see that the fracture length does not increase monotonically with time but also reduces to smaller values and at some times to the initial frac-pack length (the injector was initially hydraulically fractured). This was a case study done to history match and injection well's performance with known injection rates and injected solids concentration. The fracture lengths were estimated from WID 7.2 as a result of a reasonable history match for the well's injectivity.

Based on field studies we have conducted, we believe that fracture opening and closing occurs in most injection wells as the injection rates change significantly with time. The injection rate history for this well and the history matched injectivity is also shown.

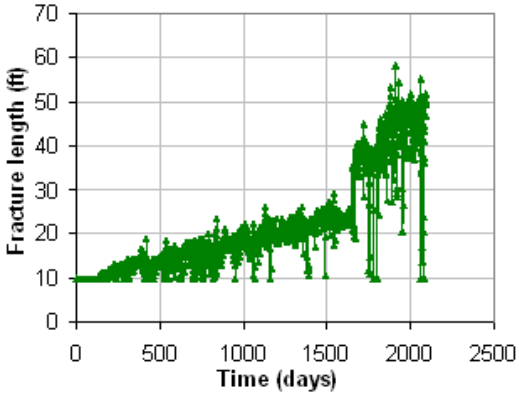

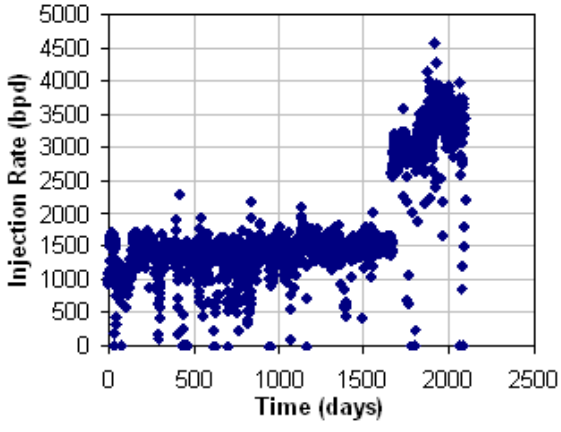

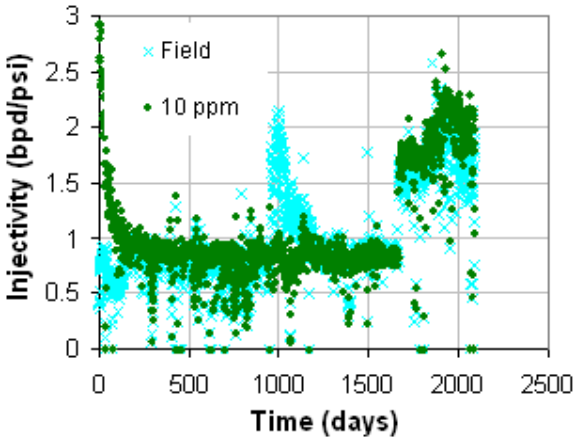

9.4 Equivalent Frac Pack Porosity as it Extends or Closes

There are two options in WID to model injection into frac-packed wells. 1) Comprehensive Frac Pack Model with No Fracture Growth and 2) Injection well with Fracture Option that needs initial fracture length and porosity. The second model is needed to model injection into frac-packed wells that may have frac pack growth in length since the first model does not work after the frac pack needs to grow in length.

The porosity of the initial fracture representing a frac-packed well is termed as equivalent Frac-Pack porosity. The term equivalent is used because the second model does not actual model gravels in the fracture but apparently considers their presence by using the equivalent porosity in the fracture. Equivalent porosity is the porosity of the frac-pack without any injection solids but only with initial volume of gravels. This porosity will change if the frac-pack width and/or length changes from the initial dimensions as the constant volume of the gravels would then occupy a different bulk volume.

WID 7.0 Model

Equivalent Frac-Pack Porosity = 1 – G.V./B.V.

G.V. = gravel volume = constant

B.V. = w x h x Lf

Initial frac-pack porosity = 1 – G.V. (constant) / B.V. (w x h x Lfinitial)
Rearranging the terms to calculate the G.V. (constant)
⇨ G.V. (constant) = B.V. (w x h x Lfinitial) x (1 – Initial frac-pack porosity)

The above formula calculates the gravel volume given the initial frac-pack width, length, height and the initial porosity and then uses this to calculate the changing porosity of the frac-pack as it extends or closes. Note the frac pack can not close more than the initial B.V. due to the gravels. It can only close up to the initial dimensions after it has become wider and longer.

Case 1: Fracture Extension

The equivalent frac-pack porosity after fracture extension from its initial length can be calculated as follows (assuming frac-pack width and height to remain constant).

Equivalent New Porosity = 1 – G.V. (constant) / (w x h x Lf)

Replacing G.V. (constant) in the above equation:

Eq. New Porosity = 1 – w x h x Lfinitial x (1 – Initial frac-pack porosity) / (w x h x Lf)

Equivalent New Porosity = 1 – (Lfinitial / Lf) x (1 – Initial frac-pack porosity)

Improvements are made to the previous WID 7.0 model in WID 7.2 model:
The assumption of constant width of the frac-pack as it extends or closes is removed and the actual width of the frac-pack at any time is used instead. However there is one flaw in the equivalent frac-pack (fracture) model that it does not honor the initial width of the frac-pack but rather calculates its width based on the PKN model. The initial width of the equivalent frac-pack as calculated by PKN model is very small (~ 1 mm) which would give a very small volume of the fracture as compared to the actual volume of the frac-pack.

The solution used: The porosity of the equivalent frac-pack is assumed to be equal to the initial actual frac-pack porosity until the equivalent frac-pack volume is <= the actual initial frac-pack volume. After that the gravels are uniformly distributed in the fracture with higher bulk volume and the equivalent new porosity is recalculated. The equation would for the equivalent frac-pack porosity is then calculated as followed:

Based on the previous time step width and new time step fracture length the porosity of the frac-pack with the gravels but no solids is calculated as follows:

$$\phi_g = \phi_{g\,ini} \qquad \text{when} \qquad wL_f <= w_{ini}L_{fini}$$

$$\phi_g = 1 - \frac{w_{ini}L_{fini}}{(wL_f)_{\max}}\left[1 - \phi_{g\,ini}\right] \qquad \text{when} \qquad wL_f > w_{ini}L_{fini}$$

Once the porosity is calculated, the filter cake thickness is calculated as follows:

$$h_c = \frac{\left[(t - tt)/t\right]\int_0^t qc\,dt}{(1-\phi_c)\phi_g A_f}$$

Note this equation applies to an extending or static fracture. If the fracture closes to certain length less than the maximum length that it has reached at any time during injection then the integral term is replaced by another term as calculated by the algorithm under section 9.2 of the user guide. The injected solids are not redistributed in a closing fracture but are only uniformly distributed in an extending fracture. Using the filter cake thickness and fracture length, new width of the fracture is calculated as given by Table 1 of Chapter 4 (Technical Documentation).

The new set of equations account for: a) the actual width of the fracture and b) the gravel volume is distributed uniformly in the extended fracture to its new bulk volume that it has reached at any time during injection.

Case 1: Fracture Closure

Model: Assume a fracture closes back from 100 ft to 50 ft because the pressure in the region (between 50 and 100 ft) has reduced below minimum horizontal stress (sigmahmin) due to reduction in injection rate. The model assumes that the gravels would not redistribute in the 50 ft fracture but still remain in the 100 ft fracture/reservoir with only 50 ft as effective fracture. By effective fracture (50 ft) we mean the part of the reservoir that is allowing flow while the remaining 50 ft (between 50-100 ft) even though is packed with gravels and may be some filter cake does not have any open width that allows for flow. Now actually if there is no filter cake in this region then it should allow for flow through the gravels but the model assumes that these gravels are supposedly crushed such that no open width is available in this closed region where pressure < sigmahmin. This is an area of research and thought that needs to be discussed further. As of now this is what is implemented in WID 7.2 for Equivalent Frac-Pack Porosity as Closes.

Schematic of the half frac-pack with gravels and porosity in determining the thickness of the filter cake:

1. Frac-Pack with no gravels (for reference)

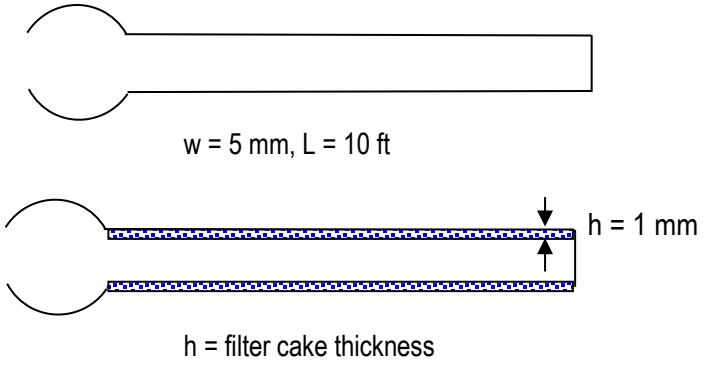

2. Frac-Pack with gravels (at initial length and width)

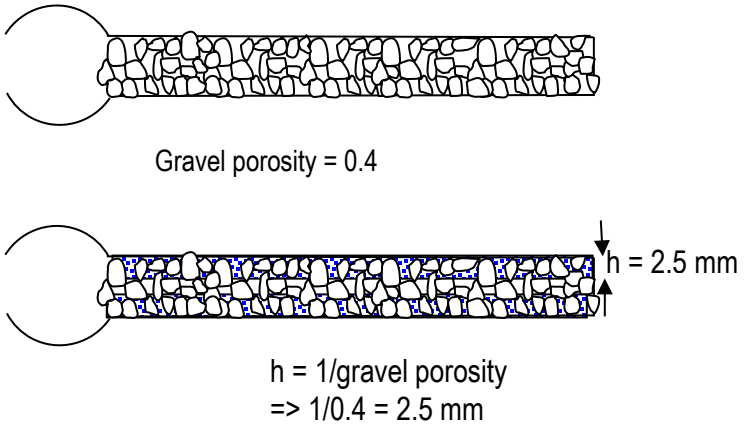

The filter cake is hard to visualize growing between the gravels (zoom to 200 % for a better view of the filter cake between the gravels) but basically if you calculate the thickness of the same filter cake volume as in 1) you would get 2.5 mm of its thickness.

3. Frac-Pack is extended to width of 7 mm and length of 12 ft (with same volume of initial gravels and same volume of filter cake)

$$\phi_g = 1 - \frac{w_{ini} L_{fini}}{(wL_f)_{\max}} \left[1 - \phi_{g\,ini}\right] \quad => \quad \phi_g = 1 - \frac{5x10}{7x12}\left[1 - 0.4\right] \quad => \quad \phi_g = 0.643$$

$$h_c = \frac{\left[(t - tt)/t\right] \int_0^t qc\,dt}{(1 - \phi_c)\phi_g A_f} \quad => \quad \frac{h_c}{h_{cini}} = \frac{\phi_{gini} A_{fini}}{\phi_g A_f} \quad => \quad \frac{h_c}{2.5} = \frac{0.4x5x10}{0.643x7x12} \quad =>$$

$$h_c = 0.926\,\text{mm}$$

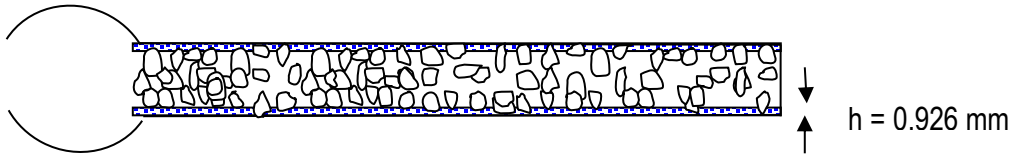

4. Frac-Pack (with same volume of gravels and same volume of filter cake) that has closed back to the initial length (10 ft) from the extended length of 12 ft. Note up to the point in the fracture where the pressure ~ sigmahmin, the schematic remains similar as above (shown below) with same width and the same filter cake thickness. However in the part of the fracture where p<sigmahmin, the fracture is conceived to be as shown below

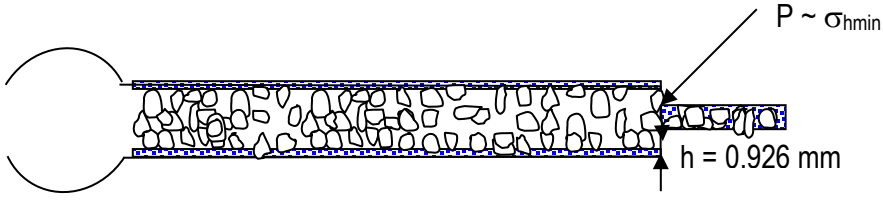

Even though the porosity of the gravels and the filter cake thickness is the same in the effective fracture as 7 mm and 0.926 mm, the porosity and the thickness of the filter cake in the closed part of the fracture is not and may be between the proppant size (1 mm) and the filter cake thickness of 2.5 mm. The program assumes that the ineffective fracture would have no conductivity while in reality it may have some conductivity due to proppants keeping the fracture open. However due to the filter cake that has compressed in this region would make this region quite impermeable. Moreover the minimum horizontal stress on this region which is higher than the fluid pressure would even reduce the porosity lower than 0.4 making the permeability really low. So saying that this part of the fracture is ineffective seems reasonable.

Chapter 10: Skin Distribution and Cross-Flow in Vertical Well Layers

10.1 Skin Distribution between Layers with Initial Well Skin

Definition: Skin of a layer in an injection well is defined as:

$$s_l = \frac{2\pi\left(\frac{kk_{rw}h}{\mu_{wi}}\Delta p_s\right)_l}{q_l} \qquad (1)$$

Note ΔPs is the pressure drop due to skin around the well / fracture. The flow properties used in the above equation are for the injection fluid and could be different from the actual flowing fluid around the well. The reader is cautioned that the pressure drop due to the skin should be calculated using the injected phase properties even if the well has two phases flowing around it.

Definition: Skin of the entire injection well is calculated from the skin of each layer:

Given the skin of N layers s1, s2, .. sN, skin of the well is calculated as followed:

$$\frac{\sum_{i=1}^{N}\left(\frac{kk_{rw}h}{\mu_{wi}}\right)_i}{\ln\left(\frac{r_e}{r_w}\right)+s} = \frac{\left(\frac{kk_{rw}h}{\mu_{wi}}\right)_1}{\ln\left(\frac{r_e}{r_w}\right)+s_1} + \frac{\left(\frac{kk_{rw}h}{\mu_{wi}}\right)_2}{\ln\left(\frac{r_e}{r_w}\right)+s_2} + .. \qquad (2)$$

Only s (skin of the entire well) is unknown.

Given the initial skin of the well, how to distribute the skin to its layers (what is the skin of all the layers)

If the skin of the well is known but the well has multiple layers, then there can be multiple solutions to it and therefore the question on how to distribute the well skin to its layers originates. Distributing the skin of the well to all its layers evenly and equal to the initial well skin seems to be good first guess if the layers skin is not known. Let's make sure if it is so.

$$q_l = \frac{2\pi\left(\frac{kk_{rw}h}{\mu_{wi}}\right)_l \Delta p}{\ln\left(\frac{r_e}{r_w}\right) + s_l} \tag{3}$$

The equation above is application of Darcy's law for calculating the flow rate in any layer of the well with a known skin of the layer. We see that the flow rate is proportional to the (k*krw*h/mu) of the layer. If sl is 0, the flow rate would be proportional to (k*krw*h/mu). Therefore, it seems reasonable to distribute the skin of the well evenly to all the layers since the flow distribution would be proportional to the (k*krw*h/mu) which it was when there was no skin (s=0) and the total skin will remain equal to the well skin. However if the the well is frac packed (discussion of the next section) or some other form of skin in any layer is known, then the skin of the well should not be evenly and equally distributed to its layers, i.e. the skin of the layers should not be equal to the well skin.

Example: Skin of a well with one or more layers frac packed

If the initial skin of the well is known and the well is frac packed (either all the layers, or some of the layers), then the skin of the layers should not be equal to the well skin. Let's find out why.
The flow rate into an infinitely conductive frac packed layer is given as followed:

$$q_l = \frac{2\pi\left(\frac{kk_{rw}h}{\mu_{wi}}\right)_l \Delta p}{\ln\left(\frac{2r_e}{lf_l}\right)} \tag{4}$$

$$\Rightarrow q_l = \frac{2\pi\left(\frac{kk_{rw}h}{\mu_{wi}}\right)_l \Delta p}{\ln\left(\frac{r_e}{r_w}\right) + s_{fl}} \tag{5}$$

$$\Rightarrow \text{where } s_{fl} = \ln\left(\frac{2r_e}{lf_l}\right) - \ln\left(\frac{r_e}{r_w}\right) \tag{6}$$

$$\Rightarrow s_{fl} = \ln\left(r_w\right) - \ln\left(\frac{lf_l}{2}\right) \tag{7}$$

$$\Rightarrow s_{fl} = \ln\left(\frac{2r_w}{lf_l}\right) \quad (8)$$

Note sfl would be negative because of the frac pack (lf > 2rw). If a layer does not have a frac pack then sfl is zero.

Now suppose the well has some skin, then well skin needs to be in the flow rate equation of a layer. If the well's skin is evenly distributed (sl = swell) then the equation for flow rate into the frac packed layer would become the following:

$$q_l = \frac{2\pi\left(\frac{kk_{rw}h}{\mu_{wi}}\right)_l \Delta p}{\ln\left(\frac{r_e}{r_w}\right) + s_w} \quad (9)$$

This would mean that sfl (negative skin due to the frac pack) has no impact on the layer's flow rate. It would be as if the layer is not frac packed in terms of flow distribution. It would be more reasonable to get sl by honoring sfl too rather than just making it equal to sw. The flow would then be distributed in proportionality to (k*krw*h/mu) and sfl (i.e. both the layer transmissibility and frac pack are honored).
Finding the additional skin in the layer due to the well skin which also has an effect of the initial frac pack skin can be done as followed:

$$s_l = s_{fl} + A \quad (10)$$

Using s (skin of the well) and skin of the fracture or any other form of skin known in any layer, A is obtained. This would distribute the skin of the well in accordance to both (k*krw*h/mu) and the frac pack.

$$\frac{\sum_{i=1}^{N}\left(\frac{kk_{rw}h}{\mu_{wi}}\right)_i}{\ln\left(\frac{r_e}{r_w}\right) + s} = \frac{\left(\frac{kk_{rw}h}{\mu_{wi}}\right)_1}{\ln\left(\frac{r_e}{r_w}\right) + s_{f1} + A} + \frac{\left(\frac{kk_{rw}h}{\mu_{wi}}\right)_2}{\ln\left(\frac{r_e}{r_w}\right) + s_{f2} + A} + .. \quad (11)$$

It seems obtaining A is not simple in the above equation because it a polynomial of nth order with n roots.

Solution:

1. Trial and Error:

First guess: (1E-2, 1E+2)
Assume that A exists between 0.01 (Amin) and 100 (Amax). To make sure first, calculate the value of the polynomial with Amin.

$$f(A_{\min}) = -\frac{\sum_{i=1}^{N}\left(\frac{kk_{rw}h}{\mu_{wi}}\right)_i}{\ln\left(\frac{r_e}{r_w}\right)+s} + \frac{\left(\frac{kk_{rw}h}{\mu_{wi}}\right)_1}{\ln\left(\frac{r_e}{r_w}\right)+s_{f1}+A_{\min}} + \frac{\left(\frac{kk_{rw}h}{\mu_{wi}}\right)_2}{\ln\left(\frac{r_e}{r_w}\right)+s_{f2}+A_{\min}} + .. \quad (12)$$

Let's say the value of the function is positive. Next we calculate the value of the polynomial with Amax.

$$f(A_{\max}) = -\frac{\sum_{i=1}^{N}\left(\frac{kk_{rw}h}{\mu_{wi}}\right)_i}{\ln\left(\frac{r_e}{r_w}\right)+s} + \frac{\left(\frac{kk_{rw}h}{\mu_{wi}}\right)_1}{\ln\left(\frac{r_e}{r_w}\right)+s_{f1}+A_{\max}} + \frac{\left(\frac{kk_{rw}h}{\mu_{wi}}\right)_2}{\ln\left(\frac{r_e}{r_w}\right)+s_{f2}+A_{\max}} + .. \quad (13)$$

The value of the function should be negative if the value of A lies between Amin and Amax. If the value of the function is positive, we start increasing the range between Amin and Amax.

Second guess of the range, increase the range by two orders (one at min side and one at max side), i.e. decrease Amin to 1E-3 and increase Amax to 1E+A. Calculate the value of the polynomial again to see if the function changes sign. Keep increasing the range until the range is found where the by the function changes the sign. Let's say with Amin the sign is negative and Amax the sign is positive.

Find the value of the polynomial with A = 0.5(Amin+Amax). If the sign is negative then Amin = A, else if sign is positive then Amax = A else A (solution) = A.

Repeat the above loop until f(A)<tolerance (say 1E-15).Routine implemented in FORTRAN and cross checked with EXCEL

10.2 Skin Evolution with Injection

Skin of an injection increases due to injection of solids getting deposited around the well. Note the change in injection fluid mobility compared to the reservoir fluid mobility does not change the well skin. However due to thermal stresses caused by cold fluids injected result in thermal fracturing to such an extent that well injectivity can become higher than the initial (example Prudhoe Bay in Alaska). In most injection wells however the injectivity is reduced due to the combined effect of permeability reduction due to solids deposition in the reservoir around the well (ΔP_{int}), filter cake deposition in the well / fracture (ΔP_c), pressure drop in the frac pack / fracture (ΔP_f), and pressure change due to increase in fracture length. The first three usually increase the well skin as they are positive while the fourth one reduces the well skin as it is usually negative. These four are added along with the pressure drop due to initial well skin (ΔP_{s0}) to calculate the total pressure drop that would then used to calculate the final well skin.

$$\Delta p_s = \Delta p_{s0} + \Delta p_{\text{int}} + \Delta p_c + \Delta p_f + \frac{q_l}{2\pi\left(\frac{kk_{rw}h}{\mu_{wi}}\right)_l}\ln\left(\frac{2r_w}{lf_l}\right) \tag{14}$$

Skin of a layer is calculated after knowing the pressure drop due to damage and fracture in a layer.

$$s_l = \frac{2\pi\left(\frac{kk_{rw}h}{\mu_{wi}}\Delta p_s\right)_l}{q_l} \tag{15}$$

Equation 3 is used knowing all the layers skin to calculate the evolved skin of the well.

Once sl is known during injection, equation 11 is used to calculate the total well skin.

It is questionable how to define skin of the well for a non-hydrostatic reservoir since there can be cross flow. WID uses hydrostatic formulation for calculating total well skin from the skin of its layers even if the reservoir is non-hydrostatic.

Non-hydrostatic Reservoir

$$\frac{\sum_{i=1}^{N}\frac{kk_{rw}h}{\mu_{wi}}\left[P_{wf}-\frac{1}{N}\left(P_{R1}+P_{R2}+..\right)\right]}{\ln\left(\frac{r_e}{r_w}\right)+s} = \frac{\left(\frac{kk_{rw}h}{\mu_{wi}}\right)_1\left(P_{wf}-P_{R1}\right)}{\ln\left(\frac{r_e}{r_w}\right)+s_1} + \frac{\left(\frac{kk_{rw}h}{\mu_{wi}}\right)_2\left(P_{wf}-P_{R2}\right)}{\ln\left(\frac{r_e}{r_w}\right)+s_2} + .. \tag{16}$$

The formulation above for the non-hydrostatic reservoir does not seem right. The L.H.S. is not equal to the R.H.S. The R.H.S is the sum of all the injection rates into the different layers but L.H.S is arbitrary. I can't think of writing an equation in the form of Darcy's radial form for the non-hydrostatic reservoir as a whole. More discussion is provided in the next section on flow distribution in a non-hydrostatic reservoir.

10.3 Flow Distribution when Layers are not in Hydrostatic Equilibrium

Let's suppose there are 3 layers with their own permeability, thickness and fluid type. The layers are divided by thin shales making their pore pressure non-hydrostatic. A schematic of this layer system is shown below. The pore pressures (Pr1, Pr2, and Pr3) in these layers are constant at the boundary (re). The injection rate is Q. The problem is to find out the flow distribution (q1, q2, and q3).

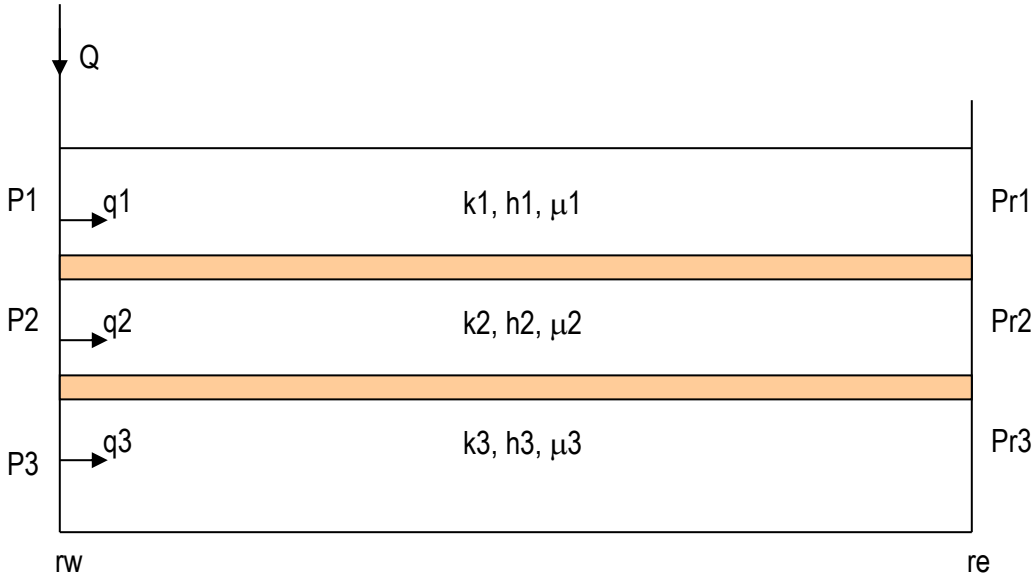

The first thing is to write the flow equation for each layer:

$$q_1 = \frac{2\pi\left(\frac{kk_{rw}h}{\mu_{wi}}\right)_1 (P_1 - P_{r1})}{\ln\left(\frac{r_e}{r_w}\right) + s_1};$$

$$q_2 = \frac{2\pi\left(\frac{kk_{rw}h}{\mu_{wi}}\right)_2 (P_2 - P_{r2})}{\ln\left(\frac{r_e}{r_w}\right) + s_2};$$

$$q_3 = \frac{2\pi\left(\frac{kk_{rw}h}{\mu_{wi}}\right)_3 (P_3 - P_{r3})}{\ln\left(\frac{r_e}{r_w}\right) + s_3}$$

Note P1, P2 and P3 are the pressures in the wellbore and should be hydrostatic. We first find out the excess pore pressures in the 3 layers as followed (with reference as the pore pressure in the first layer):

$$\Delta P_i = \left(P_{ri} - P_{r1}\right) - \left(P_i - P_1\right)$$

If the pore pressures were hydrostatic, the two terms in the bracket would cancel out and the excess pore pressure would be zero for any given layer. Rearranging the equation:

$$\Delta P_i = \left(P_{ri} - P_i\right) + \left(P_1 - P_{r1}\right); \qquad \left(P_i - P_{ri}\right) = \left(P_1 - P_{r1}\right) - \Delta P_i$$

Writing the flow equations in terms of flow resistance (R = ΔP/q)

$$R_i = \frac{\left(P_i - P_{ri}\right)}{q_i} = \frac{\ln\left(\frac{r_e}{r_w}\right) + s_i}{2\pi\left(\frac{kk_{rw}h}{\mu_{wi}}\right)_i}$$

The flow resistance is a constant for a given layer and does not depend on the flow rate or the pressures. Writing the flow rates in terms of flow resistances,

$$q_1 = \frac{\left(P_1 - P_{r1}\right)}{R_1}; \qquad q_2 = \frac{\left(P_2 - P_{r2}\right)}{R_2} = \frac{\left(P_1 - P_{r1}\right) - \Delta P_2}{R_2};$$

$$q_3 = \frac{\left(P_3 - P_{r3}\right)}{R_3} = \frac{\left(P_1 - P_{r1}\right) - \Delta P_3}{R_3}$$

$$Q = q_1 + q_2 + q_3$$

$$Q = \frac{\left(P_1 - P_{r1}\right)}{R_1} + \frac{\left(P_2 - P_{r2}\right)}{R_2} + \frac{\left(P_3 - P_{r3}\right)}{R_3}$$

$$Q = \frac{\left(P_1 - P_{r1}\right) - \Delta P_1}{R_1} + \frac{\left(P_1 - P_{r1}\right) - \Delta P_2}{R_2} + \frac{\left(P_1 - P_{r1}\right) - \Delta P_3}{R_3}$$

$$Q = \left(P_1 - P_{r1}\right)\left[\frac{1}{R_1} + \frac{1}{R_2} + \frac{1}{R_3}\right] - \frac{\Delta P_1}{R_1} - \frac{\Delta P_2}{R_2} - \frac{\Delta P_3}{R_3}$$

Defining total flow resistance as followed:

$$\frac{1}{R_T} = \frac{1}{R_1} + \frac{1}{R_2} + \frac{1}{R_3}$$

$$Q = \frac{\left(P_1 - P_{r1}\right)}{R_T} - \frac{\Delta P_1}{R_1} - \frac{\Delta P_2}{R_2} - \frac{\Delta P_3}{R_3}$$

$$Q + \frac{\Delta P_1}{R_1} + \frac{\Delta P_2}{R_2} + \frac{\Delta P_3}{R_3} = \frac{\left(P_1 - P_{r1}\right)}{R_T}$$

$$\left(P_1 - P_{r1}\right) = R_T \left[Q + \frac{\Delta P_1}{R_1} + \frac{\Delta P_2}{R_2} + \frac{\Delta P_3}{R_3} \right]$$

Using this for the flow rate in the first layer:

$$q_1 = \frac{R_T}{R_1} \left[Q + \frac{\Delta P_1}{R_1} + \frac{\Delta P_2}{R_2} + \frac{\Delta P_3}{R_3} \right]$$

$$q_2 = \frac{R_T}{R_2} \left[Q + \frac{\Delta P_1}{R_1} + \frac{\Delta P_2}{R_2} + \frac{\Delta P_3}{R_3} \right] - \frac{\Delta P_2}{R_2}$$

$$q_3 = \frac{R_T}{R_3} \left[Q + \frac{\Delta P_1}{R_1} + \frac{\Delta P_2}{R_2} + \frac{\Delta P_3}{R_3} \right] - \frac{\Delta P_3}{R_3}$$

Note ΔP1 is zero therefore the above equations can be generalized for any layer (ith layer in an N layer system.

$$q_i = \frac{R_T}{R_i} \left[Q + \sum_{i=1}^{N} \frac{\Delta P_i}{R_i} \right] - \frac{\Delta P_i}{R_i}$$

These results are applicable to any flow geometry that can be represented by flow resistances (example, linear geometry, elliptical geometry etc). However when the flow resistances have flow rate dependence (for ex. polymer flow, Non-Darcy flow), then flow resistance has to be iteratively calculated. However for approximate results the previous flow distribution solution could be used.

The above equation implies that the flow rate in a layer can be negative depending upon the pore pressures, total injection rate and the layer flow resistances.

Chapter 11: 3-Dimensional Fracture Propagation Model

11.1 Introduction

Fracture Height Growth

The process of fracture growth induced by long-term water injection is different from the process of hydraulic fracturing. Some differences which must be accounted for in the water injection fracturing are particle plugging due to solids in the injected water, and thermal stress changes due to the injection of large volumes of cold water. The traditional (Carter's) fluid leak-off model may not be appropriate for water injection fractures due to the above effects.

Similarly to hydraulic fracturing, it is also important to predict the accurate fracture dimensions and the leak-off behavior to understand the injectivity of the water injection project. This data will be the basis of the water quality selection and the subsequent design for the water treatment facility. The fracture growth into the bounding layer, when it is not properly addressed, may significantly distort all aspects of the mechanical and fluid flow behavior. In addition, the time for the induced fracture to reach the bounding layer when the water injection initiates is not negligible in thick zones [1]. However, the breach of the fracture to the adjacent layers cannot be properly predicted by constant height fracture growth model, e.g., PKN model. When water is injected into multiple layers, complicated in-situ stress conditions will require the utilization of the 3-dimensional fracture growth calculation.

Fluid Leak-off Model

The Carter's leak-off model [2] is a conventional fluid leak-off (fluid loss) model for hydraulic fracturing simulations. Many commercial fracturing simulations assume the leak-off coefficient to be constant and use it to calculate the leak-off rate in the fluid material balance. This coefficient is normally specified based on the field injection test or estimated from the reservoir and injection properties. The constant leak-off coefficient from hydraulic fracturing, when used for the water injection projects, may not represent the proper leak-off behavior due to the long-term internal and external filter cake formation. Hence, to calculate the proper leak-off behavior for water injection, we recommend that the particle plugging, stress changes and the fracture mechanics are comprehensively taken into account for the water injection fracture modeling. The leak-off coefficient of water injection fractures will vary with time because the effect of the particle plugging and the in-situ stress change will vary with the long period of the injection. This also requires the calculation of the leak-off rate in the course of the fracturing simulation combined with particle filtration modeling and fluid flow simulations.

Water Injection Models

Since Pang and Sharma [3] and Wennberg and Sharma [4] had built a comprehensive water injection model based on Perkins and Gonzales [5] model, various aspects of improvements have been implemented to the model to build the latest injection well model by Suri *et al.* [6]. An internal filtration model to calculate permeability reduction was improved by Gadde and Sharma [7]. The filtration model by Rajagopalan and Tien [8] was utilized for these improvements to predict the filtration coefficient. The filtration coefficient of this semi-empirical model describes the degree of particle filtration in the formation near fracture faces. The permeability reduction model proposed by Sharma et al. [9] predicts the permeability profiles by the particle plugging on the fracture face. (Appendix A.1.)

The fluid flow and relevant pressure drops for composite reservoir zones use the infinite conductivity

solution by Gringarten *et al.* [10]. Assuming a vertical fracture with two wings, the dimensions and pressure drops of the stepwise fluid and thermal fronts are analytically calculated. The fluid and thermal fronts are assumed to be ellipses confocal with the fracture. For the fracture growth calculation used in water injection models, Perkins and Gonzales [5] predicted the changes in in-situ stress by thermo- and poro-elastic effect induced by long-term injection. They introduced the fracture propagation model to calculate the fracture length induced by water injection. These models were combined into a semi-analytical numerical simulation to simulate fractured or unfractured vertical openhole gravel-packed wells, cased and perforated wells, horizontal wells with transverse or longitudinal fractures [11], and vertical frac-packed well [12].

Fracture Growth Criteria of the 2-D Model

The water injection model by Suri *et al.* [6] describes the fracture propagation by a 2-D model. This model was used as a reference model for the new 3-D model as its particle plugging, reservoir fluid flow, and stress change models are used as a part of the new model. Its fracture growth model is reviewed here for comparison. The fracture is assumed to initially grow as an enlarging penny shaped crack. Once the height of the fracture reaches the height of the formation, it is assumed to be confined between the bounding formations. The fracture tip is assumed to be circular while it is growing, but the fracture height remains to be constant. The basis of the fracture propagation used is the linear elastic fracture mechanics. The Griffith's energy balance theory [13] was used for mode I fracture propagation in plain strain condition. This condition applies to fractures with the penny shaped crack tip.

$$K_I = K_{IC} \tag{1}$$

where K_I is a stress intensity factor in mode I fractures and K_{IC} is a critical stress intensity factor in mode I fractures. A previously existing crack reinitiates when K_I exceeds K_{IC}. By definition, both terms can be written as:

$$\frac{2}{\pi}\Delta\sigma_I\sqrt{\pi r_f} = \sqrt{\frac{2\gamma E}{1-\nu^2}} \tag{2}$$

where γ is a specific surface energy, and E is Young's modulus. The driving stress of mode I fractures, $\Delta\sigma_I$, can be expressed with the fracture propagation pressure, P_{frac} and the in-situ stress, $S_{h\min}$.

$$\Delta\sigma_I = P_{frac} - S_{h\min} \tag{3}$$

By using this definition and rearranging the equation, the fracture propagation pressure can be calculated as below.

$$P_{frac} = S_{h\min} + \sqrt{\frac{\pi\gamma E}{2(1-\nu^2)r_f}} \tag{4}$$

The penny shaped fracture tip radius, r_f in the above equation can be replaced with the fracture height, $h_f/2$, once the top and bottom of the fracture tip reach the bounding layers. The square root term in the above equation is practically negligible compared to $S_{h\min}$ value. Then, the fracture propagation at the tip happens when the tip pressure exceeds $S_{h\min}$ value. This is well applied to the water injection projects in the unconsolidated sand formation. When a simulation for a single layer water injection is required, the 2-D fracture growth criteria will serve as a good estimation for the mechanics part of the simulation.

11.2 Model Formulation

Features and Assumptions of the Model

The objective of the new water injection model is to predict the injectivity decline by addressing the combined effect of the fracture geometry in 3-dimension, the degree of the particle plugging, and the change in the in-situ stress. There are several assumptions made to accomplish the calculations:

- The reservoir is homogeneous and isotropic.
- The fracture is the single two-winged fracture in the vertical direction. ($S_{vert} > S_{horiz}$)
- The degree of the particle plugging is uniform over the entire fracture face.
- The fluid loss is one-dimensional and perpendicular to the fracture face.
- Darcy's law is valid to the reservoir fluid flow.
- The fluid displacement and the temperature profile in the reservoir are piston-like.
- Heat conductions between layers are neglected.
- Water injection rate is constant.

Based on the above assumptions, the simulation model is composed of mainly two modules. One is the fracture propagation module and the other is the formation damage module. The formation damage module is composed of particle filtration, reservoir fluid flow, and stress change calculations. The latter eventually calculates the fluid leak-off coefficient, and this coefficient is used in the fracture propagation module again for the next time step. The schematic calculation sequence is shown in **Error! Reference source not found.**.

The model grid blocks are the finite element mesh composed of the regular triangular elements in the middle of the fracture and the singular quadrilateral elements at the fracture tip. The fracture propagation module calculates the fracture width, pressure, and the leak-off rate at the mesh nodes. The fracture propagation distance, relevant time step and remeshing calculations are also conducted.

Based on the fracture calculation at a specific propagation time step, the formation damage module calculates both internal and external particle filtration on the fracture face with the transition time calculation. The calculated particle filtrations are represented to resistances of reservoir fluid flow calculations. These resistances are converted to the leak-off coefficient, and this will be used for the fracture propagation calculation for each time step progression.

The overall simulation utilizes a combined numerical system composed of finite element methods for the fracture propagation module, and the semi-analytic calculation schemes for the formation damage module. The detailed algorithm of the model is explained in the Sec. 11.3. The following sub-sections explain the formulations and schemes used in fracture propagation module and the formation damage module.

Material Balance in the Fracture

The material balance equation can be calculated for the entire fracture, and it can be derived in the differential form representing the control volume as well. We use both forms of fluid flow equation in the simulation for different purposes. First, the overall material balance for the fracture and the fluid injection can be written as below:

$$V_{inj} = V_{frac} + V_L \qquad (5)$$

where V_{frac} is the fracture volume and V_L is the cumulative leak-off volume. In this equation, the cumulative injection volume, V_{inj} is simply the flow rate multiplied by the injection time when the

injection flow rate is maintained constant.

$$V_{inj} = q_{inj} \cdot t_{inj} \quad (6)$$

Meanwhile, for the time duration of Δt, the material balance for the fluid in a fracture is:

$$q_{inj} \cdot \Delta t = \Delta V_{frac} + q_L \cdot \Delta t \quad (7)$$

The leak-off flowrate for the short period of time can be assumed:

$$q_L(t) = q_{inj} - \frac{\Delta V_{frac}}{\Delta t} \quad (8)$$

For any specific time step, the leak-off flowrate, $q_L(t)$ can be calculated with this equation assuming that it is constant within that time step. This will serve as one way to calculate the average leak-off rate and is to be compared with $q_L(t)$ calculated from the formation damage module which will be explained later.

We also use the differential form of the material balance equation in the fracture propagation module based on Yew [14] and Gu [15]'s model. The fracture width is narrow compared to the areal dimension of the fracture. This leads to assumptions that pressure in the fracture is dependent on *x* and *y* directions (area), but not *z* direction (width). The velocity components of *x* and *y* directions are only accounted in the fracture and the fluid flow in *z* direction is taken as the fluid leak-off. The fluid is assumed to be Newtonian and incompressible. The material balance equation for the control volume, which has dimensions of Δx, Δy and $w(x,y)$ inside the fracture, is:

$$-\frac{\partial q_x}{\partial x} - \frac{\partial q_y}{\partial y} - q_L = \frac{\partial w}{\partial t} \quad (9)$$

where q_x and q_y terms are then related to the fluid pressure, $P(x,y)$ inside the fracture:

$$\frac{\partial}{\partial x}\left(\frac{w^3\,\partial P}{12\mu\,\partial x}\right) + \frac{\partial}{\partial y}\left(\frac{w^3\,\partial P}{12\mu\,\partial x}\right) = \frac{\partial w}{\partial t} + 2 \cdot u_L(t,x,y) \quad (10)$$

By the finite element formulation, the equation can be transformed to the following matrix equations.

$$[K]\{P\} = -\{f_L\} - \{f_w\} + \{f_p\} \quad (11)$$

where f_L, f_w and f_p are forcing function terms which are originated from the fluid leak-off, fracture width change, and the fluid injection respectively. The detailed derivation of the formulation can be found from Yew, Gu and Ouyang [14]–[16].

Fracture Mechanics

The fracture mechanics in the model are based on the linear elastic fracture mechanics. The fracture opening equation is required along with the fluid flow equation to calculate the fracture geometry and pressure distribution in the fracture model. Economides [17] stated that the width, *w* near the tip of a stress-free crack is a function of the stress intensity factor, K_I for the plain strain assumption.

$$w(r) = \frac{4(1-\nu)}{G} K_I \sqrt{\frac{r}{2\pi}} \quad (12)$$

where *r* is the inward normal distance from the fracture front. The definition of the stress intensity factor, K_I can be inserted to give the following equation including the stress and the pressure terms.

$$w(r) = \frac{4\sqrt{2}}{\pi}\frac{1-\nu}{G}\left(P - S_{h\min}\right)r \qquad (13)$$

This relation was formulated for arbitrarily shaped fractures in an infinite elastic medium by Bui [18]:

$$\begin{aligned} &-P(x,y) + S_{h\min}(x,y) \\ &= \frac{G}{4\pi(1-\nu)}\iint_{\Omega}\left[\frac{\partial}{\partial x}\left(\frac{1}{r}\right)\frac{\partial w}{\partial x'} + \frac{\partial}{\partial y}\left(\frac{1}{r}\right)\frac{\partial w}{\partial y'}\right]dx'dy' \end{aligned} \qquad (14)$$

Gu [15] and Yew [14] reformulated the above equation into a weak form as in the following equation:

$$\begin{aligned} &\frac{G}{4\pi(1-\nu)}\iint_{\Omega\Omega}\frac{1}{r}\left(\frac{\partial v}{\partial x}\frac{\partial w}{\partial x'} + \frac{\partial v}{\partial y}\frac{\partial w}{\partial y'}\right)dxdydx'dy' \\ &= \int_{\Omega}\left\{P(x,y) - S_{h\min}(x,y)\right\}v(x,y)\,dxdy \end{aligned} \qquad (15)$$

where the test function, $v(x,y)$ is a continuous function which satisfies that the fracture width is zero at the fracture tip. It is notable that the singular term $1/r$ was moved to the test function, $v(x,y)$. The opening displacement equation can also be transformed to the following form by the finite element formulation:

$$[A]\{w\} = \{f\} \qquad (16)$$

Readers again are recommended to refer to Yew, Gu and Ouyang [14]–[16] for the detailed finite element formulation, the algorithms and iterative method schemes for the fracture width, pressure and propagation calculations.

Fracture Propagation

One of the assumptions of the previous 2-dimensional fracture model by Suri *et al.* [6] is that the fluid injected is all leaked off. This assumption is valid as the fracture efficiency (fracture volume divided by injected volume), which is commonly calculated for the hydraulic fracturing jobs, is almost zero when calculated for water injection projects. Instead, the fracture lengths are calculated by an iteration method which satisfies the fracture propagation criteria at the fracture tip as explained in Sec. 0. In contrast, the 3-D fracture growth model does not use this assumption, and the fluid loss (the leak-off flowrate) calculation is required along with fracture propagation criteria.

Based on the finite element formulation for the fluid flow equation in a fracture and the fracture opening equation, Yew [14] and Gu [15] developed the iterative scheme for the 3-D fracture propagation calculation for hydraulic fracturing simulations. We modified their model and used it in the fracture propagation module of our simulation. The original model is working for the time scale of the hydraulic fracturing, which is normally in the order of an hour. Hence, the model was modified to accommodate the time scale of the water injection, which normally extends to several years. The other major change in the model was that the leak-off coefficient, which was specified by user in the previous model, is now calculated by the formation damage module. The leak-off coefficient is varying with time as it is dependent on the degree of the formation damage which is also affected by the history of the fracture growth.

For the fracture propagation criteria, stress intensity factors at the mesh points of the fracture tip are compared with their critical value, the fracture toughness. The process is composed of: (i) discretization of the material balance equation in the time domain, (ii) solving for the pressure and width by Picard iterative method, and (iii) fracture front movement calculation by the stress intensity factor. This can be further explained as follows: (i) The discretization of material balance in the time domain is combined with the global mass balance equation for the entire fracture. By combining Eq.

(7) and (11), the time step is implicitly decided during the iterative scheme. (ii) The resulting time step becomes the basis for the solution of width and pressure. The convergence is tested during Picard iterative scheme for the solution of the pair of the width and pressure equations. (iii) Once the fracture width is calculated for the fracture mesh, the stress intensity factor again is calculated from Eq. (12). In the course of the propagation, if the fracture is assumed to be stationary for a short period of time, the incremental stress intensity factor from its critical value, $K_I - K_{IC}$, at each node can determine the tip propagation distances [19].

$$\Delta d = \frac{K_I - K_{IC}}{K_{IC} + \frac{S_{tip} H_l}{\sqrt{h_d}}} \qquad (17)$$

where S_{tip} is the local in-situ stress at the tip, H_l is the local fracture height, and h_d is the depth of the fracture in the high in-situ stress layer.

The Adaptive Leak-off Calculation

In many fracturing simulations, the leak-off coefficient is specified by the user and remains constant during the injection periods. However, this assumption is not valid for water injection simulations because the leak-off behavior is a strong function of the formation damage of which the degree changes significantly with time by the long term nature of the injection. It is also dependent on the fracture growth behavior until the fluid loss is calculated at a specific time. Hence, the leak-off rate and the relevant leak-off coefficient shall be calculated at each time step.

A 2-D analytical radial flow reservoir model and the formation damage model near fracture faces were used to calculate the leak-off rate, q_L for the 3-D fracture propagation at a certain time step. With a known reservoir boundary pressure, P_e, the pressure drops for each fluid flow region were calculated by the following equations.

$$\Delta P_1 = q_L R_1 = q_L \frac{\mu_o}{2\pi k k_{ro} h} \ln\left(\frac{2r_e}{a_2 + b_2}\right) \qquad (18)$$

$$\Delta P_2 = q_L R_2 = q_L \frac{\mu_{wr}}{2\pi k k_{rw} h} \ln\left(\frac{a_2 + b_2}{a_1 + b_1}\right) \qquad (19)$$

$$\Delta P_3 = q_L R_3 = q_L \frac{\mu_{wi}}{2\pi k k_{rw} h} \ln\left(\frac{a_1 + b_1}{a_0 + b_0}\right) \qquad (20)$$

$$\Delta P_4 = q_L R_4 = q_L \frac{\mu_{wi}}{2\pi k k_{rw} h} \ln\left(\frac{a_0 + b_0}{L_f}\right) \qquad (21)$$

where, ΔP_1 is a pressure rise between the water flood front and the far-field drainage boundary. ΔP_2 is a pressure increase between the connate water flood front and the injected water flood front. ΔP_3 is a pressure increase between the injected water flood front and the thermal front. ΔP_4 is a pressure increase between the thermal front and the fracture. (See Fig. .)

A pressure increase across a skin damage at the fracture face, ΔP_s, can be obtained from the particle filtration and permeability reduction model [3, 18, 19]. It is composed of the flow resistances of the internal filtration of particles in the matrix near the fracture face and the external filter cake formation on the fracture face.

$$\begin{aligned}\Delta P_s &= q_L R_s \\ &= q_L \left(\max\left(R_{\text{int}} - R_{undamaged}, 0 \right) + R_c \right) \\ &= q_L \left(\max\left(\frac{\mu_{wi}}{A_f} \int_0^{L_{DZ}} \frac{dx}{k(x)} - \frac{\mu_{wi} L_{DZ}}{A_f k}, 0 \right) + \frac{\mu_w h_c}{A_f k_c} \right)\end{aligned} \tag{22}$$

Then, the pressure drop from the reservoir boundary to the fracture tip can be calculated by combining the above equations which leads to the explicit expression for the leak-off rate at a certain time.

$$\begin{aligned}\Delta P_{tip-e} &= P_{tip} - P_e \\ &= \Delta P_1 + \Delta P_2 + \Delta P_3 + \Delta P_4 + \Delta P_s \\ &= q_L \left(R_1 + R_2 + R_3 + R_4 + R_s \right)\end{aligned} \tag{23}$$

$$q_L(t) = \frac{P_{tip} - P_e}{R_1 + R_2 + R_3 + R_4 + R_s} \tag{24}$$

By explicitly solving resistances with the superficial velocity and fracture length of the previous time step, the leak-off rate is obtained by Eq. (24). This leads to a calculation for the leak-off coefficient, C_L at a specific time by assuming Carter's fluid loss correlation.

$$C_L(t) = \frac{q_L(t)}{A_f(t)} \sqrt{t} \tag{25}$$

The validity of the Carter's correlation will be discussed later. At this stage, this leak-off coefficient is assumed to represent the degree of fluid loss based on the uniform leak-off assumption over the entire area of the fracture. This coefficient becomes useful as the leak-off calculation is dependent on time and location when used in 3-D fracture propagation module. The fluid-loss calculation in the fracture propagation module is based on the equation as shown below.

$$u_L(x, y, t) = \frac{C_L(t)}{\sqrt{t - \tau(x, y)}} \tag{26}$$

The resulting linear leak-off velocity is directly used for the material balance equation in 3-dimensional fracture propagation models. After substituting the leak-off rate in Eq. (10), the pressure distribution and width are obtained from the fracture propagation module accordingly.

11.3 Model Algorithm

Method for Time Step Handling

The new injection well model is composed of two calculation modules: The fracture growth module and the formation damage module. The fracture growth calculation requires a discrete time step which starts from the moment the fracture growth criterion is met at the tip. The resulting time step (days or months) can be relatively long when the fracture growth rate is low. However, the particle plugging model requires the calculation for the duration before the fracture growth, and it needs a smaller time step than that of the fracture propagation module after fracture initiation. We used two different time steps for respective modules as in Fig. 3. The variables and results of each module were interchanged as necessary.

Before the fracture initiation, the formation damage module is conducted to predict the fracture

initiation time. After the fracture initiation, the fracture module calculates one propagation time step. The resulting fracture geometry and an incremental time, Δt_n^{3D} from the fracture propagation module is now used for the formation damage module. For the recently calculated time step duration from the fracture propagation module, the formation damage module calculates the change in the reservoir fluid flow, stress changes, and particle plugging with smaller time steps. This requires smaller time steps as the particulate plugging need cumulative information with time-dependent properties, e.g., flow resistances in the reservoir, thermal- and poroelastic stress changes. The increment in the time step of the formation damage module, Δt^{2D} is a constant value smaller than Δt^{3D}. The leak-off coefficient is calculated when $t^{2D} = t^{2D}_{n,\,final}$ for the next time step of the 3-D fracture module. This will properly address the fluid leak-off behavior during the recent fracture propagation time step.

Calculation Algorithm

At the beginning of the simulation, the time when the fracture starts to propagate is calculated. The fracture propagation module is not used for this stage. The particle plugging, thermal and poro-elastic stress change and the reservoir flow resistances are calculated to check whether the in-situ stress condition is above the fracture initiation pressure. The equations in Sec. 2 are used for the reservoir flow resistance calculation, permeability reduction, and stress change models. The 2-D fracture propagation criterion in Sec. 1 is used to determine the fracture initiation as well. When the fracture is initiated either from the un-fractured or fractured well, the fracture propagation module begins from the fracture initiation time.

After the fracture initiation, the simulation algorithm uses the 3-dimentional propagation module as an outer loop and the formation damage module an inner loop. Based on the leak-off coefficient from the particle filtration model of the previous time step, the fluid losses are determined for the following fracture growth calculation. The fluid flow equations and the fracture width calculation are performed by the iterative scheme described in Sec. 0 to give the fluid loss rate depending on time and location. Subsequently, the fracture propagation distances at the tip, the new dimensions and the pressure of the fracture are determined. In this iterative scheme, the time step corresponding to the fracture growth is calculated.

The discrete fracture growth requires the calculations for the necessary changes in the formation damage properties, the stress condition, and the reservoir fluid flow during the time step of the fracture propagation module. To address variations within one time step of the fracture propagation module, the formation damage module uses the refined time step smaller than that of the fracture propagation module. The fracture dimension is linearly interpolated at the refined time step as the dimension information is necessary for the calculation of the particle plugging and flow resistances. The validity of the linear interpolation will be reviewed by the simulation results. This intermediate calculation is important as the change in it determines the subsequent leak-off coefficient for the outer loop calculation. The leak-off coefficient is now used for the subsequent time step's fluid flow equation in the fracture propagation module. The necessary parameters for the fluid flow and fracture opening formulation are prepared for the fracture growth module in the following time step. This procedure will be repeated until the simulation ending time.

11.4 Discussion

Comparison with 2-D Model

The new model was tested by using typical parameters of a water injection project. The results of the new model is compared with the model by Suri *et al*. [6] which utilizes the 2-D fracture propagation scheme for a water injection project. The previous 2-D model uses the same formation damage model with the current 3-D model. However, it does not employ the algorithm or leak-off calculation explained in the previous sections. The base case model is explained as follows:

The injection well is assumed to be initially a fractured vertical well with the initial fracture length of 100 ft and the height of 150 ft. The initial shape of the fracture was assumed to be penny-like. The fracture width at the initiation was calculated by 3-dimensional model with the pressure distribution at the moment of fracture initiation. The stress contrast was 200 psi to the bounding layers to ensure fracture containment. The input parameters are the injection fluid, reservoir, thermal, and mechanical properties used for the base case simulation.

The fracture initiation time for this specific case was predicted to be about 0.6 year as in Fig. 5. The fracture length grows from 100 to about 300 ft in 15 years. However, the 2-D model predicted the fracture growth to be about 350 ft in the same time duration. The length predicted by the 3-D model was generally shorter than that by the 2-D model. This is believed to be due to the stricter fracture propagation criteria of the 3-D model in which the stress intensity factors along the tip are compared with their critical values. In Fig. 5, the bottomhole pressure is shown along with the fracture tip pressure. In the 2-D model, the fracture tip pressure is almost the same as the minimum in-situ stress. This is in accordance with the 2-D fracture propagation criteria explained in Sec. 11.1. In the 3-D model, the fracture criteria is independent of this global criteria, but the stress intensity factors are compared locally and hence, more strictly than in the 2-D model. The 3-D model's shorter length leads to the thicker external filter cake deposition. The pressure drop across thicker filter cake in the 3-D model was higher than 2-D case. This increased the bottomhole pressure to be higher in the 3-D model than in the 2-D simulation. If the 3-D fracture length is shorter than the 2-D, the opposite result is expected, and the 3-D bottomhole pressure would be lower than that of 2-D.

The injectivity is directly predicted from the bottomhole pressure. The injectivity of the fractured injection wells is directly related to the fracture growth. Before the fracture initiation, the injectivity normally decreases, and the rate of decrease is a function of the particle plugging of the well. After fracture initiation, the newly propagated area of the fracture is subject to the additional particle plugging, and the injectivity is stabilized. The stabilized injectivity and the time for the stabilization is a strong function of the injection water quality and formation properties. The injection water quality shall be specified to maintain the high injectivity as long as possible within the economic tolerances. This is one of the most important objectives of the injection well model.

Leak-off Behavior

The leak-off coefficient calculated by the formation damage module, which includes the particle filtration model, the reservoir fluid flow model, and the stress change model, is used as a crucial parameter for the 3-dimensional fracture propagation module. The leak-off coefficient, C_L, by definition, is only valid assuming that Carter's correlation is valid. We use the leak-off coefficient by assuming the Carter's correlation, but the coefficient is calculated for each fracture growth time step. Eventually, the linear rate of the fluid loss to the fracture face is the parameter we need for the fluid flow equation in the fracture. The calculated leak-off coefficient is dependent only on time and based on the assumption of the formation damage module that the fluid loss is uniform along the fracture face. But, by using the leak-off coefficient, the 3-D fracture propagation module generates the linear fluid loss rate, $u_L(t,x,y)$, which is dependent on time and location at the fracture.

The leak-off coefficient was calculated in two ways. The coefficient from the formation damage module was compared with those calculated from simulation results as in Fig. 6. The coefficients acquired from simulation results are not used for any part of the simulation and do not carry any

importance in the simulation procedure. They were calculated from the average leak-off rate in Eq. (8) for reference purposes. They represent the ratio of the resultant fluid loss to the injection flow rate. They can be understood as the reference values used to check whether the formation damage module plays a significant role in the overall fracture model. In Fig. 6, the difference between them represents the significance of the formation damage module in water injection fracturing. The degree of calculated coefficient change with time would result in a significant change in fracture dimensions when it remains constant.

When we look into the change of the averaged linear fluid loss velocity with time, the validity of the Carter's model can be addressed. The Carter's model assumes that the velocity changes inversely proportional to the square root of time. In Fig. 6, the velocity and time correlated with the exponent of approximately 0.4 for water injection simulations. Some other simulations in following figures also showed exponent values lower than 0.5. The lower exponents, e.g., 0.4, results in the lower values in linear leak-off velocity than those from the exponent of 0.5. This is the combined effect of additional fluid resistances caused by particle filtration, reservoir fluid flow, and stress change. They tend to give additional flow resistances in the long time scale of water injection. This effect may not be significant in hydraulic fracturing.

The adaptive leak-off calculation was applied for the hydraulic fracturing simulation to investigate the leak-off behavior. The same calculation and algorithm was used based on the particle plugging model, reservoir fluid flow model, and the stress change model for the shorter injection time steps. For this time domain, the effect of reservoir fluid flow and thermal stress change were negligible as in Fig. . The leak-off coefficient remained constant compared to the water injection cases. The order of the leak-off coefficient predicted was lower than those of water injections, and they were close to the typical values known for hydraulic fracturing. The coefficients from the leak-off calculation module and results of the simulation did not present any significant difference between them. The exponent of the correlation between velocity and time was approximately 0.5. This is very close to the exponent of the traditional Carter's correlation. The fluid leak-off behavior predicted from our model for hydraulic fracturing resulted in a very similar result with that of Carter's model. This indicates again that the dominating effects in water injection are not significant in the hydraulic fracturing with slick water. Our model can be used to estimate the leak-off coefficient when it is not available from other tests. It is important to note that we simulated the slick water as an injection fluid. If any other fluid with different rheology and wall building properties are used, the result may deviate from Carter's correlation. This requires further investigation.

Effect of Injection and Reservoir Properties

The effect of the injection water quality, in-situ stress, and reservoir properties were investigated. Different simulation cases were conducted to observe the sensitivity of the model to injection and reservoir properties including the particle concentration in the injection water and the stress contrast between sand and bounding layers.

The effect of the particle concentration is shown in Fig. . The particle concentration directly affects the cumulative amounts of particles and the filtration properties on the fracture face. The higher concentrations in the injection water led to a quicker decline of the injectivity and earlier fracture initiations. The bottomhole pressure is expected to be higher in a high concentration. Eventually, the longer fracture is expected. As can be expected, the lower concentration of particles leads to a higher fluid loss. The exponents for Carter's correlation were approximately 0.4, but any specific correlation with the concentration was not seen from the results.

The fracture dimensions generated from different in-situ stress conditions were compared in Fig. 9. In the base case simulations, the stress contrast between the target and bounding layer was 200 psi, and this ensured the fracture containment within the target layer. When the stress contrast was

lowered to 50 psi, the fracture was predicted to breach into the bounding layers. The effects of fracture breaching and the fluid loss into the bounding layer are effectively addressed by a 3-dimensional fracture model. The pressure and width distribution are mainly calculated during the process of propagation. When the fracture dimension becomes different by a different stress conditions, the exposed fracture area and particle filtration becomes different. This will lead to a different behavior in the fluid loss in the fracture. The simulation can be applied to more complex in-situ stress conditions.

11.5 Conclusion

Traditional fracture models used the constant leak-off coefficient and compared the intensity factor with fracture toughness. This applied to both the hydraulic fracture modeling and water injection simulations. We used an alternative approach. We changed the leak-off coefficient with time based on the filtration model. From that leak-off coefficient, the coupled fluid flow and fracture dimension equations were solved. The stress intensity factor at the tip of the fracture mesh was compared to the fracture toughness in the fracture propagation scheme. The 3-D fracture module and the leak-off calculation module were combined in the special time step handling mechanism and the model algorithm. The major findings of this work are:

- The leak-off coefficient of the water injection fracturing can change with time depending on the particle filtration behavior.
- The exponent to time in Carter's correlation can be approximately 0.4 when used for water injection fracturing, which is lower than the conventional value of 0.5.
- The adaptive leak-off calculation used for hydraulic fracturing simulation suggested the conventional (Carter's) leak-off calculation is appropriate.
- The adaptive leak-off calculation can be used independently for estimations of the leak-off coefficient from the injection and reservoir properties.
- The 3-dimensional fracture model can properly address the fracture growth into bounding layers.

11.7 Nomenclature

A_f = Area of fracture face (ft^2)
a_0 = Major axis of the thermal front ellipse (ft)
a_1 = Major axis of the waterflood front ellipse (ft)
b_0 = Minor axis of the thermal front ellipse (ft)
b_1 = Minor axis of the waterflood front ellipse (ft)
C_L = Leak-off coefficient in Carter's correlation (ft/√min)
E = Young's modulus (psi)
G = Shear modulus (psi)
h_c = Thickness of external filter cake (mm)
h_d = depth of the fracture in the high in-situ stress layer
H_l = Local fracture height
I = Injectivity ($=q_{inj}/(P_{iwf}-P_e)$) (bpd/psi)
k = Permeability of formation (md)
k_c = Permeability of filter cake (md)
K_I = Stress intensity factor (psi√in)
K_{IC} = Critical stress intensity factor (psi√in)
k_{ro} = End point relative permeability to oil (-)
k_{rw} = End point relative permeability to water (-)

L_{DZ} = Depth of internal damaged zone (ft)
L_f = Fracture length (ft)
P = Pressure (psi)
P_e = Pressure at reservoir boundary (psi)
P_{frac} = Fracturing pressure at the tip of 2-D fracture (psi)
P_{iwf} = Flowing injection pressure at bottomhole (psi)
P_{tip} = Pressure at fracture tip (psi)
q_{inj} = Injection flowrate (bbl/d)
q_L = Volumetric leak-off flowrate (bbl/d)
R_1 = Fluid flow resistance corresponding to ΔP_1 (psi/bpd)
R_2 = Fluid flow resistance corresponding to ΔP_2 (psi/bpd)
R_3 = Fluid flow resistance corresponding to ΔP_3 (psi/bpd)
R_4 = Fluid flow resistance corresponding to ΔP_4 (psi/bpd)
r_f = Radius of circular fracture tip (ft)
R_{int} = Fluid flow resistance by internal filter cake (psi/bpd)
R_s = Fluid flow resistance corresponding to ΔP_s (psi/bpd)
R_{und} = Fluid flow resistance of undamaged zone (psi/bpd)
S = Total stress (psi)
S_{hmin} = Minimum horizontal in-situ stress (psi)
S_{tip} = local in-situ stress at the tip (psi)
t_{inj} = Injection time (min)
t_n^{2D} = Simulation time used in formation damage module (s)
t_n^{3D} = Simulation time used in fracture growth module (s)
u_L = Linear velocity of fluid leak-off (ft/min)
V_{frac} = Volume of the fracture (ft^3)
V_{inj} = Cumulative injection volume (ft^3)
V_L = Cumulative leak-off volume (ft^3)
w = Fracture Width (inch)
γ = Specific surface energy (Pa·m)
Δd = Increment frontal displacement of fracture node (ft)
ΔP_1 = Pressure rise between connate waterflood front and reservoir boundary (psi)
ΔP_2 = Pressure rise between connate waterflood front and injected waterflood front (psi)
ΔP_3 = Pressure rise between injected waterflood front and thermal front (psi)
ΔP_4 = Pressure rise between thermal front and the fracture (psi)
ΔP_s = Pressure increase by particle deposition on fracture face (psi)
$\Delta\sigma_I$ = Driving stress of mode-I fracture (net pressure) (psi)
μ = Viscosity (cp)
μ_o = Viscosity of oil (cp)
μ_{wi} = Viscosity of water at injection temperature (cp)
μ_{wr} = Viscosity of water at reservoir temperature (cp)
ν = Poisson's ratio (-)
σ = Effective stress (psi)

11.7 References

1. Abou-Sayed, A.S., Sinha, K.P. and Clifton, R.J. 1984. Evaluation of the Influence of In-Situ Reservoir Conditions on the Geometry of Hydraulic Fractures Using a 3-D Simulator: Part 1-Technical Approach. paper SPE 12877 presented at the *SPE Unconventional Gas Recovery Symposium, 13-15 May 1984, Pittsburgh, Pennsylvania*. doi:10.2118/12877-MS.

2. Carter, R.D. 1957. Appendix I - Derivation of the General Equation for Estimating the Extent of the Fractured Area. *Optimum Fluid Characteristics for Fracture Extension by G.C. Howard and C.R. Fast,* pp.261–269, American Petroleum Institute.

3. Pang, S. and Sharma, M.M. 1997. A Model for Predicting Injectivity Decline in Water-Injection Wells. *SPE Formation Evaluation*, 12: 194–201.

4. Wennberg, K.E. and Sharma, M.M. 1997. Determination of the Filtration Coefficient and the Transition Time for Water Injection Wells. paper SPE 38181 presented at the *SPE European Formation Damage Conference, 2-3 June 1997, The Hague, Netherlands*. doi:10.2118/38181-MS.

5. Perkins, T.K. and Gonzalez, J.A. 1985. The Effect of Thermoelastic Stresses on Injection Well Fracturing. *Society of Petroleum Engineers Journal*, 25: 78–88.

6. Suri, A., Sharma, M. and Peters, E. 2011. Estimates of Fracture Lengths in an Injection Well by History Matching Bottomhole Pressures and Injection Profile. *SPE Reservoir Evaluation & Engineering*, 14: 385–397.

7. Gadde, P. and Sharma, M. 2001. Growing Injection Well Fractures and Their Impact on Waterflood Performance. paper SPE 71614 presented at the *SPE Annual Technical Conference and Exhibition, 30 September-3 October 2001, New Orleans, Louisiana*. doi:10.2118/71614-MS.

8. Rajagopalan, R. and Tien, C. 1976. Trajectory analysis of deep-bed filtration with the sphere-in-cell porous media model. *AIChE Journal*, 22: 523–533.

9. Sharma, M.M., Pang, S., Wennberg, K.E. and Morgenthaler, L.N. 2000. Injectivity Decline in Water-Injection Wells: An Offshore Gulf of Mexico Case Study. *SPE Production & Facilities*, 15: 6–13.

10. Gringarten, A., Henry J., R. and Raghavan, R. 1974. Unsteady-State Pressure Distributions Created by a Well With a Single Infinite-Conductivity Vertical Fracture. *Society of Petroleum Engineers Journal*, 14: 347–360.

11. Suri, A. and Sharma, M. 2009. Fracture Growth in Horizontal Injectors. paper SPE 119379 presented at the *SPE Hydraulic Fracturing Technology Conference, 19-21 January 2009, The Woodlands, Texas*. doi:10.2118/119379-MS.

12. Suri, A. and Sharma, M. 2010. A Model for Water Injection Into Frac-Packed Wells. *SPE Reservoir Evaluation & Engineering*, 13: 449–464.

13. Griffith, A.A. 1921. The Phenomena of Rupture and Flow in Solids. *Philosophical Transactions of the Royal Society of London. Series A, Containing Papers of a Mathematical or Physical Character*, 221: 163–198.

14. Yew, C.H. 1997. *Mechanics of Hydraulic Fracturing*. Gulf Professional Publishing.

15. Gu, H. 1987. Study of Propagation of Hydraulically Induced Fractures. Dissertation, The University of Texas at Austin, USA.

16. Ouyang, S. 1994. Propagation of Hydraulically Induced Fractures with Proppant Transport. Dissertation, The University of Texas at Austin, USA.

17. Economides, M.J. and Nolte, K.G. 2000. *Reservoir Stimulation*. 3rd ed. John Wiley & Sons.

18. Bui, H.D. 1977. An integral equations method for solving the problem of a plane crack of arbitrary shape. *Journal of the Mechanics and Physics of Solids*, 25: 29–39.

19. Mastrojannis, E.N., Keer, L.M. and Mura, T. 1980. Growth of planar cracks induced by hydraulic fracturing. *International Journal for Numerical Methods in Engineering*, 15: 41–54.

20. Saripalli, K., Bryant, S. and Sharma, M. 1999. Role of Fracture Face and Formation Plugging in Injection Well Fracturing and Injectivity Decline. paper SPE 52731 presented at the *SPE/EPA Exploration and Production Environmental Conference, 1-3 March 1999, Austin, Texas*. doi:10.2118/52731-MS.

11.8 Figures

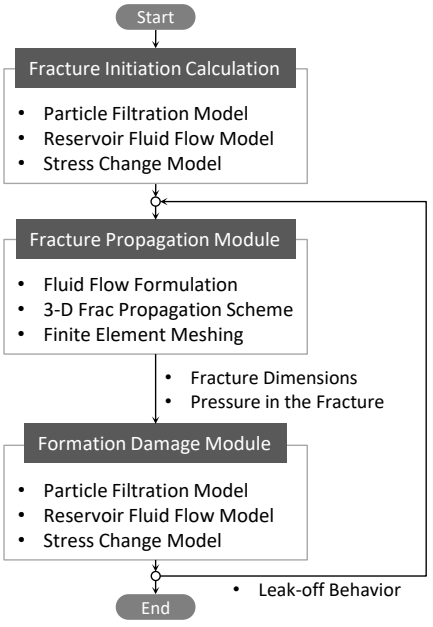

Fig. 1. Simulation flow chart.

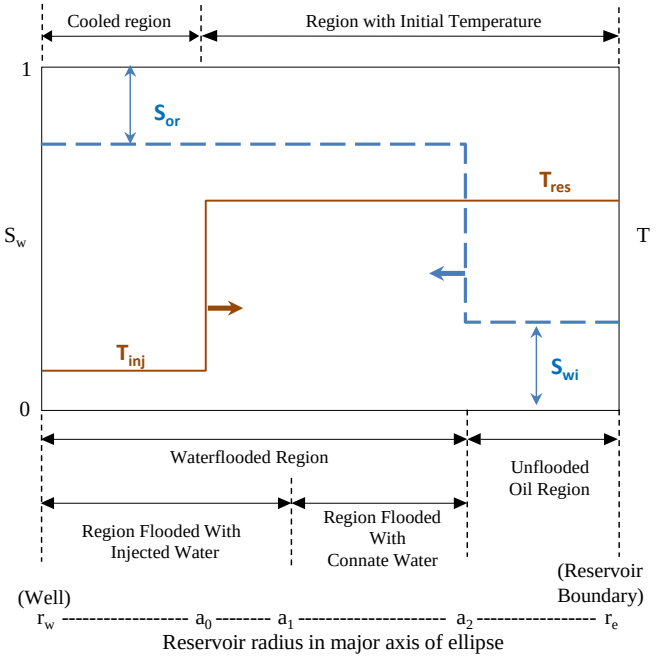

Fig. 2. Water saturation and temperature profile in the reservoir model.

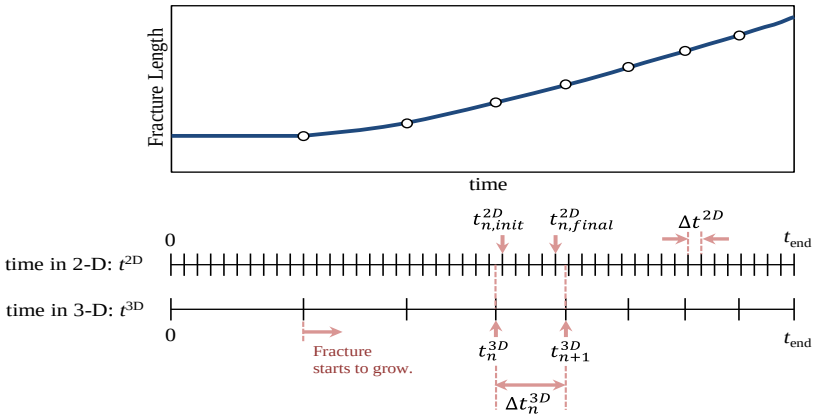

Fig. 1. Time steps used in the simulation. The time step in 2-D, t^{2D} is for the calculation of the particle plugging model, reservoir fluid flow, and stress changes. The time step in 3-D, t^{3D} is for the calculation of the fracture propagation.

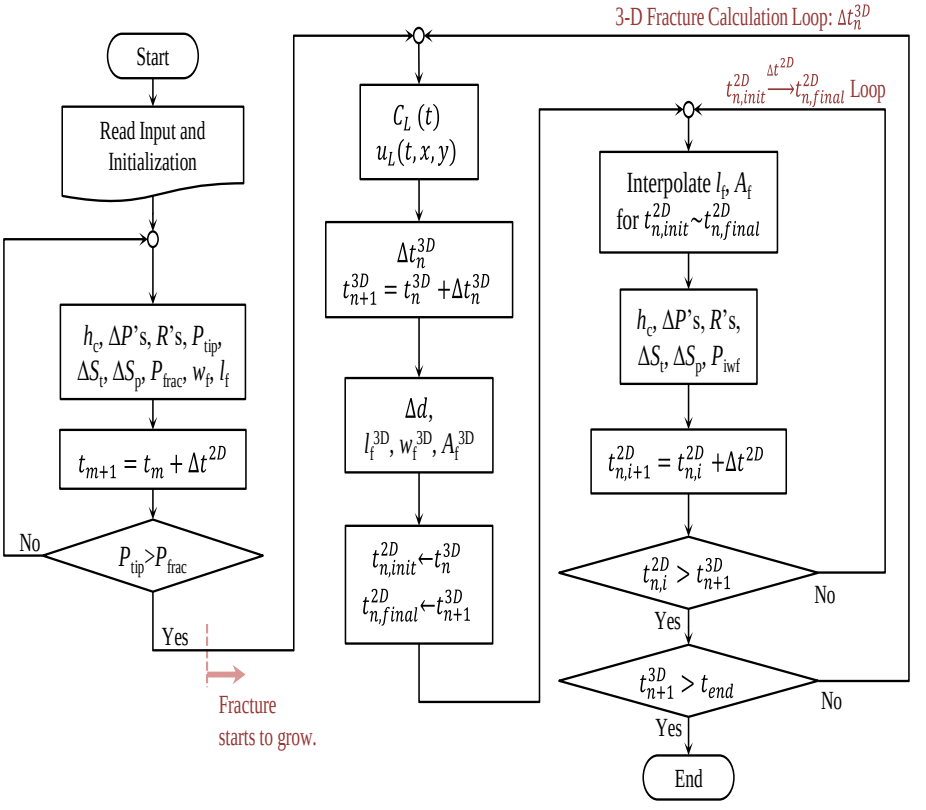

Fig. 2. Main algorithm. The outer loop conducts calculations for the fracture propagation (for time step $t^{3D}{}_n \longrightarrow t^{3D}{}_{n+1}$) and the inner loop calculates the particle plugging model, fluid flow equations in the reservoir, and the stress changes for the time steps ($t^{2D}{}_{n,\text{init}} \longrightarrow t^{2D}{}_{n,\text{final}}$).

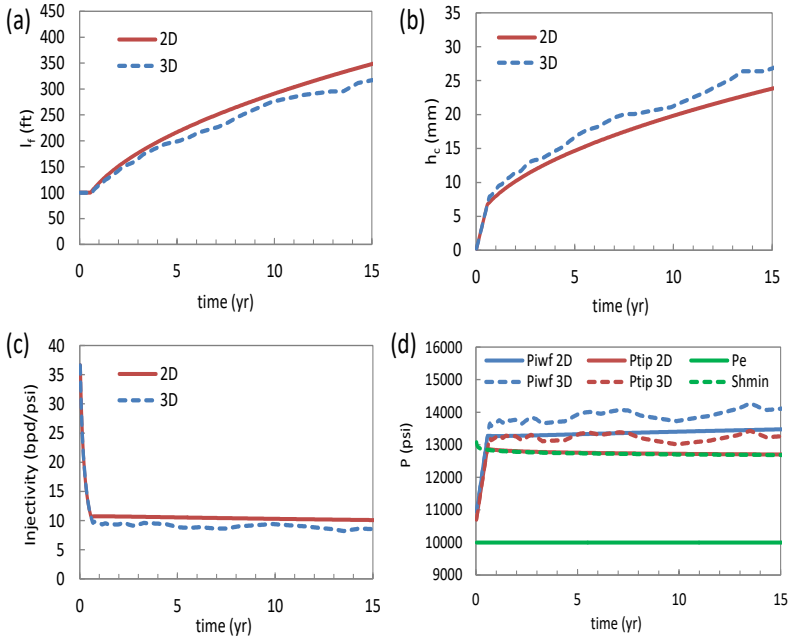

Fig. 3. Results of the base case model. (a) Fracture half length with time, (b) Thickness of the external filter cake on the fracture faces, (c) Injectivity of the well, (d) Flowing injection bottom hole pressure and fracture tip pressure compared to the minimum horizontal stress and the reservoir boundary pressure. The results were compared to those of water injection well model with 2-dimensional fracture propagation.

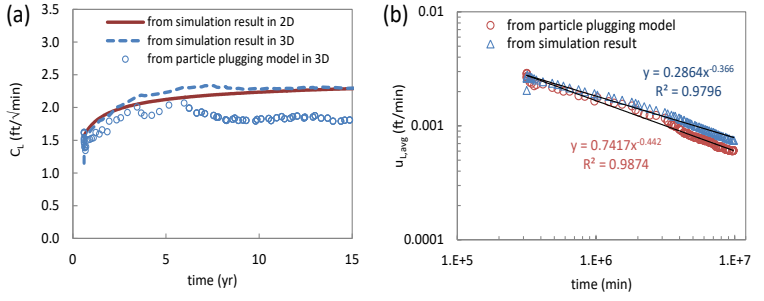

Fig. 4. The leak-off behavior from the base case results. (a) The leak-off coefficient used in Carter's leak-off equation. The leak-off coefficient calculated from the particle plugging model is compared to the effective leak-off coefficients calculated from the simulation results. (b) The Carter's leak-off behavior was tested by correlating the linear leak-off velocity to time. The exponent to time is

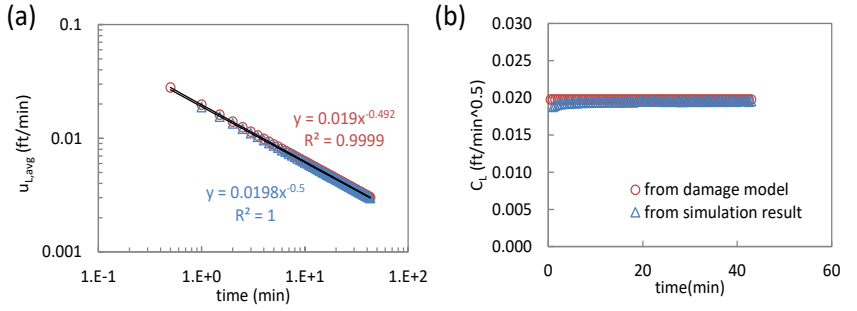

Fig. 7. Leak-off Behavior calculated by the adaptive leak-off model for hydraulic fracturing simulation. The leak-off behavior from the adaptive leak-off calculation and simulation results follows the conventional Carter's leak-off correlation.

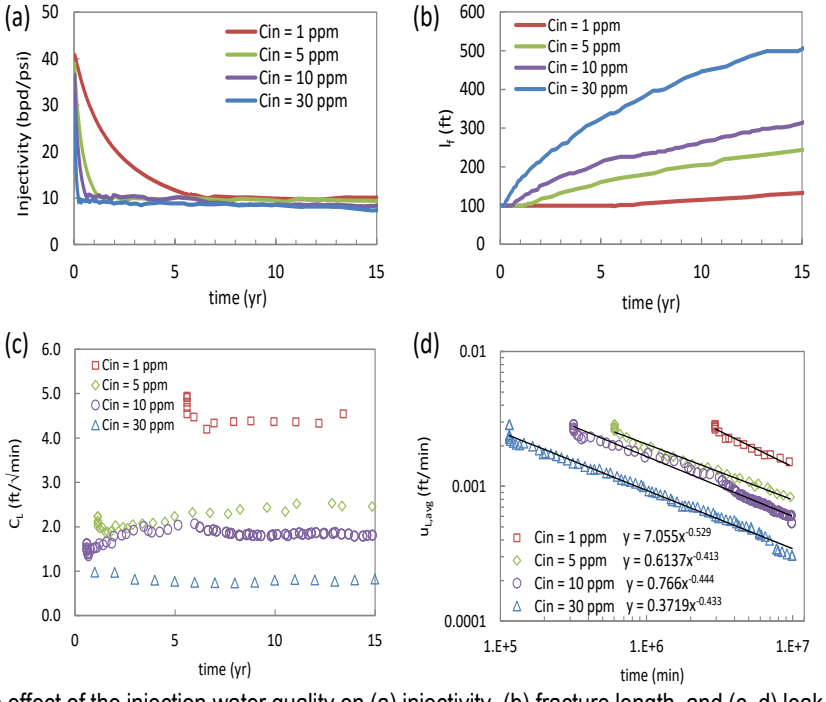

Fig. 8. The effect of the injection water quality on (a) injectivity, (b) fracture length, and (c, d) leak-off behavior. Higher particle concentration in the injection water led to less leak-off and higher rate of fracture growth.

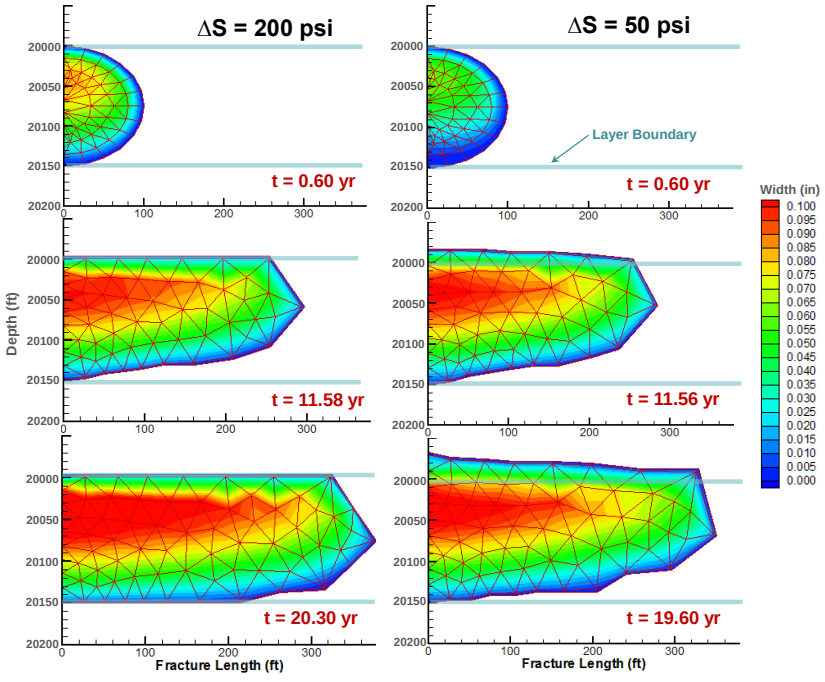

Fig. 5. Effect of the stress difference between the target and bounding layers on the fracture dimensions. Higher stress contains the fracture within the sand layer, but the fracture breaches into the bounding layers when the stress contrast is lower.